SYNTHESIS AND PHOTOPHYSICAL INVESTIGATION OF SUPRAMOLECULAR COMPLEXES DEVELOPED FOR PHOTOINITIATED ELECTRON COLLECTION

by

Sharon Marie Molnar

Dissertation submitted to the Faculty of the

Virginia Polytechnic Institute and State University

in partial fulfillment of the requirements for the degree of

DOCTOR OF PHILOSOPHY

in

Chemistry

APPROVED:

Karen J. Brewer, Chair

Mark R. Anderson

John G. Dillard

Brian E. Hanson

Joseph S. Merola

January, 1996
Blacksburg, Virginia

key words: polypyridyl, ruthenium, photochemistry

SYNTHESIS AND PHOTOPHYSICAL INVESITGATION OF SUPRAMOLECULAR COMPLEXES DEVELOPED FOR PHOTOINITIATED ELECTRON COLLECTION

by
Sharon M. Molnar

Karen J. Brewer, Chair

Chemistry

(ABSTRACT)

In this research, photochemical molecular devices were designed to perform photoinitiated electron collection. These devices were synthesized, characterized and their spectroscopic, photochemical and electrochemical properties investigated. The general formula for these systems is $\{[(bpy)_2Ru(BL)]_2MCl_2\}^{5+}$ (M = Ir^{III} and BL = dpq (2,3-bis(2-pyridyl)quinoxaline) or dpb (2,3-bis(2-pyridyl)benzoquinoxaline), or M = Rh^{III}, BL = dpp (2,3-bis(2-pyridyl)pyrazine)). The functioning of these devices as photoinitiated electron collectors was determined. Through the use of a sacrificial electron donor in a photolysis experiment, the functioning of the $\{[(bpy)_2Ru(dpb)]_2IrCl_2\}^{5+}$ trimetallic complex as a photochemical molecular device for photoinitiated electron collection was established. The interaction of the electron donor with the trimetallic complex was also investigated through a Stern-Volmer quenching study.

To tune the properties of the chromophoric units, $[Ru(bpy)_2(BL)]^{2+}$, the bridging ligand was varied. The dpq bridging ligand was modified through the incorporation of electron donating and electron withdrawing substituents. The 6,7-dimethyl-2,3-bis(2'-pyridyl)quinoxaline and 6,7-chloro-2,3-bis(2'-pyridyl)quinoxaline bridging ligands were synthesized and characterized. The ruthenium mono- and bimetallic complexes utilizing these bridging ligands, as well as dpb, were synthesized and investigated. It was shown that the light absorbing and electrochemical properties of these $[Ru(bpy)_2(BL)]^{2+}$ chromophores can be varied by altering the π-acceptor nature of the bridging ligand.

To my Parents, David E. and Geraldine K. Molnar

and

Miss Darcie.

ACKNOWLEDGMENTS.

Getting to this point of being able to write the acknowledgments section to my doctoral thesis has been a long and arduous task. It has been a journey I would not have been able to complete on my own. There have been countless people both academically and personally, too numerous to adequately encompass here, that I am deeply grateful to have encountered throughout my journey.

Academically, I would first like to thank my research director Dr. Karen J. Brewer. A simple written thank you seems trivial for the amount of patience and understanding she has extended to me from the start of my graduate career. When I didn't have faith in myself (academically and otherwise), she had enough for the both of us. Thanks to "Doc" ... you've not only given me a shoulder to lean on, but also an occassional well needed, and well placed, kick in the butt; which was always followed by a laugh and a smile. I have learned much from you. The members of my committee have been incredibly helpful and extraordinarily patient through the thesis process. So to Drs. Joseph Merola, Brian Hanson, John Dillard, and Mark Anderson I'd like to extend my enormous gratitude.
I would also like to acknowledge the National Science Foundation (CHE-9313642) for funding my research.

Other influences throughtout my academic career have been: Dr. Roger Willett, Dr. Helen Place, Sr. Mary Thompson, Sr. Adele Rothan, Dr. Patricia Fish, Dr. Susan Molnar, and Dr. E. Brady Williams. I'd also like to take a line to acknowledge the help of

Analytical Services at Virginia Tech, specifically Bill Bebout and Geno Iannacconne, and Tom Glass.

On a personal level of gratitude there are, again, numerous people...too many to write down here. First, I'd like to thank my best bud Elizabeth Raub Bullock...I love ya, man !!!...Enough said. I've also been lucky to have made many cherished friends along the way: Heather Hall, Gail Reed, J. Marnita Douglas, Steven Lee Alam, Mark and Lisa Vrana, Jeff and Tami Staub, Michelle Stabile, Sumner Weston Jones, R. Gary Brewer, and last, but by no means least ...Todd Fletcher and, my personal angel, Diedre Smith.

Family wise I have had support from my two brothers Mark and Paul, and my two new sisters Tanya and Kathy. Some other family members that have been important too me are: Mary Kantrow, Marilyn Kantrow, Anna Clingingsmith, Jim and Jenny Kantrow, Andy and Sonya Molnar, and Kay and Jerry Shaw. Finally, I like to show my heart felt gratitude to two people who have given me unconditonal support...my two cherished and immensely loved parents...Dave and Gerri Molnar.

TABLE OF CONTENTS

LIST OF ABBREVIATIONS

Q	**Q**uencher
BL	**B**ridging **L**igand
bpy	**bipy**ridine
Cl_2dpq	6,7-dichloro-2,3-bis(2'-pyridyl)quinoxaline
DMA	N,N'- **dim**ethyl**a**niline
TPA	**Tri**phenyl**a**mine
dpp	2,3-bis(2'-pyridyl)pyrazine
dpq	2,3-bis(2'-pyridyl)quinoxaline
dpb	2,3-bis(2'-pyridyl)benxoquinoxaline
EC	**E**lectron **C**ollector
ED	**E**lectron **D**onor
ILCT	**I**ntra**l**igand **C**harge **T**ransfer
LA	**L**ight **A**bsorber
LA*	**L**ight **A**bsorbing Species in the Excited State
LMCT	**L**igand-to-**M**etal **C**harge **T**ransfer
MD	**M**olecular **D**evice
Me_2dpq	6,7-dimethyl-2,3-bis(2'-pyridyl)quinoxaline
MLCT	**M**etal-to-**L**igand **C**harge **T**ransfer
MO	**M**olecular **O**rbital
PIEC	**P**hotoinitiated **E**lectron **C**ollection
PMD	**P**hotochemical **M**olecular **D**evice

LIST OF FIGURES.

LIST OF TABLES.

CHAPTER 1.

INTRODUCTION.

The goals of the research detailed herein were to design, synthesize, and determine the photophysical properties and functioning of a photochemical molecular device (PMD) developed for photoinitiated electron collection (PIEC). An orbital energy level diagram for a photoinitiated electron collector has been proposed in the literature[1], yet an actual functioning device had not materialized.

Photochemical Molecular Devices.

A device by definition is: "device (dé vîs): a thing that is made, usually for a particular working purpose."[2] A molecular device (MD) is a device on the molecular scale composed of subunits. Each subunit is designed to execute a specific task. Multiple subunits executing their task in a given sequence yields an overall function that the device has performed. Supramolecular complexes are often thought of as the connective assemblies of such molecular subunits. Many of these devices involve the absorption and/or emission of light, and, therefore, have been termed photochemical molecular devices. Photobiological devices perform a variety of functions, such as photosynthesis and vision.[1] Natural systems are remarkably complex and their exact replication would be synthetically challenging. Artificial systems that carry out similar tasks, however, can be devised.

In 1987 Vincenzo Balzani proposed orbital energy diagrams for a multitude of photochemical molecular devices.[1] One specific PMD described by Balzani was a

photoinitiated electron collector. The purpose of such a device was to use light energy to initiate a sequence of events which, in the end, yielded the collection of multiple electrons. Once collected, the electrons could subsequently be used to facilitate the multielectron reduction of a variety of substrates. Figure 1 shows a modified depiction of Balzani's orbital energy diagram corresponding to a photoinitiated electron collector. The device is constructed of three main subunits: an electron donor (ED); a light absorber (LA); and an electron collector (EC). Multiple electrons are collected on the device through a sequence of events. Mapping the flow of such a sequence of events is facilitated by focusing on one half of the device, prior to viewing the system as a whole. The sequence of events for a ED–LA–EC section of the device are: (1) the LA absorbs a photon; (2) the ED donates an electron to fill the hole created; and (3) the promoted electron, resulting from step 1, propagates to lower energy orbital on the central EC. After the performance of all three steps, the result is one oxidized ED and a singly reduced EC. Duplication of the same sequence of events, by the other half of the device, produces two oxidized electron donors and a doubly reduced electron collector. For the purposes of the work detailed herein, it should be noted that all subunits are covalently attached in his proposed PMD for PIEC.

The PMDs designed for PIEC in this research are mixed-metal trimetallic systems of the form $\{[(bpy)_2Ru(BL)]_2MCl_2\}(PF_6)_5$ (M= Ir^{III} and BL = dpq (2,3-bis(2-pyridyl)quinoxaline) and dpb (2,3-bis(2-pyridyl)benzoquinoxaline), M = Rh^{III}, BL = dpp (2,3-bis(2-pyridyl)pyrazine)). Some of the device's monometallic subunits device have been previously studied. Before highlighting the research pertaining to these monometallic complexes, and discussing the research herein, a brief prologue is provided

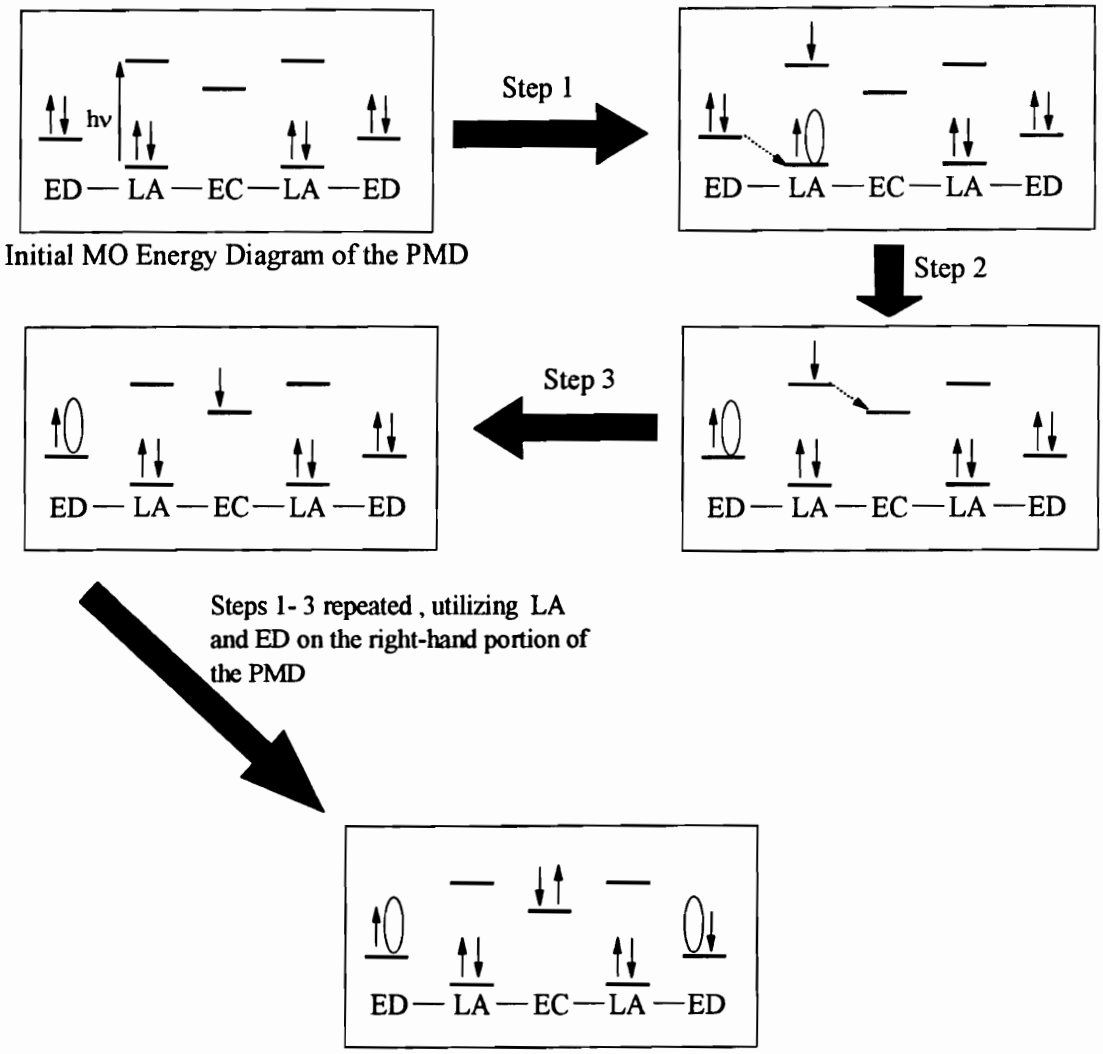

Figure 1. *Orbital Energy Diagram for the Design of a Molecular Device for Photoinitiated Electron Collection.* The first diagram shows the initial orbital energy diagram of the device. The abbreviations for these subunits are electron donor (ED), light absorber (LA), and electron collector (EC). The final diagram shows the orbital energy diagram of the device after it has performed its function.

to orient the reader to pertinent concepts and establish a terminology basis. This discussion will give a cursory overview of electronic transitions, cyclic voltammetry, and excited state phenomena.

Electronic Transitions.

In discussing the characterization and photophysical parameters of the PMDs it will be useful to use a localized molecular orbital approach. The transition metal centers contained in the trimetallic PMDs for PIEC, and their monometallic subunits, possess pseudo-octahedral symmetry. The molecular orbital (MO) diagram for an octahedral complex involving both σ and π bonding is shown in Figure 2.[3] This "block–MO" diagram is a simplified molecular orbital representation incorporating a localized MO concept.[4] Each 'block' represents multiple molecular orbitals. The MO block's subscript denotes the predominant contributor to that set of MOs ($(block)_M$ = dominant metal contribution and $(block)_L$ = a dominant ligand contribution). Various types of optical exitations can occur between these orbitals.

Octahedral complexes can undergo many types of optical excitations. Referring to Figure 2[4], there are three general types of transitions for octahedral metal complexes: metal-centered transitions, ligand-centered transitions, and transitions involving both metal and ligand based orbitals. Metal-centered transitions (1) are referred to as d-d transitions or ligand field (LF) transitions. Ligand based transitions (2) are referred to as intraligand transitions (IL). Intraligand transitions commonly involve the π bonding, nonbonding N based orbitals and antibonding orbitals ($n_L \rightarrow \pi^*_L$, $\pi_L \rightarrow \pi^*_L$). Transitions involving both

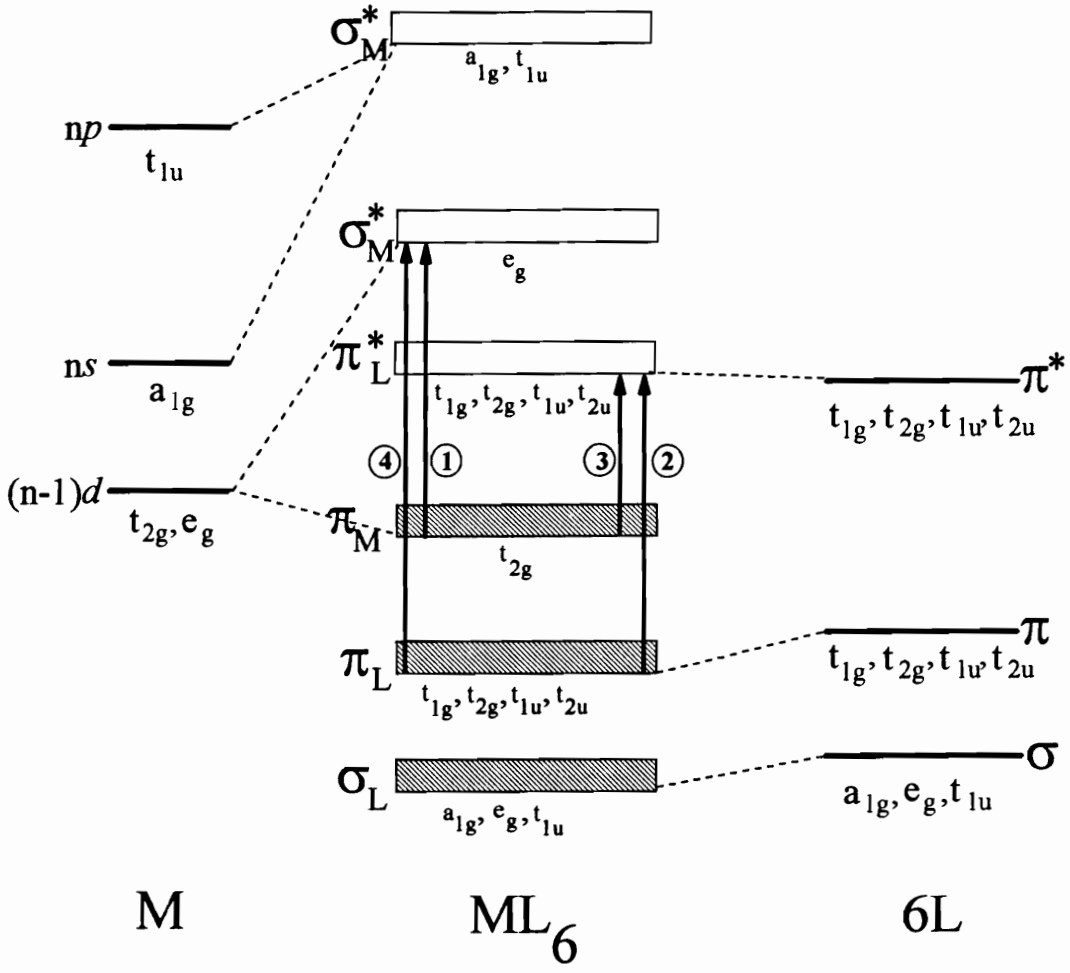

Figure 2. *Block Molecular Orbital Energy Diagram for an Octahedral Complex, ML_6.* The cross-hatching of a 'block' denotes the extent of electron occupation of that block.

metal and ligand based orbitals are classified as either a metal-to-ligand charge transfer (MLCT) or a ligand-to-metal charge transfer (LMCT).[3] MLCT transitions (3) may be from the filled t_{2g} or partially filled e_g^*. The most common example of a MLCT transition is ($\pi_M \rightarrow \pi^*_L$). A LMCT transition originates from any of the filled ligand orbitals (π_L or σ_M) and terminates in any of the empty metal orbitals. A common LMCT (4) transition is from the π_L to the σ_M^*.[4] After excitation of a molecule there is an alteration of the electronic state of the complex. There are many ways to deactivate and characterize the excited state created by the promotion of an electron to a higher energy orbital.

Excited State Phenomena.

An excited state may lose energy by radiative, nonradiative and quenching pathways. A state diagram, or Jablonski diagram, for a d^6 octahedral complex can be used to visually illustrate these basic pathways (Figure 3).[5] Radiative deactivation occurs through both fluorescence (k_f, emission from S_1) and phosphorescence (k_p, emission from T_1). Although other deactivation pathways include heat loss (k_{nr} and $k_{nr'}$, nonradiative decay), and interaction with another molecule (k_{rxn}, quenching), phosphorescence deactivates most complexes of the type described herein.

Quantum Yields. A mathematical relationship, known as quantum yields, is used to indicate the efficiences of excited state processes. An example would be the emission quantum yield (Φ^{em}). The ratio of the quanta of light emitted versus quanta of light absorbed by the system, (Equation 1), yields a numerical value for the emission quantum yield.

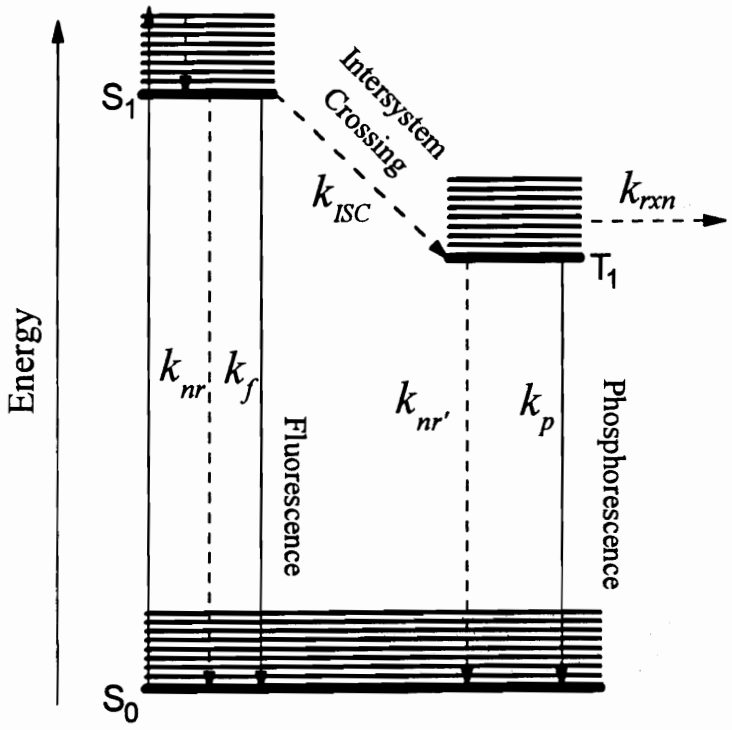

Figure 3. *Jablonski Diagram.*

$$\Phi^{em} = \text{(Quanta of photons emitted)/(Quanta of photons absorbed)} \qquad (1)$$

Quantum yields can be expressed for any process. For instance, one can determine the quantum yields for intersystem crossing, phosphorescence, fluorescence, or for the production of products from a photochemical reaction. The quantum yield for any process resulting from a directly and optically populated state is expressed by equation 2.[6]

$$\Phi_{process} = k_{process} / \Sigma k_i \qquad (2)$$

The quantum yield for any process ($\Phi_{process}$) from an optically populated state is the ratio of the rate constant for that process ($k_{process}$) and the summation of all the rate constants for all processes (Σk_i) that deactivate that state. This equation, however, becomes more complicated when considering an indirectly and optically populated state,[6]

$$\Phi_{process} = \Phi_{population} (k_{process} / \Sigma k_i) \qquad (3)$$

Phosphorescence is an example of an indirectly and optically populated state. The quantum yield expression for phophorescence is shown below, as seen in Equation 3 and expressed exclusively in terms of relevant rate constants.

$$\Phi_p = \Phi_{ISC}(k_p / [k_p + k_{nr'}])$$

$$= \left[\frac{k_{ISC}}{k_{ISC} + k_{nr} + k_f}\right]\left[\frac{k_p}{k_p + k_{nr'}}\right] \qquad (4)$$

Excited State Lifetimes. Another characteristic of the excited state is its lifetime. An excited state lifetime is an important characteristic to know since it determines the amount of time in which excited state reactions may occur.

When photochemists perform measurements to determine excited state lifetimes, a pulse of light excites the sample and decay of the sample's excitation is observed. The light pulse produces a high concentration of excited state molecules. For an emissive excited state, the intensity of the emitted radiation is monitored over time. The intensity of light decreases over time after the light pulse, and the observation of this decrease in radiation intensity versus time yields the excited molecules rate of decay. Radiative emission from an excited state is a random process, and therefore follows first-order kinetics. The rate of the excited state's decay can be expressed as [7]

$$\frac{-\,d\,[LA^*]}{dt} = k_{obs}\,[LA^*] \qquad (5)$$

The rate of decay should fit a single-exponential function, $y = a + b[\exp(-k_{obs}t)]$. Given k_{obs} one can calculate τ, the excited state lifetime, $\tau_r = 1/k_{obs}$. The rate constant for an excited state's deactivation is the summation of all of the rate constants associated with each depletion pathway for such a state. In the case of phosphorescence from the T_1 state, the observed rate constant for loss of that state, k_{obs}, would be the sum of k_p, $k_{nr'}$, and k_{rxn}.

Quenching. Interactions of LA^* with a quencher (Q) can result in the deactivation of LA^*. This quenching may be through electron transfer, energy transfer, or some other bimolecular deactivation pathway. A dynamic (or diffusional) quenching scheme is outlined below.[5]

$LA + h\nu$	$\rightarrow$	LA^*	Excitation (I_a)
LA^*	$\rightarrow$	$LA + h\nu'$	Radiative Decay (k_1)
LA^*	$\rightarrow$	LA + heat	Nonradiative Decay (k_2)
$LA^* + Q$	$\rightarrow$	$LA^- + Q^+$	Electron Transfer Quenching (k_q)
$LA^* + Q$	$\rightarrow$	$LA + Q$	All Other Bimolecular Quenching (k_3)

Through observing the response of the light absorber's excited state physical properties as a function of quencher concentration, one can determine the rate at which the two species interact. The use of the above dynamic scheme to determine that rate is known as Stern-Volmer kinetics.[5]

All unimolecular rate constants are grouped into one rate constant, k_t ($k_t = k_1 + k_2$). Similarly, all bimolecular quenching rate constants are grouped into k_q' ($k_q' = k_q + k_3$). During a steady state photochemical experiment, the [LA*] does not change appreciably over time. Therefore, application of the steady state approximation to the rate of decay of the concentration of the excited light absorber [LA*] over time, yields

$$d[LA^*]/dt = I_a[LA] - k_t[LA^*] - k_q'[LA^*][Q] = 0$$

Therefore,
$$[LA^*] = I_a[LA] / (k_t + k_q'[Q]) \qquad (6)$$

The change in the concentration of LA^- over time can be related to the concentration of the light absorbing species and the concentration of the quenching species

$$d[LA^-]/dt = k_q[LA^*][Q]$$

$$= k_q[Q]\{I_a[LA] / (k_t + k_q'[Q])\} \qquad (7)$$

The quantum yield for the production of LA^- is expressed as

$$\Phi_{[LA^-]} = \{d[LA^-]/dt\}/ I_a \quad (8)$$

Given equations 5,6 and 8

$$\{d[LA^-]/dt\}/I_a = k_q[LA][Q]/(k_t + k_q'[Q]) \quad (9)$$

and through the combination of equations 8 and 9

$$1/\Phi_{[LA^-]} = k_t/k_q[LA][Q] + k_q'/k_q[LA]$$

Therefore, a plot of $(1/\Phi_{[LA^-]})$ versus $(1/[Q])$ will yield a straight line, with

$$\text{slope} = k_t/k_q[LA] \quad \text{and} \quad y\text{-intercept} = k_q'/k_q[LA]$$

The ratio of the *y*-intercept to the slope yields the Stern-Volmer quenching constant, K_{SV}. From this constant one may determine k_q', if the excited state lifetime of the light absorbing species is known.

$$(y\text{-intercept/slope}) = [k_q'/k_t] = \tau\, k_q' = K_{SV}$$

Cyclic Voltammetry.

A useful characterization method for the complexes in this research is cyclic voltammetry. This technique will lend insight into the redox properties of the PMD and its subunits. Figure 4 shows a representative cyclic voltammogram. A cyclic voltammogram is obtained by scanning potential and monitoring current response. From the voltammogram, one may obtain the anodic and cathodic peak currents (i_p^a and i_p^c, respectively) and the anodic and cathodic peak potentials (E_p^a and E_p^c, respectively). The separation of the anodic and cathodic peak potentials, ΔE_p, will give a rough estimation of

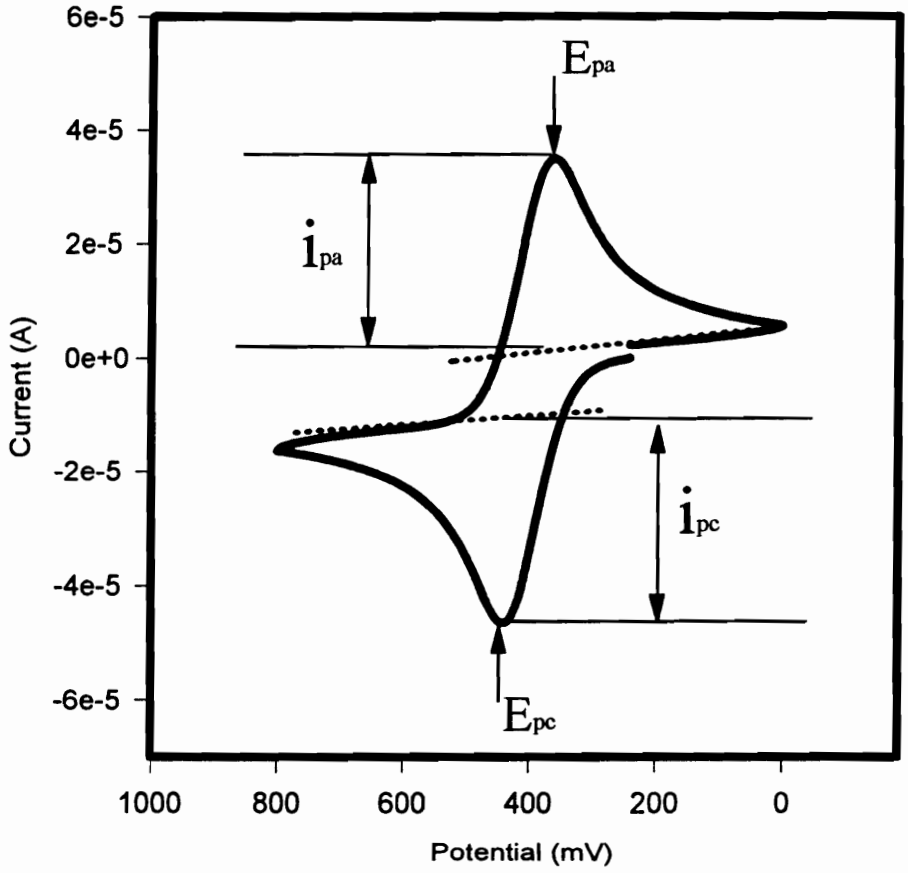

Figure 4. *Cyclic Voltammogam of Ferrocene.* This voltammogram was taken at room temperature in HPLC grade acetonitrile with 0.1 M tetrabutylammonium hexafluorophosphate for the supporting electrolyte (scan rate = 200 mV/s.) The working, auxiliary, and reference electrodes were platinum disk, platinum wire, and Ag/AgCl (0.26 vs. NHE).

the number of electrons transferred in that process. For a reversible couple, $\Delta E_p(V) = 0.059/n$ (where n is the number of electrons transferred). The formal potential of the couple, $E_{1/2}$, is the value usually reported in tables of cyclic voltammetric data, and is equal to the average of the anodic and cathodic peak potentials ($E_{1/2} = [E_p^a + E_p^c]/2$).[8,9]

The Photochemical Molecular Device's Subunits.

The goal of this research is to construct a photochemical molecular device for photoinitiated electron collection. Creation of the PIEC will involve the utilization of ruthenium based MLCT chromophores as the LA, and both iridium and rhodium based ECs. PIEC involves the separation of charge. The task of photoinitiated charge separation has been achieved by many researchers. A device that performs photoinitiated charge separation is referred to as a molecular photovoltaic.[1] It contains an electron donor (ED), an electron acceptor (EA), and a light absorber (LA). Researchers have employed many different types of components to achieve photoinitiated charge separation (PICS).[10-26]

The construction of photovoltaic devices has taken on a 'natural' and an 'abiotic' design. Researchers have employed components such as porphyrins and peptides, as well as non-biologically oriented units. The literature holds a vast number of photovoltaic devices, therefore ,only few will be highlighted here. Moore et al. have created pentads[10, 11] and tetrads[12] which contain carotenoid, porphyrin and quinone units. A pentad device can successfully undergo charge separation with a quantum yield (Φ_{CS}) of 0.83 and a charge separated lifetime (τ_{CS}) of 55 μs, in dichloromethane.[10] In the case of

the free-base tetrad, a quantum yield of 0.87 and a charge separated lifetime of 7.4 μs in dichloromethane was observed. The use of this carotenoid and porphyrin unit assembly has also been examined by Nishimura.[13] Another example of the use of porphyrin type complexes is in Jean-Pierre Sauvage's research. One zinc and one gold containing porphyrin unit surround a Cu^{I} centered rotaxane (τ_{CS} = 20 ps). In this case, charge separation between a zinc and gold center has been mediated through the Cu^{I} center.[14]

Abiotic components of photovoltaic devices have been explored with a variety of metal centers, electron donors and electron acceptors. T. J. Meyer et al. have undertaken the exploration of Re^{I} and Ru^{II} monometallic,[15] as well as bimetallic,[16] photovoltaic devices. A bimetallic rhenium tricarbonyl complex containing the coordinated electron donor pyridyl phenothiazine,[16,17] has been shown to successfully undergo photoinduced charge separation.

Variations of ruthenium 2,2'-bipyridine (bpy) complexes function as photovoltaics with bipyridine acting as the electron acceptor and pyridyl-phenothiazine[15], or functionalized bipyridines[18], as the electron donor. Functionalization of bipyridine can create an electron acceptor or an electron donor[18-24] to successfully accomplish photoinitated charge separation. Schanze and co-workers have investigated photovoltaic Re^{I} tricarbonyl monometallic systems containing donor ligands which contain α-amino and alcohol funtionalities and their affect on the lifetime of charge separation (achieving Φ_{CS} = < 0.001, τ_{CS} = 15 ns).[25] C. M. Elliott has explored ruthenium based chromophores $(bpy)_2Ru^{II}$ attached to a functionalized bipyridine moiety to accomplish PICS.[23] This

functionalized bipyridine has a variety of spacer units between the main bipyridine unit and the electron acceptor (these complexes yielded a varying τ_{CS} of 28-147ns in acetonitrile).[23] The functionalization of bipyridine has created bridging bimetallic species. Scandola et al. has created a Ru^{II} /Rh^{III} bimetallic photovoltaic device in which the metal centers are bridged through two covalently attached bipyridine units (in the case of Rh^{III} MLCT excitation the τ_{CS} is 5 ns, and for Ru^{II} MLCT excitation the τ_{CS} is 35 ps).[20] Meyer's complex $Ru(bpy)_2(LL')$ contains a functionalized bipyridine (LL'). In one case LL' has incorporated a lysine chain that separates an electron donor and a quinone electron acceptor (in acetonitrile $\Phi_{CS} = 0.26$ and $\tau_{CS} = 174$ns).[26]

$Ru(bpy)_3^{2+}$ and its $Ru(bpy)_2(BL)^{2+}$ Analogs.

Burstall[27] synthesized $[Ru(bpy)_3]^{2+}$ in 1936. To many photochemists and inorganic chemists he had synthesized an extremely fascinating and useful complex. Not only did it possess a long-lived metal-to-ligand charge transfer excited state at room temperature (τ = 0.62 μs, in aqueous solvents[28]), it could also undergo excited state electron and energy transfer.[28, 29] Given these photophysical attributes, $[Ru(bpy)_3]^{2+}$ could be utilized in solar energy conversion schemes. Analogs of this complex have varied from bipyridine functionalization to varying combinations of the ligand types bound to the metal center, i.e. $Ru^{II}(LL)_x(LL')_{3-x}$.[28] The utilization of these analogs has branched out into many areas of chemistry involving energy/electron transfer. One notable area is in the development of supramolecular systems to be used as photochemical molecular devices.[28,30-33]

A vast number of ligand types have be used to create $[Ru(bpy)_3]^{2+}$ analogs which can be covalently coupled to other metals through the use of bridging ligands. A subdivision of such ligands are α-diimine bidentate, dinucleating ligands, which were highlighted in a review article by Peter J. Steel.[35] Figure 5, shows a number of such ligands, as well as those utilized in this research.[35] One specific mixed-ligand analog is shown in Figure 6.[36-38] The substitution of one bipyridine for a bridging ligand (such as dpq (2,3-bis(2-pyridyl)pyrazine)) not only allows for two metal centers to be bridged, but also provides a venue for covalent attachment of the LA to another subunit. There are two important aspects of the $[Ru(bpy)_2(dpp)]^{2+}$ complex that should be noted: (1) Regardless of excitation energy, the complex always decays to its lowest lying excited state with $\Phi = 1$ and (2) the lowest lying excited state is $Ru(d\pi) \rightarrow dpp(\pi^*)$ charge transfer. Therefore, regardless of excitation energy, the electron is transferred from the ruthenium metal center to the dpp ligand. This promotes directed electron flow toward the site at which an additional metal center can be bound.

Electrochemistry can lend insight into the nature of the highest-occupied molecular orbital (HOMO) and the lowest-unoccupied molecular orbital (LUMO) associated for these complexes. In the electrochemical window of −2.0 V to +2.0 V (vs Ag/AgCl), $[Ru(bpy)_3]^{2+}$ [36], $[Ru(bpy)_2(dpp)]^{2+}$ [36-38], and $[Ru(bpy)_2(dpq)]^{2+}$ [39-42] exhibit one oxidation and three reductions (Table 1). The reversible one electron oxidation, for all three

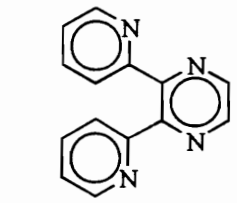

2,3-Bis(2-pyridyl)pyrazine

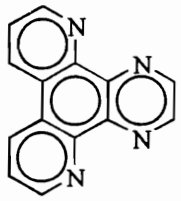

1,4,5,12-tetraaazatriphenylene

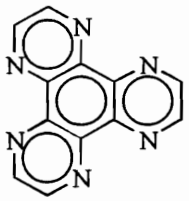

1,4,5,8,9,12-hexaazatriphenylene

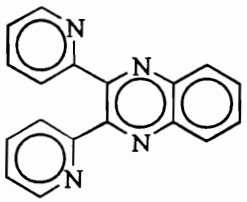

2,3-Bis(2-pyridyl)quinoxaline

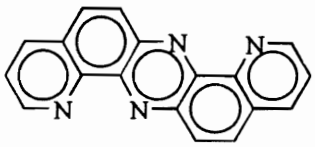

1,2:5,6-di-2-pyridino-9,10-diazaanthracene

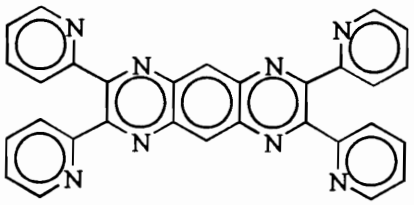

2,3,7,8-tetra-2-pyridyl-pyrazino[2,3-*g*]quinoxaline

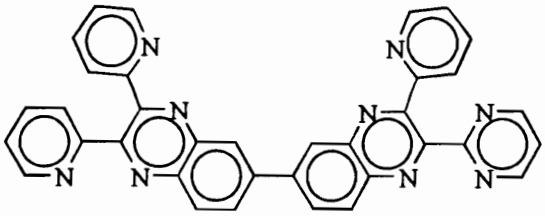

2,2',3,3'-tetra-2-pyridyl-6,6'-biquinoxaline

Figure 5. *Examples of Polypyridyl Bidentate Bridging Ligands. (Continued on next page.)*

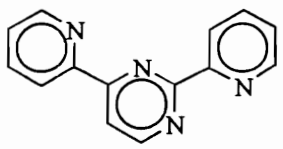

2,4-Bis(2-pyridyl)pyrimidine

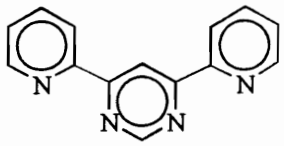

4,6-Bis(2-pyridyl)pyrimidine

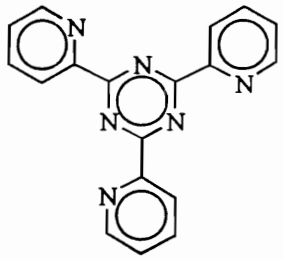

2,4,6-tri-(2-pyridyl)-1,3,5-triazine

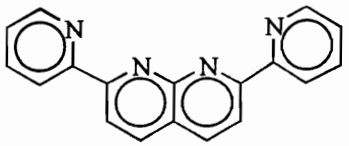

2,7-Bis(2-pyridyl)-1,8-naphthyridine

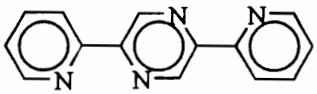

2,5-Bis(2-pyridyl)pyrazine

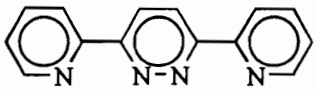

3,6-Bis(2-pyridyl)pyridazine

2,5-Bis(2-pyridyl)tetrazine

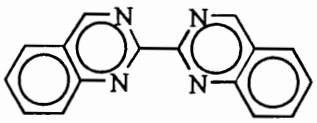

2,2'-biquinazoline

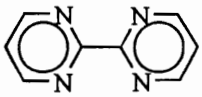

2,2'-bipyrimidine

Figure 5*(continued)*. *Examples of Polypyridyl Bidentate Bridging Ligands. (Continued on next page.)*

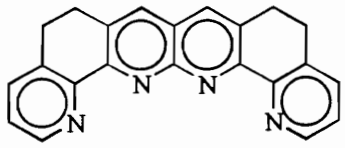

5,6,9,10-tetrahydro-15,16-diazadipyrido[2,3-a:3',2'-n]tetracene

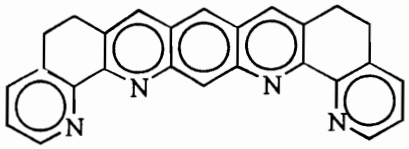

5,6,10,11-tetrahydro-16,18-diazadipyrido[2,3-a:3',2'-n]pentacene

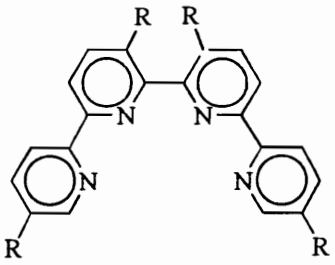

R = H, CH_3

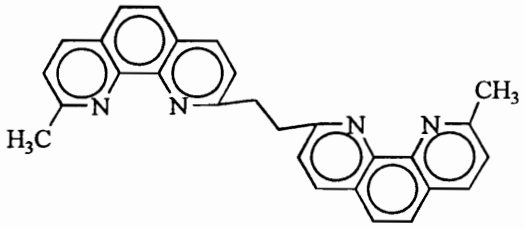

bis(9-methyl-1,10-phenathroline)ethylene

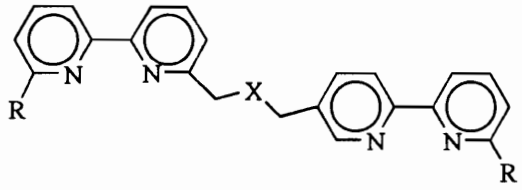

X= $C(CO_2Et)_2$, R = H;
X=$C(CO_2Et)_2$, R = CH_3;
X = O, R = CH_3

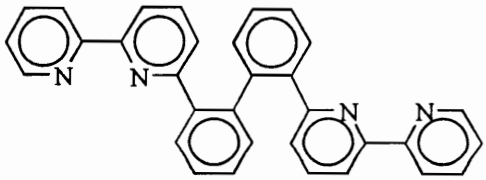

2,2'-bis(2,2'-bipyrido)biphenyl

Figure 5*(continued).* *Examples of Polypyridyl Bidentate Bridging Ligands.*

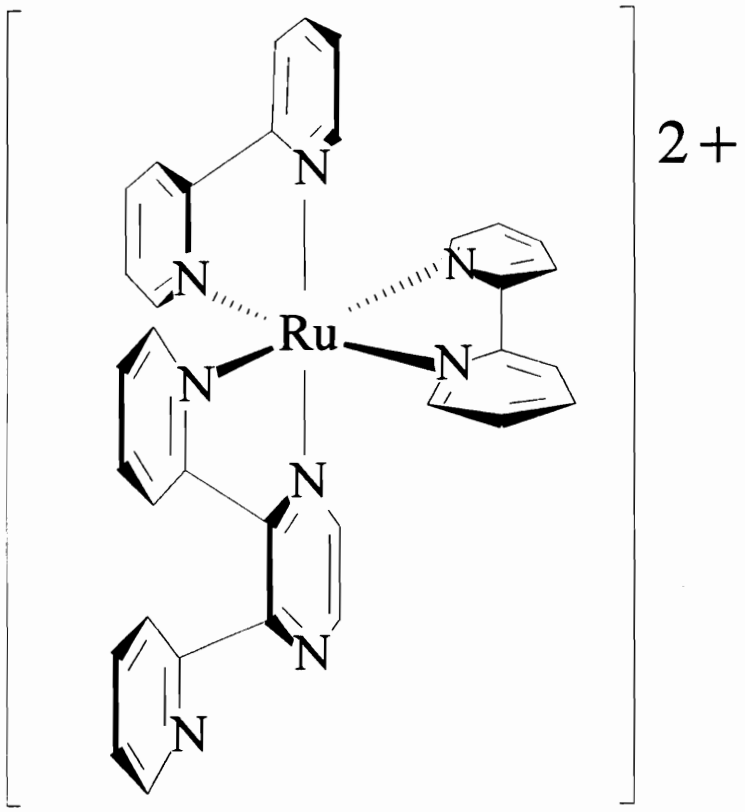

Figure 6. *The $Ru(bpy)_3^{2+}$ Analog $[Ru(bpy)_2(dpp)]^{2+}$, (dpp = 2,3-bis(2-pyridyl)pyrazine).*

Table 1. Cyclic Voltammetric Data[a] for a Series of Ruthenium Monometallic Bipyridyl Complexes. (bpy = 2,2'-bipyridine, dpp = 2,3-bis(2-pyridyl)pyrazine, and dpq = 2,3-bis(2-pyridyl)quinoxaline)

COMPLEX	Oxidation		Reductions	
	$E_{1/2}$(V)	Assignment	$E_{1/2}$(V)	Assignment
$[(bpy)_3Ru]^{2+}$ [c]	+1.27	Ru^{II}/Ru^{III}	-1.31	bpy,bpy,bpy / bpy,bpy,bpy^-
			-1.50	bpy,bpy,bpy^-/ bpy,bpy^-,bpy^-
			-1.77	bpy,bpy^-,bpy^-/ bpy^-,bpy^-,bpy^-
$[(bpy)_2Ru(dpp)]^{2+}$ [c]	+1.34	Ru^{II}/Ru^{III}	-1.14	dpp / dpp^-
			-1.53	bpy, bpy / bpy^-, bpy
			-1.74	bpy^-, bpy / bpy^-, bpy^-
$[(bpy)_2Ru(dpq)]^{2+}$ [b]	+1.39	Ru^{II}/Ru^{III}	-0.78	dpq / dpq^-
			-1.45	bpy, bpy / bpy^-, bpy
			d	

[a] All data present was taken in room temperature acetonitrile, 0.1 M Bu_4NPF_6 solution, and potentials reported are vs. SSCE.
[b] Ref. 39.
[c] Ref. 36.
[d] Determination of $E_{1/2}$ potential obscured by an adsorption wave.[39]

complexes, corresponds to a ruthenium based oxidation, Ru^{II}/Ru^{III}.[36-42] All three reductions in $[Ru(bpy)_3]^{2+}$ are bipyridine based.[33] The first reduction couple for $[Ru(bpy)_2(dpp)]^{2+}$ [36-38] and $[Ru(bpy)_2(dpq)]^{2+}$ [39-42] corresponds to a reversible one electron bridging ligand reduction. The following two reduction couples in the $[Ru(bpy)_2(dpp)]^{2+}$ and $[Ru(bpy)_2(dpq)]^{2+}$ complexes are bipyridine reductions. From this data one can assert that in $[Ru(bpy)_3]^{2+}$ the HOMO is a ruthenium based $d\pi$ orbital, and the LUMO a π^* based orbital on the bipyridine.[33] The $[Ru(bpy)_2(dpp)]^{2+}$ and $[Ru(bpy)_2(dpq)]^{2+}$ complexes have a ruthenium based HOMO and a bridging ligand based π^* LUMO.[36-42]

Given the nature of the HOMO and LUMO in this series of ruthenium complexes, it is interesting to consider their oxidation and reduction trends. The ruthenium oxidation potential increases when a bipyridine is exchanged for a bridging ligand, and when the bridging ligand is changed from dpp to dpq. This potential shift is due to the increasing π-accepting ability of the bridging ligand stablizing the ruthenium $d\pi$ orbital.[43]

The first reduction shifts to a more positive potential upon going from $[Ru(bpy)_3]^{2+}$ to $[Ru(bpy)_2(dpp)]^{2+}$ to $[Ru(bpy)_2(dpq)]^{2+}$. This increased stabilization of the LUMO is attributed to the increasing stabilization of the BL π^* orbital energy in dpq vs. dpp vs. bpy.[33, 36-42] The shift in the first ligand reduction potential is much more pronounced than the shift in the Ru^{II}/Ru^{III} couple.

The variation in the energy of the HOMO and LUMO of these complexes is also reflected in the electronic absorption spectroscopy. The electrochemical data has shown that the HOMO-LUMO gap decreases in the series from $[Ru(bpy)_3]^{2+}$ to

$[Ru(bpy)_2(dpp)]^{2+}$ to $[Ru(bpy)_2(dpq)]^{2+}$. The lowest lying MLCT transitions of these complexes are Ru(dπ) → bpy(π*) CT, for $[Ru(bpy)_3]^{2+}$ [33], and Ru(dπ) → BL(π*) CT based for $[Ru(bpy)_2(dpp)]^{2+}$ [36-38] and $[Ru(bpy)_2(dpq)]^{2+}$ [39-42]. Therefore, when transversing the series from $[Ru(bpy)_3]^{2+}$ to $[Ru(bpy)_2(dpp)]^{2+}$ to $[Ru(bpy)_2(dpq)]^{2+}$, the lowest energy absorption maxima should red shift due to the corresponding decrease in the HOMO-LUMO energy gap as shown in Table 2.

To achieve the collection of electrons, and subsequent delivery of the electrons to a substrate, $[Ir^{III}(BL)_2Cl_2]^{1+}$ [44] and $[Rh^{III}(BL)_2Cl_2]^{1+}$ [44] monometallic subunits will be utilized. These subunits have been studied free of the supramolecular structure by Brewer and co-workers.[44] In studying the supramolecular arrays created from these electron collectors one must understand the properties of the $[Ir^{III}(BL)_2Cl_2]^{1+}$, and $[Rh^{III}(BL)_2Cl_2]^{1+}$ complexes (BL = dpp, dpq, and dpb).

Iridium Monometallic Complexes Containing Polypyridyl Bridging Ligands.

Electrochemistry. The cyclic voltammetric data for the $[Ir(BL)_2Cl_2]^{1+}$ [+] (BL = dpp, dpq, and dpb) monometallic complexes, originally synthesized by the Brewer group[44], are presented in Table 3. This table contains data for the bipyridine analog for comparison purposes.[45] As expected, there are no oxidations present in the –2.0 to +2.0 V vs. Ag/AgCl window, but three reductions are observed, the third reduction being irreversible. This behavior is quite similar to the earlier studied $[Ir(bpy)_2Cl_2]^{+}$ complex.[45] The first two reductions observed for the $[Ir(BL)_2Cl_2]^{1+}$ complex are bridging ligand based. The two equivalent BLs are electronic coupled through the iridium metal center and therefore

Table 2. Electronic Absorption Spectral Data for a Series of Ruthenium Monometallic Bipyridyl Complexes.[a] (bpy = 2,2'-bipyridine, dpp = 2,3-bis(2-pyridyl)pyrazine, and dpq = 2,3- bis(2-pyridyl)quinoxaline.)

COMPLEX	λ_{max}^{abs}(nm)	$10^{-3}\ \varepsilon$ $M^{-1}cm^{-1}$	λ_{max}^{em}(nm)	τ(ns)
$[Ru(bpy)_3]^{2+}$ [b]	452	14	600	620
$[(bpy)_2Ru(dpp)]^{2+}$ [c]	464	12	658	276
$[(bpy)_2Ru(dpq)]^{2+}$ [d]	517	8	760	71

[a] Measurements taken in deoxygenated acetonitrile at room temperature.
[b] Ref. 28.
[c] Ref. 37.
[d] Ref. 39.

Table 3. Cyclic Voltammetric Data[a] for a Series of Iridium Monometallic Complexes Containing Polypyridyl Bridging Ligands. (bpy = 2,2'-bipyridine, dpp = 2,3-bis(2-pyridyl) pyrazine, dpq = 2,3- bis(2-pyridyl)quinoxaline, and dpb = 2,3-bis(2-pyridyl) benzoquinoxaline.)

COMPLEX	Reductions	
	$E_{1/2}$ (V)	Assignment
$[Ir(bpy)_2Cl_2]^{1+}$ [b]	-1.18	bpy, bpy / bpy, bpy$^-$
	-1.39	bpy, bpy$^-$ / bpy$^-$, bpy$^-$
	-2.12 [d]	Ir^{III} / Ir^{I}
$[Ir(dpp)_2Cl_2]^{1+}$ [c]	-0.83	dpp, dpp / dpp, dpp$^-$
	-1.06	dpp, dpp$^-$ / dpp$^-$, dpp$^-$
	-1.75 [d]	Ir^{III} / Ir^{I}
$[Ir(dpq)_2Cl_2]^{1+}$ [c]	-0.47	dpq, dpq / dpq, dpq$^-$
	-0.66	dpq, dpq$^-$ / dpq$^-$, dpq$^-$
	-1.50 [d]	Ir^{III} / Ir^{I}
$[Ir(dpb)_2Cl_2]^{1+}$ [c]	-0.33	dpb, dpb / dpb, dpb$^-$
	-0.55	dpb, dpb$^-$ / dpb$^-$, dpb$^-$
	-1.34[d]	Ir^{III} / Ir^{I}

[a] All cyclic voltammograms were recorded at room temperature in spectral grade acetonitrile with 0.1 M Bu_4NPF_6 as the supporting electrolyte. The electrodes employed were a platinum working electrode, a platinum wire auxiliary electrode, and a Ag/AgCl reference electrode (0.286 vs NHE).
[b] Ref. 45.
[c] Ref. 44.

reduce at different potentials. The third reduction is a two-electron irreversible reduction of the iridium metal center. The cyclic votammetric data exhibits two trends. One trend involves the BL reductions and another involves the metal center reduction. The bridging ligand reductions shift to a more positive potential through the series bpy, dpp, dpq, dpb. This trend is observed in the free ligands as well.[36, 39, 46] This shift can be attributed to decreasing energy of the bridging ligand π^* orbital through this series.

The iridium metal center in $[Ir(BL)_2Cl_2]^+$ undergoes an irreversible two electron reduction which corresponds to the Ir^{III}/Ir^{I} reduction couple.[44] This reduction is irreversible due to a change in the metal's coordination environment. In the reduction from a 3+ to a 1+ state, the metal center converts from a d^6 to a d^8 configuration. Now that the metal has a d^8 configuration, it no longer favors an octahedral environment, but prefers a square planar one. To accommodate this preference, the chlorides bound to the metal irreversibly dissociate. Hence, once reduced, the iridium center cannot be reoxidized, at this potential, to its original state, resulting in the observation of an irreversible two electron reduction.[44]

In examining the values for the iridium's irrreversible reduction, the potentials shift to a more postive potential through the series (bpy, dpp, dpq, dpb). As the ligands π-accepting ability increases, more electron density is donated by the metal center. This in turn decreases the electron density on the iridium and creates a more easily reduced metal center.

Electronic Absorption Spectroscopy. The electronic absorption spectroscopy data for the Ir^{III} monometallic complexes is presented in Table 4.[44, 45] The lowest lying

Table 4. Electronic Absorption Spectral Data for a Series of Iridium Monometallic Dichloro Complexes Containing Polypyridyl Bridging Ligands. (bpy = 2,2'-bipyridine, dpp = 2,3-bis(2-pyridyl)pyrazine, dpq = 2,3-bis(2-pyridyl)quinoxaline, and dpb = 2,3-bis(2-pyridyl)benzoquinoxaline.)

COMPLEX	λ_{max} (nm)[c]	10^{-3} ε
	Absorption[d]	$M^{-1}cm^{-1}$
$[Ir(bpy)_2Cl_2]^{1+}$ [c]	430	1.1
$[Ir(dpp)_2Cl_2]^{1+}$ [d]	480	< 0.20
$[Ir(dpq)_2Cl_2]^{1+}$ [d]	514	1.2
$[Ir(dpb)_2Cl_2]^{1+}$ [d]	528	2.0

[a] All spectra were recorded in room temperature spectral grade acetonitrile.
[b] The lowest energy absorption maxima for the complex.
[c] Ref. 45.
[d] Ref. 44.

absorption maxima for the $[Ir(BL)_2Cl_2]^+$ systems is a $Ir(d\pi) \rightarrow BL(\pi^*)$ charge transfer transition. In the monometallic complexes, the λ_{max}^{abs} shifts to lower energy (red shift) as bipyridine is substituted by dpp, dpq, and dpb, consistent with the observed stabilization of the π^* orbital through this series.

Rhodium Monometallic Complexes Containing Polypyridyl Bridging Ligands.

Rhodium analogs of the $[Ir^{III}(BL)_2Cl_2]^{1+}$ monometallic complexes have also been studied by the Brewer group.[44] Modification of the $[Ir^{III}(BL)_2Cl_2]^{1+}$ by changing the metal center is significant in that the LUMO of the complex is no longer BL based, but metal centered. This type of behavior has been observed in the bpy complexes, $[M(bpy)_2Cl_2]^+$ (M = Rh^{III} [47] or Ir^{III} [45]).

Electrochemistry. The electrochemical data for the series of complexes, $[Rh(BL)_2Cl_2]^{1+}$ (BL = dpp, dpq, and dpb) and bpy analog is given in Table 5.[44, 47] From the comparison of this data with that of the iridium systems, one can see that the rhodium metal center is easier to reduce. This is also seen in the iridium and rhodium bpy analogs.[47] As the bridging ligand π-accepting ability increases through the series (dpp < dpq < dpb), the reduction potential of the Rh metal center increases. The reduction potential of the ligands increases through the series (dpp < dpq < dpb). This is due to the lower π^* orbital energy of the dpb vs. dpq vs. dpp ligand.

From the electrochemistry, it can be seen that the Rh^{III} ($d\sigma^*$) based orbitals lie below the $BL(\pi^*)$ based orbitals. The ordering of the metal centered and BL based reduction is reversed in comparison to the Ir^{III} systems. This will be important in the

Table 5. Cyclic Voltammetric Data[a] for a Series of Rhodium Monometallic Dichloro Complexes Containing Polypyridyl Bridging Ligands. (bpy = 2,2'-bipyridine, dpp = 2,3-bis(2-pyridyl)pyrazine, dpq = 2,3- bis(2-pyridyl)quinoxaline, and dpb = 2,3-bis(2-pyridyl) benzoquinoxaline.)

COMPLEX	Reductions	
	$E_{1/2}$ (V)	Assignment
$[Rh(bpy)_2Cl_2]^{1+}$ [b]	-1.30	Rh^{III} / Rh^{I}
	-1.50	bpy, bpy / bpy, bpy$^-$
$[Rh(dpp)_2Cl_2]^{1+}$ [c]	-1.05	Rh^{III} / Rh^{I}
	-1.19	dpp, dpp / dpp, dpp$^-$
$[Rh(dpq)_2Cl_2]^{1+}$ [c]	-0.85	Rh^{III} / Rh^{I}
	-1.49	dpq, dpq / dpq, dpq$^-$
$[Rh(dpb)_2Cl_2]^{1+}$ [c]	-0.72	Rh^{III} / Rh^{I}
	-1.24	dpb, dpb / dpb, dpb$^-$

[a] All cyclic voltammetric data was taken in room temperature spectral grade acetonitrile with 0.1 M Bu_4PF_6 as the supporting electrolyte. The electrodes employed were a platinum working electrode, a platinum wire auxiliary electrode, and a Ag/AgCl reference electrode (0.286 vs NHE).
[b] Ref. 47.
[c] Ref. 44.

construction of photochemical molecular devices. The HOMO of these $[Rh(BL)_2Cl_2]^{1+}$ complexes is Rh^{III} ($d\pi^*$) based and the LUMO is Rh^{III} ($d\sigma^*$) based. Given the nature of the HOMO and LUMO, the lowest lying excited state of these complexes is expected to be ligand-field (LF) in nature.[48]

Electronic Absorption Spectroscopy. The electronic absorption spectral data for a series of Rh^{III} monometallic complexes is shown in Table 6.[44, 49] The lowest lying absorption observed in the 190 - 820 nm electronic absorption spectroscopy window, in acetonitrile, is $Rh^{III}(d\pi^*) \rightarrow BL(\pi^*)$ CT based. This transition decreases in energy when the bridging ligand is changed from dpp to dpq to dpb.[44] A lowest lying LF state is expected for these $[Rh(BL)_2Cl_2]^{1+}$ complexes. Although this is not observed in the electronic absorption spectra due to a low extinction coefficient, it is observed in their emission spectra. The emission maxima, taken in the solid state at 77 K, for the $[Rh(bpy)_2Cl_2]^{1+}$, $[Rh(dpp)_2Cl_2]^{1+}$, and $[Rh(dpq)_2Cl_2]^{1+}$ complexes, are 660, 707 , and 737 nm, respectively.[44, 49]

These monometallic building blocks have the appropriate properties to function as the components of a PMD for PIEC. The goal of this project is to use these building blocks to construct a PMD for PIEC, study the properties of these new supramolecules and investigate their functioning as a PMD for PIEC.

Table 6. Electronic Absorption Spectral Data for a Series of Rhodium Monometallic Complexes Containing Polypyridyl Bridging Ligands. (bpy = bipyridine, dpp = 2,3-bis(2-pyridyl)pyrazine, dpq = 2,3-bis(2-pyridyl)quinoxaline, and dpb = 2,3-bis(2-pyridyl) benzoquinoxaline.)

COMPLEX	λ_{max} (nm)[a]	10^{-3} ε
	Absorption[b]	$M^{-1}cm^{-1}$
$[Rh(bpy)_2Cl_2]^{1+}$ [c]	311	27
$[Rh(dpp)_2Cl_2]^{1+}$ [d]	328	19
$[Rh(dpq)_2Cl_2]^{1+}$ [d]	376	11
$[Rh(dpb)_2Cl_2]^{1+}$ [d]	408	15

[a]All spectra were recorded in room temperature spectral grade acetonitrile.
[b]The lowest energy absorption maxima for the complex.
[c] Ref. 49.
[d] Ref. 44.

CHAPTER 2.

EXPERIMENTAL METHODS.

Materials.

All materials were reagent grade and used as received and were purchased from Fisher Scientific or Aldrich unless otherwise noted. The size exclusion gel, Sephadex LH-20, was purchased from Sigma Chemical Company. Burdick and Jackson spectral grade acetonitrile (Baxter Scientific) was used in electronic absorption spectroscopy, electrochemistry, spectroelectrochemistry, photolysis, emission and lifetime studies. Tetrabutylammonium hexafluorophosphate (Bu_4NPF_6) was the supporting electrolyte in all electrochemical experiments. This electrolyte was produced by metathesis of aqueous tetrabutylammonium bromide using aqueous potassium hexafluorophosphate. The resulting salt was purified by several recrystallizations from 100% ethanol, dried in a vacuum oven for 4 hours, tested for purity by cyclic voltammetry, and stored in a vacuum desicator. Iridium trichloride hydrate, ruthenium trichloride hydrate, and rhodium trichloride hydrate were purchased from Johnson Matthey, or acquired via Johnson Matthey's precious metal loan program. The $\{[(bpy)_2Ru(dpb)]_2IrCl_2\}(PF_6)$ was synthesized by Girlie Nallas.[50] Elemental Analysis was conducted by Galbraith Laboratories.

Size-Exclusion Chromatography.

Size-exclusion chromatography (SEC) is a technique in which sample components are separated based on their molecular size. Retention of the different components is related to the ability of the component to fit into the cavities of the porous stationary

phase. Molecules that are too large to enter the pore (fully or partially) elute rapidly from the column, while retention times of smaller components are proportional to their ability to fit inside the pore.[51-53]

Size exclusion chromatography utilizes three general types of stationary phases: (1) soft gels; (2) semi-rigid gels; and (3) highly rigid gels. Soft gels, the type utilized in this research, consist of polymeric materials that are able to expand or contract. An example of these polymeric types is cross-linked cellulose based polymers (e.g., Sephadex) or polyacrylamides (e.g. Bio-Gel).[51] The molecular weight of each component should fall between the permeation limit (the largest molecular weight that will fit, to any degree, into the gel pore) and exclusion limit (the smallest molecular weight that will not fit into the gel pores) for proper separation of sample components. Sephadex LH-20, the soft gel used to purify the trimetallic complexes in this research, has a 5,000 molecular weight exclusion limit. This limit was determined based on the assumption that the molecules to be separated were spherical. Normally this assumption would not need further consideration since, generally, molecular size is proportional to molecular weight. Due to the non-spherical nature of the trimetallic systems, however, the elution time for these complexes are faster than expected for corresponding predicted molecular weights.[51-53]

Column preparation for gel filtration chromatography involves initial preparation of the gel. To ensure expansion of the beads to their maximum capacity, the Sephadex LH-20 gel was allowed to soak overnight in the mobile phase (2:1 (vol./vol.) ethanol/acetonitrile) prior to being poured into a glass column (48 cm × 2.2 cm I.D., with

a gel height of 32 cm). The sample, 5 mL of a highly concentrated solution of the crude complex, was loaded onto the column and chromatographed. Fractions of the eluent were collected manually and monitored via electronic absorption spectroscopy. The fractions that had identical spectra were combined.

High Performance Liquid Chromatography (HPLC).

A Rainin Rabbit HPLC connected to a Gilson fraction collector, automated via a Gilson fraction controller, was used to purify the trimetallic systems in this research. The stainless steel column (4 ft. long, 3/8" I. D.) was packed with Sephadex LH-20 using 2:1 (vol./vol.) ethanol/acetonitrile. There was a three minute delay time between the sample (1mL) injection/loading stage and the initiation of fraction collecion. Each fraction consisted of 20 drops of eluent. Electronic absorption spectroscopy was used to determine which fractions contained pure trimetallic complex. This was done by comparing their spectra to a spectrum of a known sample. The spectrum of the trimetallic should also resemble the spectra of the combination of monometallic fragments. Fractions containing pure trimetallic were combined and rotoevaporated to dryness. The trimetallic complex was dissolved in 5 mL of acetone and flash precipitated with 75 mL of diethyl ether. The resulting solid was isolated by vacuum filtration and its purity was determined by electronic absorption spectroscopy and cyclic voltammetry.

Electronic Absorption Spectroscopy.

The electronic absorption spectroscopy in this research was conducted on a Hewlett Packard 8452A diode array spectrophotometer (2 nm resolution, 190-820 nm range) interfaced to a Hewlett Packard Vectra computer. The UV-visible general

scanning and kinetics computer programs, contained in the Hewlett Packard Software package, were used for data collection. All spectra were recorded at room temperature in acetonitrile using 1 cm quartz cuvettes.

Electrochemistry.

Cyclic voltammetry. Cyclic voltammograms were obtained on a BioAnalytical Systems Inc. 100W electrochemical system with the use of a platinum working electrode (5.5 cm long, 6.5 mm OD, 1.6 mm platinum disk, with Kel-F™ plastic casing), a platinum wire auxiliary electrode (0.25 mm wire soldered to a gold-plated connector mounted in Kel-F™plastic), and a Ag/AgCl gel reference electrode (0.29 V vs. NHE). The reference electrodes were calibrated against ferrocene. This calibration was accomplished by taking a cyclic voltammogram of ferrocene in acetonitrile, using the reference electrode to be calibrated, and comparing the Fe^{2+}/Fe^{3+} to the standard NHE value. In room temperature acetonitrile, the value the Fe^{2+}/Fe^{3+} oxidation couple of ferrocene vs. NHE is 0.665 V.[8] Prior to analysis of a sample a background scan was recorded of the solvent and electrolyte system, 0.1 M Bu_4NPF_6 in acetonitrile. This background scan ensured the working capability of the system (i.e., to test for proper computer-instrument communication, instrumental sensitivity and scan rate, electrode placement/operation, electrolyte purity, solvent dryness, etc.)

Bulk electrolysis. Bulk electrolysis was carried out utilizing the BAS 100W system. The bulk electrolysis cell was a H-cell, as seen in Figure 7, with fine-fritted glass [e] separating the two compartments. The working compartment consisted of a 0.1 M Bu_4NPF_6 solution in CH_3CN, the desired analyte, a platinum wire cage working electrode

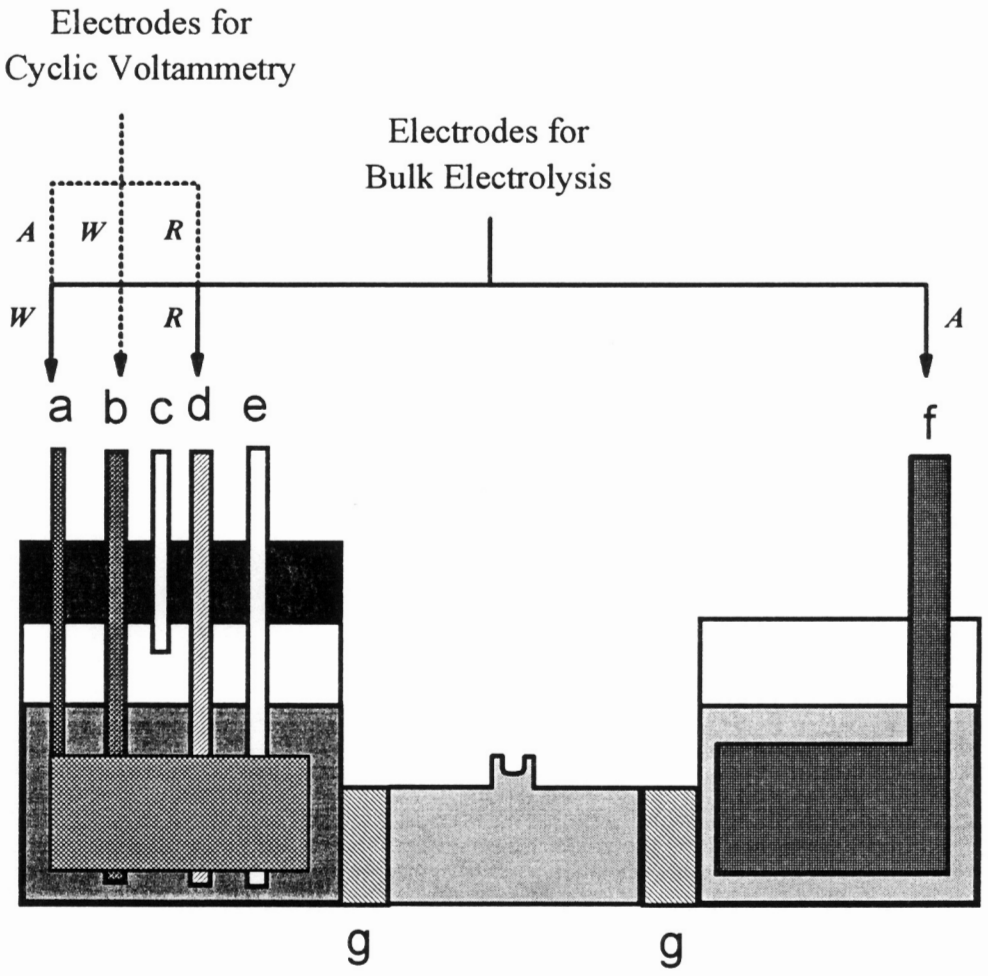

Figure 7. *Bulk Electrolysis Cell.* The electrodes for each experiment are denoted: *W* for the working electrode; *A* for the auxiliary electrode; and *R* for the reference electrode. The working compartment (left) contains the analyte, 0.1 M Bu_4NPF_6 in acetonitrile, and the following: (a) platinum cage working electrode; (b) platinum disk working electrode; (c) argon gas blanketing teflon tube; (d) Ag/AgCl reference electrode; (e) argon gas fritted glass bubbler. The auxiliary compartment (right) contains 0.1M Bu_4NPF_6 in acetonitrile and a carbon cloth auxiliary electrode (f). The compartments are connected by a glass bridge, but separated by fine porous fritted glass disks (g). All experimentation was conducted at room temperature.

[a], and a Ag/AgCl gel reference electrode [d]. The system used a fritted glass bubbler [e], and a small inlet tube to stir via bubbling and blanket the system with argon [c].) The auxiliary compartment contained a carbon cloth auxiliary electrode [f] and a 1.0 M Bu_4NPF_6 in CH_3CN solution. The bridge contained a solution of 0.1 M Bu_4NPF_6 in CH_3CN. All of the cell compartments contained varying volumes of the same 0.1 M Bu_4NPF_6 in CH_3CN stock solution. During the bulk electrolysis the number of coulombs passed into the system, the current ratio, and run time were monitored simultaneously.

Although the same cell was used to take the cyclic voltammogram during the bulk electrolysis experiment, different electrodes were utilized for each procedure. When bulk electrolysis was combined with cyclic voltammetry, the first step was to take a cyclic voltammogram using, in the left compartment, a platinum working electrode [b], a Ag/AgCl gel reference electrode [d], and the platinum wire cage [a] as the auxiliary electrode. The bulk electrolysis was then carried out using the electrodes described above. Once the sample had been electrolyzed to the desired potential another cyclic voltammogram was taken. This bulk electrolysis system allowed for the changing of the electrodes utilized for bulk electrolysis and cyclic voltammetry without exposing the sample to the atmosphere.

Spectroelectrochemistry. Electronic absorption spectroscopy and bulk electrolysis were combined to produce an analytical experiment known as spectroelectrochemistry. Although the combination of electrochemistry and other spectroscopic techniques may be placed under this general term,[54] herein, spectroelectrochemistry will refer specifically to the technique which uses electronic absorption spectroscopy.

The spectroelectrochemistry cell was a H–type configuration. Its working compartment was constructed by fusing a glass joint to a 1 cm quartz cell, Figure 8.[55] Glass tubing bridged the working compartment and the "test tube" auxiliary compartment. A fritted glass disk segregated the auxiliary compartment to insure analyte/auxiliary electrode separation. A small, flexible teflon tube was used to supply argon gas to the system. The introduction of argon to the system in this manner served two purposes. First, to agitate the analyte solution and ensure uniform electrolysis, and secondly, to deoxygenate the system prior to, and during, the experiment. The teflon tubing and the platinum wire cage electrode had to be raised above the spectrophotometers beam path, without disturbing the reservoir cap, prior to taking a spectrum. Once the spectrum was taken, both the working electrode and teflon tubing were restationed back to the center of the quartz cell portion of the working compartment for further bulk electrolysis. Acquiring data for the system, in this manner, throughout electrolysis was a delicate task. Electronic absorption spectra were monitored frequently as the electrolysis proceeded.

Infrared Spectroscopy.

Infrared spectra were taken with the use of a Perkin-Elmer 283B. The samples were prepared in KBr pellets and only one 12 minute scan was taken. Examples of infrared spectra for the bridging ligands and their starting materials are shown in Appendix I.

Nuclear Magnetic Resonance (NMR).

Spectra for the modified bridging ligand work, both ^{1}H and ^{13}C, (Chapter 3) were recorded on a 500 MHz Varian Unity at Washington State University, Pullman, WA by

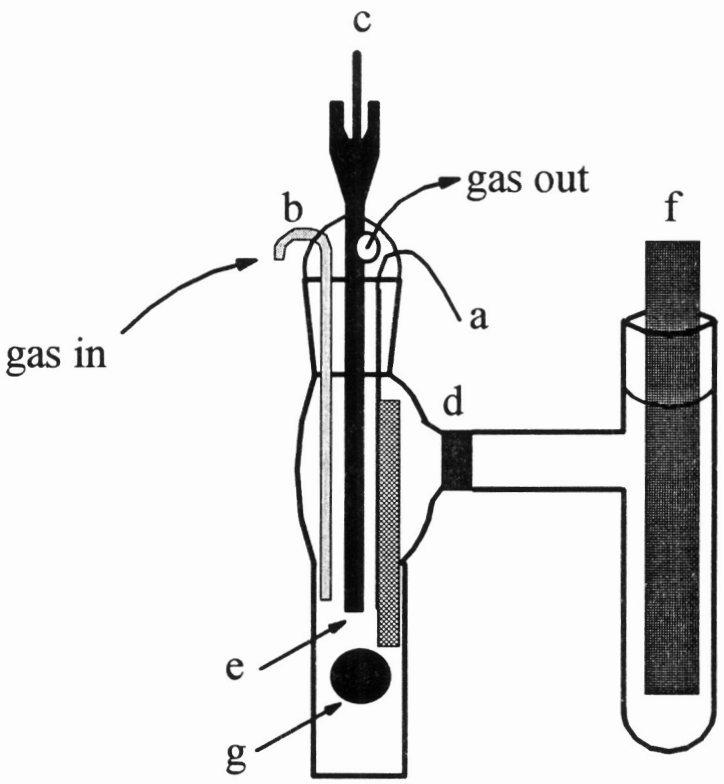

Figure 8. *Spectroelectrochemistry Cell.* The working compartment (left) contains 0.1M Bu_4NPF_6, the analyte and the following: [a] narrow platinum wire cage working electrode; [b] argon gas inlet tube; [c] Ag/AgCl reference electrode; and [e] vicor tipped glass tube. The reference electrode rests in a reservoir at the top of the glass tube that is filled with the 0.1M Bu_4NPF_6 in CH_3CN solution. Contact between the reference electrode and analyte is achieved through the vicor tip. The auxiliary compartment (right) contains 0.1 M Bu_4NPF_6 in CH_3CN with a carbon cloth auxiliary electrode [f]. Both compartments are segregated by a fine porous glass fritted disk [d]. The beam of the spectrometer passed through the main body of the quartz cuvette as denoted by the circle [g]. All experimentation was conducted at room temperature.

Dr. Steven Alam. All other ^{1}H and ^{13}C spectra were recorded on a 400 MHz Varian Unity, or on a Bruker WP 270, at Virginia Polytechnic Institute and State University, Blacksburg, VA.

Emission Spectroscopy.

Emission spectra were taken of room temperature acetonitrile solutions of a given analyte on a Photon Technology Inc. (PTI), MSIII spectrofluorometer. This spectrofluorometer was modified to detect low quantum yield, red-shifted emissions. The system consisted of a 150 W Xenon arc lamp excitation source, and a detection system with a thermoelectrically cooled, single photon counting Hammamatsu R666S red-sensitive photomultiplier tube (PMT), which was interfaced to an IBM compatible PC for data acquisition and handling. A diagram of a photomultiplier tube representative of the Hammamatsu R666S and R928, along with a spectral response for each PMT, are shown in Appendix II, courtesy of Hammamatsu Product Catalog and Technical Services.

Emission Lifetime.

Measurements of the emissions lifetimes (τ) were taken using a Photon Technology Inc. PL 2300 nitrogen laser pumping a Photon Technology PL 201 continuously tunable dye laser as a excitation source (360 - 900 nm) [a], Figure 9. This excitation source has an energy output of 240μJ per pulse at 5,000 Å (average energy) and a pulse width of 500 ps. Prior to striking the sample holder, the laser pulse passed through the triggering system, which contained a beam splitter and a Motorola MK520 photodiode. Detection of the luminescence was at a right angle to the excitation source.

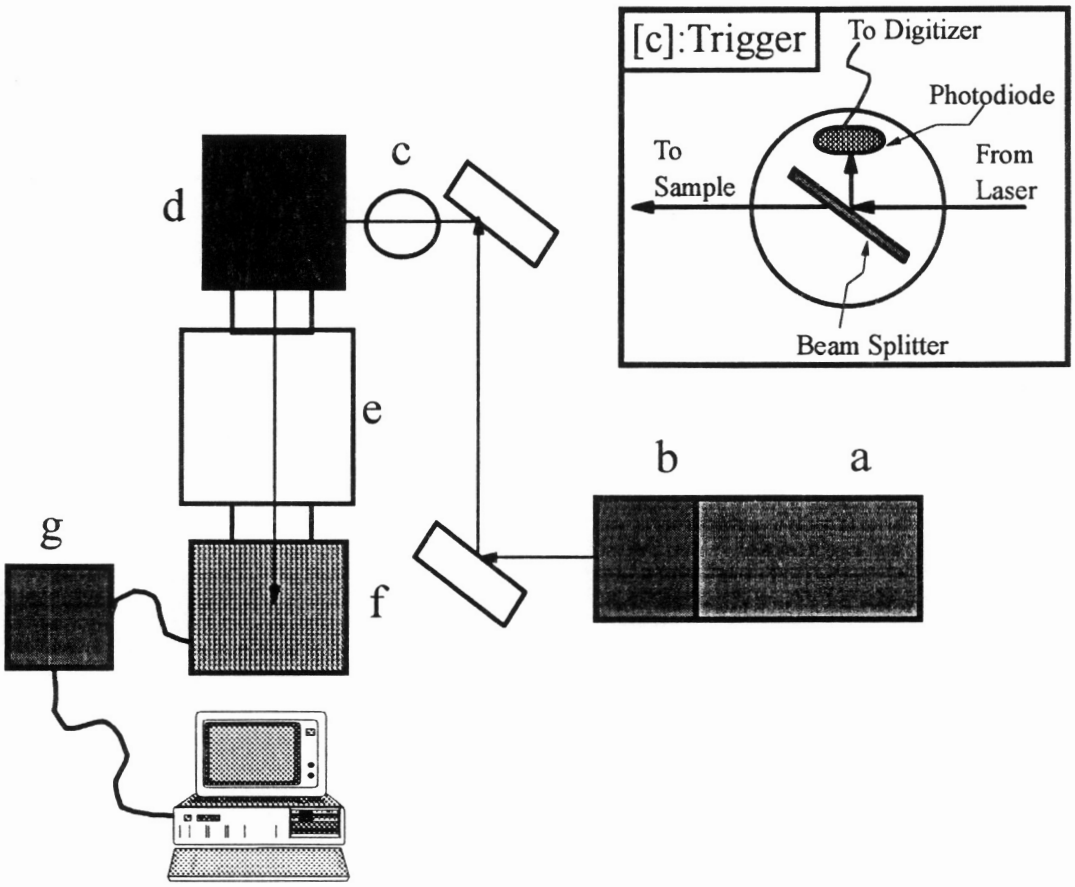

Figure 9. *Emission Lifetime System.* A tunable dye laser [a], which is pumped by a nitrogen laser [b] serves as the system's excitation source. A series of front-surfaced mirrors directs the beam to the triggering system [c], containing a Motorola MK520 photodiode. (An enlarged diagram of the triggering system is provided.) The excitation source impinges upon the sample in the cell holder [d]. The emission of the system is monitored at a right angle by passing through a PTI 01-001 monochromator and then being detected by a red-sensitive Hammamatsu R928 photomultiplier tube.

The luminescence passed through a PTI 01-001 monochromator [e], for wavelength selection. This monochromator has gratings of 1200 lines/mm. Detection of the emission was achieved with a Hammamatsu R928 red-sensitive photomultiplier tube [f]. The PTI monochromator was at a right angle to the excitation beam. Overexposure of the PMT was prevented by slits on the monochromator, which are adjustable from 0 - 6mm. These slit specifications allow for a bandpass of 4 nm/mm.(Courtesy of PTI Inc. Technical Services.) The signal was digitized and displayed on a LeCroy 9361 Dual 300 MHz oscilloscope (2.5 Gs/s). The acquired data was an average, typically of a 100 traces. Fitting the acquired data to a single exponential function ($y = a + b[\exp(-kt)]$, y = the PMT response; a, b ≡ scaling factors; t = time; and k = the rate constant) allowed for the numerical measurement of the rate constant associated with the decay of the emission intensity. The data that includes $\tau \leq$ the laser pulse and the data points at the extreme end of the data collection window were removed prior to analyses of the emission lifetime. Once the rate constant had been determined, the emission lifetime was calculated using the relationship ($\tau = 1/k$). An example of a typical trace is shown in Appendix III.

Photolysis.

The photolysis system, Figure 10, consisted of a 1000W Xenon arc lamp [a] powered by an Oriel 68820 Universal power supply (400-1000 Watts) [b]. [The output of the 1000W Xenon arc lamp, courtesy of Oriel Technical Services, is given in Appendix II.] This specific arc lamp was chosen because of its wavelength range output and irradiance capabilities. The broad band light passed through an infrared water filter [c], followed by

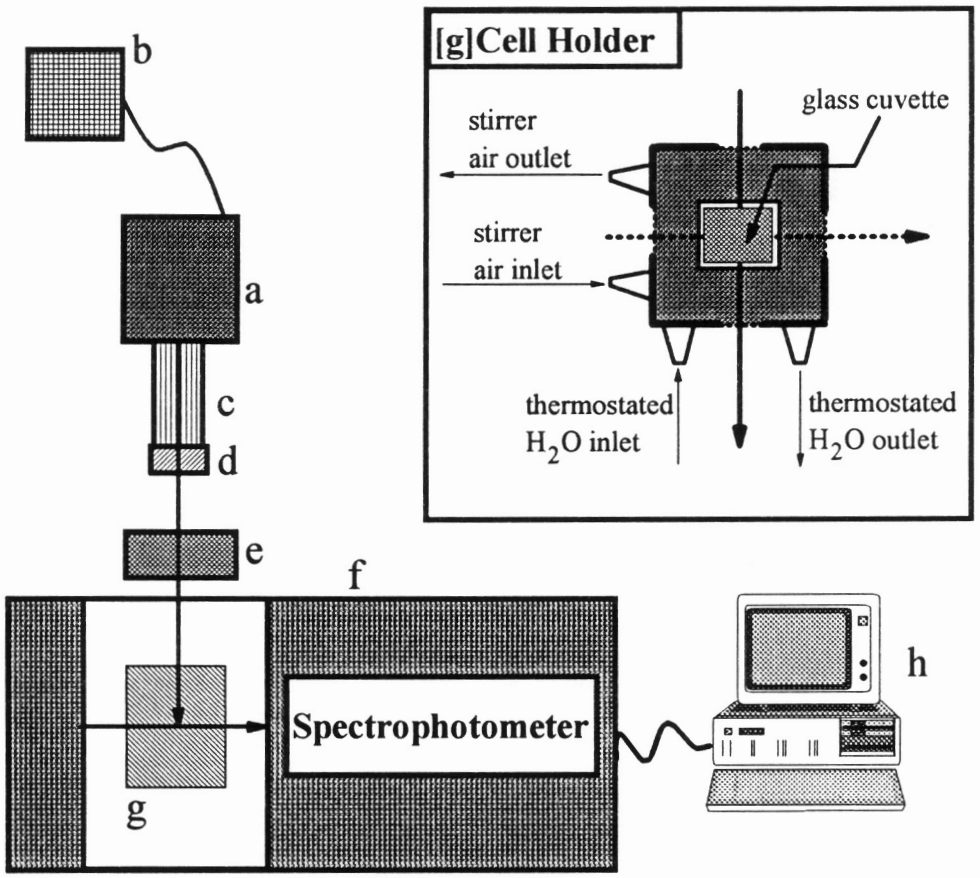

Figure 10. *Photolysis System.* A 1000 Watt xenon arc lamp[a], powered by an Oriel 68820 Universal power supply [b], whose light passed through an infrared water filter [c], an Oriel 10 nm narrow bandpass filter [d], a short-path focusing lens [e], before impinging upon the sample cell holder [g]. Electronic absorption spectra of the sample were taken with a Hewlett Packard 8452A diode array spectrophotometer.

an Oriel 10-nm narrow bandpass filter [d], and finally a short-path focusing lens [e]. (The filtering capabilities of the narrow bandpass filters utilized are given in Appendix IV in the form of a transmittance spectrum.) The filtered and focused light then impinged upon the sample cell in the cell holder [g] which was contained in a Hewlett Packard 8452A diode array spectrophotometer [f]. The thermostated cell holder was made of brass and contained a miniature air-driven magnetic stirring mechanism. During each experiment, the cell holder was thermostated to maintain a temperature of 25°C. Four openings in the walls of the cell holder allowed for both the excitation and monitoring of the sample's electronic absorption spectrum. The sample was deoxygenated via four freeze-pump-thawing cycles. A 1 mm magnetic stirring bar was introduced prior to deoxygenation. After deoxygenation, the cell was flame sealed. Once the light path of the photolysis system was checked for alignment, a blank scan of acetonitrile was taken. The analyte cell was loaded into the holder in the absence of light, and exposure began with the initiation of the spectrophotometer's kinetics program. This software is programmed to take scans at incremental time intervals and records a complete spectrum from 190 to 820 nm.

The Stern-Volmer kinetic studies of the $\{[(bpy)_2Ru(dpb)]_2IrCl_2\}(PF_6)_5$ trimetallic utilized a different photolysis system. The system described above was the improved photolysis system that integrated the spectrophotometer and light source. The system for the $\{[(bpy)_2Ru(dpb)]_2IrCl_2\}(PF_6)_5$ Stern-Volmer kinetics did not combine the light source and spectrophotometer, Figure 11. The photolysis system consisted of the same 1000 W Xenon Arc Lamp, infrared water filter, and narrow bandpass filter (10 nm), but had a different cell holder and compartment. A black box containing the sample cell holder was

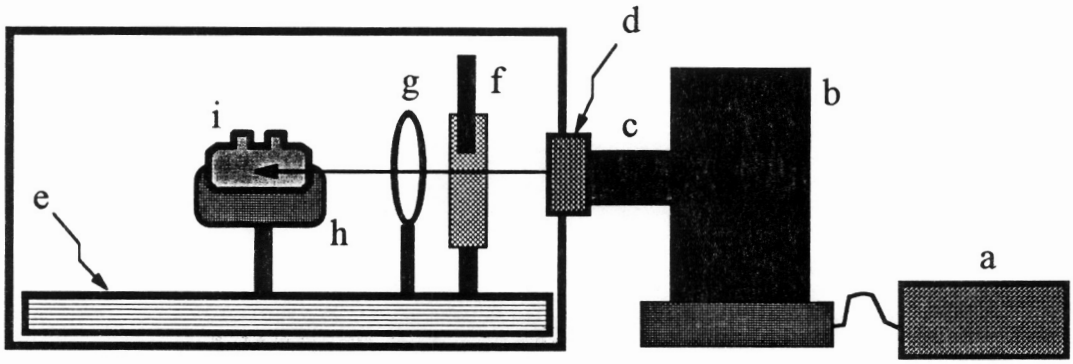

Figure 11. *Alternate Photolysis System Assembly*. A 1000 Watt xenon arc lamp[b], powered by an Oriel 68820 Universal power supply [a], whose light passed through an infrared water filter [c], an Oriel narrow bandpass filter (10 nm) [d], a shuttering mechanism [e], and a short-path focusing lens [f].

situated on an optical rail. Prior to striking the sample cell, the broad band light passed through a narrow bandpass filter (10 nm) and a focusing lens which were situated on the optical rail. The acetonitrile solution of analyte and electron donor was agitated by bubbling the system with acetonitrile saturated argon gas. The gas flowed via a hypodermic needle through the rubber septum. It should be noted that the septum also acted as a cap for the 1 cm cylindrical cell. Initially, the sample was deoxygenated by bubbling the solution for 30 minutes prior to photolysis. After exposure, the sample cell was transported to the spectrophotometer. Transportation of the sample was accomplished by placing the sample in a small light-tight black box which was in turn wrapped in black cloth.

Actinometry.

The determination of the xenon arc lamps quanta output was conducted with the use of Reinecke's salt,[56,57] $K[Cr(NH_3)_2(NCS)_4]$. A given amount of Reinecke's salt (0.199 g, 0.560 mmol) was dissolved in 250 mL of deionized water. A known aliquot of the Reinecke's salt solution was exposed to light for a given recorded time in a 5 cm cylindrical quartz cell. After the exposure had taken place, the contents of the cell were transferred to a 25 mL graduated cylinder in order to determine the volume of solution that was exposed (a typical cell volume was 13-14 mL). Following exposure, the irradiated sample and a dark control were developed. The developing solution was an aqueous solution of 0.5 M perchloric acid and 0.1 M $FeNO_3$ (aq). A 2 mL aliquot of the irradiated and dark control solution was diluted to 10 mL with developing solution. The

samples developed for 5 minutes. During photolysis the Reinecke's salt undergoes SCN^- loss in the following manner:[56, 57]

$$\textit{trans}\ [Cr(NH_3)_2(NCS)_4]^- \xrightarrow{h\nu} [Cr(NH_3)_2(NCS)_3(H_2O)] + SCN^-$$

Free SCN^-, produced from the irradiation, reacts with the Fe^{3+} in the developing solution and forms $Fe(SCN)^{2+}$. (The absorbance at 450 nm, due to the $Fe(SCN)^{2+}$, needs to undergo a change in absorbance of approximately 0.5 units.) The molar extinction coefficient of aqueous $Fe(SCN)^{2+}$ at 450 nm is $4.30 \times 10^3\ M^{-1}cm^{-1}$.[56, 57] Given the time, temperature, absorbance change, and the specific values for the filter used, the quanta per minute may be calculated for a given filter using the equation below:[56, 57]

$$I_0 = \frac{6.023 \times 10^{20}\, V_1 V_3\, \Delta A}{[\Phi\, t\, (1 - 10^{-\varepsilon_1 [A] l_1})\, V_2\, l_2 \varepsilon_2]}$$

where,

V_1 = Volume of actinometer solution irradiated (mL).

V_2 = Volume of irradiated solution used (mL).

V_3 = Final volume of V_2 after developing dilution (mL).

ΔA = Measured absorbance difference between the developed irradiated and nonirradiated Reinecke's salt solution.

Φ = Quantum yield for formation of photoproduct at the λ of irradiation (mol/einstein).

$1-10^{-\varepsilon_1[A]\ell_1}$ = Fraction of light that was absorbed by the actinometer solution.

ℓ_1 = Path length of the cell used to irradiate the actinometer solution (cm).

ℓ_2 = Path length of the cell used to measure the ΔA (cm).

ε_1 = Molar extinction coefficient of the actinometer solution at the λ of irradiation (M^{-1} cm^{-1}).

ε_2 = Molar extinction coefficient of the developed photoproduct at the measured λ (M^{-1} cm^{-1}).

This experiment was carried out three times and the quanta per minute were averaged to yield the value used in further calculations. The results of these three experiments were 6.36×10^{18}, 6.42×10^{18}, 6.62×10^{18} quanta/min. These three values yield an average of 6.5×10^{18} quanta/min.

Synthesis.

2,3-bis(2-pyridyl)quinoxaline. This bridging ligand (dpq) was synthesized according to the literature method of Goodwin and Lions.[58] An ethanolic solution (100 mL) of *o*-phenylenediamine (1.08g, 10.0 mmol) and 2,2'-pyridyl (2.12 g, 10.0 mmol) was heated at reflux for four hours. The solution was allowed to cool to room temperature and brown crystals precipitated. The product was purified through several recrystallizations in 250 mL 100% ethanol. Purity of the compound was verified through infrared spectroscopy. A typical yield for this reaction was 90%. Infrared spectra of the reaction starting materials and product are given in Appendix I.

2,3-bis(2-pyridyl)benzoquinoxaline. This ligand was first synthesized by Buu-Hoi *et al.*[59] The bridging ligand, dpb, was prepared through the modification of Goodwin and Lions' dpq synthesis.[58] Diaminonapthalene (7.91 g, 0.0500 moles) was substituted for *o*-phenylenediamine and combined with 2,2'-pyridyl (10.59 g , 0.050 moles).[44] The ligand was purified via adsorption alumina chromatography. The bright yellow band, eluted with 1:1 (vol./vol.) methylene chloride/acetonitrile, was collected and rotoevaporated to dryness and recrystallized from 250 mL 100% ethanol. A typical yield for this reaction was 90%. Purity of the compound was determined with the use of infrared spectroscopy. Infrared spectra of the starting materials and product are given in Apendix I.

6,7-dichloro-2,3-bis(2-pyridyl)quinoxaline. The ligand, Cl_2dpq, was prepared through the modification of Goodwin and Lions' dpq synthesis.[58] In this preparation *o*-phenylenediamine is substituted by 4,5-dichloro-1,2-phenylenediamine. 2,2'-pyridyl (2.12 g, 10.0 mmol) and 4,5-dichloro-1,2-phenylenediamine (1.77 g, 10.0 mmol) were combined in 100 mL of ethanol and heated at reflux for 8 hours.[60] At that time the solution was transferred to a 150 mL beaker to cool to room temperature overnight. The resulting crystals were isolated and purified by four recrystallizations in 250 mL 100% ethanol. Absence of the starting material 2,2'-pyridyl was determined with the use of infrared spectroscopy. Yields for this reaction were approximately 90%. Infrared spectra of the starting materials and product are given in Apendix I.

6,7-dimethyl-2,3-bis(2-pyridyl)quinoxaline. Preparation of this ligand, Me_2dpq, was through the modification of Goodwin and Lions' dpq synthesis.[58] 2,2'-pyridyl (2.12 g, 10.0 mmol) and 4,5-dichloro-1,2-phenylenediamine (1.3 g, 10 mmol)

were combined in 20 mL of ethanol and heated at reflux for 8 hours.[60] The warm solution was transferred to a 150 mL beaker to cool to room temperature overnight. The resulting crystals were isolated and purified by repeated recrystallizations in 250 mL 100% ethanol. A typical reaction yield was 90%. Absence of the starting material 2,2'-pyridyl was determined with the use of infrared spectroscopy. Infrared spectra of the reactions starting materials and product are given in Apendix I.

***cis*-bis(2,2'-bipyridine)dichlororuthenium(II) dihydrate** *cis*-$[Ru(bpy)_2Cl_2]\cdot 2H_2O$[61] has been prepared via a published preparation in which $RuCl_3\cdot 3H_2O$ (3.90 g,14.9 mmol), bipyridine (4.68 g, 30.0 mmol), and LiCl (4.20 g, 1.00 mmol) were combined in reagent grade dimethylformamide (25 mL) and heated at reflux, while magnetically stirring, for 8 hours. This reaction mixture was cooled to room temperature before being added dropwise to acetone (200 mL) and cooled at 0° C overnight. The red filtrate was separated from the dark green, almost black, solid using a fine glass fritted Buchner type funnel and vacuum filtration. The solid was washed with three 25 mL portions of cold water and diethyl ether to remove excess bpy, $RuCl_3\cdot 3H_2O$, LiCl, and $[Ru(bpy)_3]Cl_2$. Complete washing of the product is necessary to insure the removal of the side product $[Ru(bpy)_3]Cl_2$. After washing, the solid was allowed to dry in a vacuum dessicator overnight. A typical yield for this reaction was approximately 60%.

Dichlorobis(2,3-bis(2-pyridyl)quinoxaline)iridium(III) Hexafluorphosphate. $[Ir(dpq)_2Cl_2](PF_6)$. The preparation of this complex was a modification of the literature preparation of Brewer *et al.*[44] The literature reports a preparation wherein $IrCl_3\cdot 3H_2O$ (0.24 g, 0.80 mmol) and dpq (0.55g, 2.2 mmol) are heated in 25mL of ethylene glycol. In

this preparation the ratio of $IrCl_3 \cdot 3H_2O$ to dpq was altered from (1: 2.8) to (1:4). This Ir^{III} monometallic was synthesized by heating $IrCl_3 \cdot 3H_2O$ (0.352 g, 1.00 mmol) and dpq (1.14g, 4.00 mmol) in 15 mL of ethylene glycol at reflux for 30 minutes. The warm reaction solution was transferred dropwise to 150 mL of an aqueous saturated solution of KPF_6. The resulting precipitate was separated from the solution by vacuum filtration. This solid was washed three times with 15 mL portions of both water and diethyl ether. Purification of the solid was achieved with the use of adsorption alumina chromatography. The column (20 cm) was poured with 3:1 (vol./vol.) toluene/acetonitrile eluent. The crude product eluted as an orange band with 2:1 (vol./vol.) toluene/acetonitrile. This band was collected and rotory evaporated to dryness. This collected band was re-chromatographed in the same manner, collecting only the center portion of the band, three times to achieve purity. The final band was rotory evaporated to dryness and redissolved in 10 mL of acetone. The acetone solution was transferred dropwise to 150 mL of diethyl ether. The precipitate was isolated using vacuum filtration. A typical yield for this reaction was 75%. Thin-layer chromatography, cyclic voltammetry and electronic spectroscopy aided in the determination of purity.[44]

Dichlorobis(2,3-bis(2-pyridyl)benzoquinoxaline)iridium(III) Hexafluorphosphate. $[Ir(dpb)_2Cl_2](PF_6)$[44] Preparation of this complex was based on the synthesis of $[Ir(dpq)_2Cl_2](PF_6)$ and also a modification of the Method of Brewer *et al.*,[44] the only variation being the substitution of dpb for dpq. $IrCl_3 \cdot 3H_2O$ (0.352 g, 1.00 mmol) and dpb (1.34g, 4.00 mmol) in 15 mL of ethylene glycol at reflux for 30 minutes.

The purification of this complex differs due to the complicated reaction products. Size-exclusion chromatography (LH-20 Sephadex) was an easier purification route. The Sephadex LH-20 size-exclusion chromatography column was poured, and the analyte eluted with a 2:1 (vol./vol.) ethanol/acetonitrile solvent mixture. The desired orange product was collected and rotoevaporated to dryness and flash precipitated in diethyl ether. (Adsorption alumina chromatography can be used, but extreme expertise and additional columns are needed to achieve purity.) Although higher yields have been obtained by the Brewer group,[44] a typical reaction yield for this procedure was 20%. Purity of this complex was determined through thin-layer chromatography, cyclic voltammetry, and electronic absorption spectroscopy.

Dichlorobis(2,3-bis(2'-pyridyl)pyrazine)rhodium(III) Hexafluorophospate. $[Rh(dpp)_2Cl_2](PF_6)$.[44] Synthesis of this complex was achieved by the combination of $RhCl_3 \cdot xH_2O$ (0.245 g, 1.17 mmol) and dpp (0.548 g, 2.34 mmol) in 15 mL of a 2:1 (vol./vol.) solution of ethanol/water and refluxed for approximately 45 minutes. The warm solution was pipetted into a saturated aqueous solution of KPF_6. The solid was isolated by vacuum filtration and purified by adsorption alumina chromatography. The column was loaded with 2:1 (vol./vol.) toluene/acetonitrile and the bright-yellow product band eluted with 1:1 (vol./vol.) toluene/acetonitrile. A typical stationary phase height in a 48 cm × 2.2 cm (I.D.) column was 20 cm. Approximately 5 mL of a highly concentrated solution of crude product in the mobile phase was loaded onto the column. This purification step was repeated twice on the subsequently purified band to increase the purity with each step. A typical yield for this complex was approximately 85%. Purity of

this complex was determined through thin-layer chromatography, cyclic voltammetry, and electronic absorption spectroscopy.[44]

Dichlorobis(2,3-bis(2-pyridyl)quinoxaline)rhodium(III) Hexafluorophospate. $[Rh(dpq)_2Cl_2](PF_6)$.[44] Preparation of this complex was the same as above, except the bridging ligand dpq was used instead of dpp. $RhCl_3 \cdot xH_2O$ (0.12 g, 0.56 mmol) and dpq (0.33 g, 2.34 mmol) were refluxed in 15 mL of a 2:1(vol./vol.) solution of ethanol/water for approximately 45 minutes. The complex was purified as above and had an average yield of 67%. Thin-layer chromatography, cyclic voltammetry, and electronic absorption spectroscopy aided in determining the purity of this complex.[44]

Dichlorobis(2,3-bis(2'-pyridyl)benzoquinoxaline)rhodium(III) Hexafluorophospate. $[Rh(dpb)_2Cl_2](PF_6)$.[44] Preparation of this complex was the same as above, except the bridging ligand dpb was used instead of dpq. $RhCl_3 \cdot xH_2O$ (0.245 g, 1.17 mmol) and dpb (0.782 g, 2.34 mmol) were refluxed in 15 mL of a 2:1 (vol./vol.) solution of ethanol/water for approximately 45 minutes. The complex was purified as above and had an average yield of 72%. Purity of this complex was determined by thin-layer chromatography, cyclic voltammetry, and electronic absorption spectroscopy.[44]

Bis(2,2'-dipyridyl)(2,3-bis(2-pyridyl)pyrazine)ruthenium(II) Hexafluorophosphate. $[(bpy)_2Ru(dpp)](PF_6)_2$. This complex was first synthesized by Braunstein *et. al.*[36] The published procedure reported the synthesis of the perchlorate salt.

A revised synthesis was developed that prepares the PF_6^- salt utilizes a shorter reaction time and purification by column chromatography.[60] *Cis*-$[Ru(bpy)_2Cl_2]$ (0.400 g,

1.20 mmol) and dpp (0.571 g, 2.40 mmol) were combined in 15 mL of 2:1(vol./vol.) ethanol/water and heated at reflux for 2 hours. The warm reaction solution was pipetted into 75 mL of a saturated aqueous solution of KPF_6. After separating the solid by vacuum filtration, the crude product was purified with the use of adsorption alumina chromatography. The column was loaded in 3:1 (vol./vol.) toluene/acetonitrile and the product band (orange) eluted with 1:1 (vol./vol.) toluene/acetonitrile. A typical stationary phase height in a 48 cm × 2.2 cm (I.D.) column was 20 cm. Approximately 5 mL of a highly concentrated solution of crude product in the mobile phase was loaded onto the column. Purification in this manner was carried out several times to further purify the collected product band. A typical yield for this reaction was approximately 85 %. Purity of this complex was verified with the use of electronic absorption spectroscopy and cyclic voltammetry.[60]

Bis(2,2'-dipyridyl)(2,3-bis(2-pyridyl)quinoxaline)ruthenium(II) Hexafluorophosphate. $[(bpy)_2Ru(dpq)](PF_6)_2$. The complex was originally synthesized by Rillema *et. al.*[39] The procedure described herein is simplier and shorter.

The preparation of this complex mimics the procedure for the synthesis of $[(bpy)_2Ru(dpp)](PF_6)_2$ with the ligand dpq substituting for dpp.[60] *Cis*-$[Ru(bpy)_2Cl_2]$ (0.400 g, 1.20 mmol) was combined with dpq (0.803 g, 2.40 mmol) in 15 mL of 2:1 (vol./vol.) ethanol/water and heated at reflux for 2 hours. The warm reaction solution was pipetted into 75 mL of a saturated aqueous solution of KPF_6. After separating the solid by vacuum filtration, the crude product was purified with the use of adsorption alumina chromatography. The column was loaded in 3:1 (vol./vol.) toluene/acetonitrile and the

red-orange product band eluted with 1:1 (vol./vol.) toluene/ acetonitrile. A typical stationary phase height in a 48 cm × 2.2 cm (I.D.) column was 20 cm. Approximately 5 mL of a highly concentrated solution of crude product in the mobile phase was loaded onto the column. Purification in this manner was carried out three times to further purify the collected product band. A typical reaction yield was approximately 80%. Purity of this complex was verified with the use of electronic absorption spectroscopy and cyclic voltammetry.[60]

Bis(2,2'-dipyridyl)(2,3-bis(2-pyridyl)benzoquinoxaline)ruthenium(II) Hexafluorophosphate. $[(bpy)_2Ru(dpb)](PF_6)_2$. Synthesis of this complex was based on the synthesis used for $[(bpy)_2Ru(dpp)](PF_6)_2$, and $[(bpy)_2Ru(dpq)](PF_6)_2$.[60] *Cis*-$[Ru(bpy)_2Cl_2]$ (0.400 g, 1.20 mmol) and dpb (0.700 g, 2.40 mmol) were added to 15 mL of 2:1 (vol./vol.) ethanol/water and refluxed for 2 hours. The warm reaction solution was pipetted into a saturated aqueous solution of KPF_6. After separating the solid by vacuum filtration, the crude product was purified with the use of adsorption alumina chromatography. The column is loaded in 3:2 (vol./vol.) toluene/acetonitrile and the deep red product band eluted with 1:1 (vol./vol.) toluene/acetonitrile. A typical stationary phase height in a 48 cm × 2.2 cm(I.D.) column was 20 cm. Approximately 5 mL of a highly concentrated solution of crude product in the mobile phase was loaded onto the column. Purification in this manner was carried out two more times to further purify the collected product band. A typical yield for this reaction was approximately 85%. This complex was analyzed using electronic absorption spectroscopy and cyclic voltammetry.[60] Purity of the complex was established by thin layer chromatography.

Tetrakis(2,2'-dipyridyl)(μ-2,3-bis(2-pyridyl)pyrazine)diruthenium hexafluorophosphate. $\{[(bpy)_2Ru]_2(dpp)\}(PF_6)_4$. This bimetallic complex was first synthesized by Braunstein *et. al.*[36] The preparation utilized differs in the solvent used, the reduction in the reaction time from 72 hours to 2 hours, and purification methods.

The monometallic and bimetallic species, $[(bpy)_2Ru(dpp)](PF_6)_2$ and $\{[(bpy)_2Ru]_2(dpp)]\}(PF_6)_4$, were produced with this method.[60] *Cis*-$[Ru(bpy)_2Cl_2]$ (0.420 g, 0.868 mmol) and dpp (0.137 g, 0.584 mmol) are heated at reflux for two hours in 15 mL of 2:1 (vol./vol.) ethanol/water. A solid resulted when the red reaction solution was added to 100 mL of saturated aqueous KPF_6. This solid was separated by vacuum filtration, and washed 3 times with 20 mL of ethanol and 3 times with 20 mL of diethyl ether.

Purification of this crude product was achieved using adsorption alumina chromatography. The column was prepared with 3:1 (vol./vol.) toluene/acetonitrile. A typical stationary phase height in a 48 cm × 2.2 cm (I.D.) column was 20 cm. Approximately 5 mL of a highly concentrated solution of crude product in the mobile phase was loaded onto the column. The first band to elute was the light orange monometallic complex in 2:1 (vol./vol.) toluene/acetonitrile. This band was collected, concentrated via rotary evaporation, and then flash precipitated in diethyl ether. The second band was the purple bimetallic complex and eluted in 1:1 (vol./vol.) toluene/acetonitrile. This band was also concentrated and flash precipitated with diethyl ether. Purity of both the monometallic and bimetallic complexes was established with thin layer chromatography, electronic absorption spectroscopy, and electrochemistry.[60] The

reaction yield for the monometallic and bimetallic were 85%. This percentage is based on the assumption that the reaction mixture would produce 50% monometallic and 50% bimetallic complexes.[60]

Tetrakis(2,2'-dipyridyl)(μ-2,3-bis(2-pyridyl)quinoxaline)diruthenium hexafluorophosphate. $\{[(bpy)_2Ru]_2(dpq)\}(PF_6)_4$. This compound has been previously synthesized by Rillema *et al.*[39] The procedure employed here has a shorter reaction time, does not utilize $AgClO_4$ or $AgPF_6$, and produces both the mono- and bimetallic species with the same reaction.[60]

Cis-$[Ru(bpy)_2Cl_2]$ (0.420 g, 0.868 mmol) and dpq (0.166 g, 0.584 mmol) were combined in 15 mL of 2:1 (vol./vol.) ethanol/water. After heateing at reflux for 2 hours, the reaction solution was added to 100 mL of saturated aqueous KPF_6. The solid that formed was separated by vacuum filtration. The filtered solid was washed 3 times with 20 mL of ethanol and 3 times with 20 mL of diethyl ether. Adsorption alumina chromatography was used to purify the resulting mono- and bimetallic products. The alumina column was prepared with 3:1 (vol./vol.) toluene/acetonitrile. A typical stationary phase height in a 48 cm × 2.2 cm (I.D.) column was 20 cm. Approximately 5 mL of a highly concentrated solution of crude product in the mobile phase was loaded onto the column. The first band to elute was the orange monometallic complex, which was followed by the purple bimetallic complex. This reaction produced the monometallic complex in 85% yield, and the bimetallic complex in 80% yield. This percentage is based on the assumption that the reaction mixture would produce 50% monometallic and 50% bimetallic complexes. These complexes were analyzed using electronic absorption

spectroscopy and cyclic voltammetry. Purity of these complexes was determined using thin layer chromatography.[60]

Tetrakis(2,2'-dipyridyl)(μ-2,3-bis(2-pyridyl)benzoquinoxaline)diruthenium hexafluorophosphate. $\{[(bpy)_2Ru]_2(dpb)\}(PF_6)_4$. This bimetallic complex has not previously been reported. The procedure used here was based on the synthesis of $\{[(bpy)_2Ru]_2(dpp)\}(PF_6)_4$ and $\{[(bpy)_2Ru]_2(dpq)\}(PF_6)_4$.[60] Both the mono- and bimetallic species were produced in the reaction of *cis*-$[Ru(bpy)_2Cl_2]$ (0.420 g, 0.868 mmol) and dpb (0.195 g, 0.584 mmol) which were combined in 15 mL of 2:1 (vol./vol.) ethanol/water. The reaction mixture was added to 100 mL of saturated aqueous KPF_6 after heating at reflux for 2 hours. The solid was separated by vacuum filtration and washed 3 times with 20 mL of ethanol and 3 times with 20 mL of diethyl ether. The adsorption alumina column, used to purify both the mono- and bimetallic products, was prepared with 3:1 (vol./vol.) toluene/acetonitrile. A typical stationary phase height in a 48 cm × 2.2 cm (I.D.) column was 20 cm. Approximately 5 mL of a highly concentrated solution of crude product in the mobile phase was loaded onto the column. The first band to elute was the red-orange monometallic complex, which was followed by the maroon bimetallic complex. These bands were collected and rotoevaporated to dryness. Each solid was dissolved in 5 mL of acetone and flash precipitated in diethyl ether. The mono- and bimetallic complexes were produced in appoximately 80% yield. Again, this percentage is based on the assumption that the mono- and bimetallics would each comprise 50% of the product mixture. Thin layer chromatography determined the purity of these complexes.[60]

Bis(2,2'-dipyridyl)(6,7-dichloro-2,3-bis(2-pyridyl)quinoxaline)ruthenium(II) hexafluorophosphate and tetrakis(2,2'-dipyridyl)(μ-6,7-dichloro-2,3-bis(2-pyridyl)quinoxaline)diruthenium hexafluorophosphate. $[(bpy)_2Ru(Cl_2dpq)](PF_6)_2$ and $\{[(bpy)_2Ru]_2(Cl_2dpq)\}(PF_6)_4$. These complexes were synthesized by a modification of the $\{[(bpy)_2Ru]_2(dpq)\}(PF_6)_4$ above.[60] Both the monometallic and bimetallic complexes were synthesized in the same reaction. The two starting materials *cis*-$[Ru(bpy)_2Cl_2]$ (0.420 g, 0.868 mmol) and Cl_2dpq (0.206 g, 0.584 mmol) were heated at reflux for two hours in 15 mL of 2:1 (vol./vol.) ethanol/water. The resulting purple solution was added dropwise to 100 mL of saturated aqueous KPF_6. The resulting precipitate was separated via vacuum filtration and washed three times with 20 mL ethanol and three times with 20 mL of diethyl ether. Purification of this crude product was achieved using adsorption alumina chromatography. The column was prepared with 3:1 (vol./vol.) toluene/acetonitrile. A typical stationary phase height in a 48 cm × 2.2 cm (I.D.) column was 20 cm. Approximately 5 mL of a highly concentrated solution of crude product in the mobile phase was loaded onto the column. The first band to elute was the red monometallic complex. This band was collected, concentrated via rotary evaporation, and flash precipitated in diethyl ether. The second band was the blue-green bimetallic complex. This band was also concentrated and flash precipitated. A typical reaction yield for both the mono- and bi- metallic was on average 80%. This percentage is based on the product mixture consisting of 50% monometallic and 50% bimetallic complexes. Purity of both the monometallic and bimetallic complexes was established with thin layer chromatography. *Anal.* Calc. for $[(bpy)_2Ru(Cl_2dpq)](PF_6)_2$: C, 43.19 %; H, 2.48 %; N,

10.61 %. Found: C, 43.33 %; H, 2.46 %; N, 10.42 %. Calc. for $\{[(bpy)_2Ru]_2(Cl_2dpq)\}(PF_6)_4$: C, 39.58 %; H, 2.40 %; N, 9.55 %. Found: C, 39.12 %; H, 2.30 %; N, 9.46 %.[60]

Bis(2,2'-dipyridyl) 6,7-dimethyl-2,3-bis(2-pyridyl) quinoxalineruthenium(II) dihexafluorophosphate and tetrakis(2,2'-dipyridyl)(μ-6,7-dimethyl-2,3-bis(2-pyridyl)quinoxaline)diruthenium hexafluorophosphate. $[(bpy)_2Ru(Me_2dpq)](PF_6)_2$ and $\{[(bpy)_2Ru]_2(Me_2dpq)\}(PF_6)_4$. These complexes may be synthesized in the same manner as $[(bpy)_2Ru(Cl_2dpq)](PF_6)_2$ and $\{[(bpy)_2Ru]_2(Cl_2dpq)\}(PF_6)_4$ with slight alterations.[60] In this case, the bridging ligand Me_2dpq (0.182g, 0.582mmol) was substituted for the Cl_2dpq bridging ligand. Purification of these complexes follows the same protocol as for $[(bpy)_2Ru(Cl_2dpq)](PF_6)_2$ and $\{[(bpy)_2Ru]_2(Cl_2dpq)\}(PF_6)_4$. On average, the yield for the mono- and bimetallic complexes was approximately 80% (based on the assumption that the product mixture was 50% monometallic and 50% bimetallic complexes). Purity of the monometallic and bimetallic complexes was established with the use of thin layer chromatography. *Anal.* Calc. for $[(bpy)_2Ru(Me_2dpq)](PF_6)_2$: C, 47.30 %; H, 3.17 %; N, 11.03 %. Found: C, 47.06 %; H, 3.32 %; N, 11.06 %. Calc. for $\{[(bpy)_2Ru]_2(Me_2dpq)\}(PF_6)_4$: C, 41.92 %; H, 2.81 %; N, 9.78 %. Found: C, 41.6 2%; H, 2.85 %; N, 9.56 %.[60]

$\{[(bpy)_2Ru(dpq)]_2IrCl_2\}(PF_6)_5$. This trimetallic complex was synthesized by heating at reflux the combination of $[Ir(dpq)_2Cl_2](PF_6)_2$ (0.288 g, 0.330 mmol) and *cis*-$[Ru(bpy)_2Cl_2]$ (0.782 g, 1.00 mmol) in a 2:1 (vol./vol.) mixture of ethanol/water

(25 mL) for 24 hours.[62] The warm reaction mixture was transferred dropwise to 75 mL of a saturated solution of aqueous KPF_6. The precipitate was retrieved with the use of vacuum filtration. Purification was accomplished with the use of size exclusion chromatography. Chromatography may be done using either normal or high pressure methods. Normal pressure chromatographic technique, since the eluent is 100% ethanol, involves the metathesis of the hexafluorophosphate salt to a chloride salt. Metathesis was accomplished by combining a highly concentrated acetonitrile solution of tetrabutylammonium chloride and highly concentrated acetonitrile solution of the trimetallic complex. When utilizing the high pressure techniques, metathesis of the complex was not necessary due to the 2:1 (vol./vol.) ethanol/acetonitrile composition of the eluent. The monitoring of the fractions by electronic absorption spectroscopy allowed for the determination of which fractions contained the pure trimetallic complex. This determination was made by comparing spectra of fractions to a known sample. These fractions were rotory evaporated to dryness and dissolved in 5 mL of acetone. The trimetallic complex was flash precipitated with diethyl ether. The pure complex was blue/green in color and was produced in approximately 80 % yield.[62]

$\{[(bpy)_2Ru(dpp)]_2RuCl_2\}(PF_6)_4$. This trimetallic was synthesized by the modification of Balzani *et. al. 's* literature preparation.[63] The preparation utilized here differs slightly from that literature preparation. In this procedure KPF_6 was used to precipitate the PF_6^- salt of the crude product, instead of NH_4PF_6 as described in the literature preparation. Other alterations of the literature procedure include a longer reaction time (17 versus 7 hours) and an additional purification step.

The compounds $[(bpy)_2Ru(dpp)](PF_6)_2$ (0.161g, 0.172 mmol), $RuCl_3 \cdot 3H_2O$ (0.018 g, 0.086 mmol) and LiCl (0.024 g, 0.56 mmol) were heated at in 15 mL of ethanol for 17 hours. The hot reaction solution was precipitated in 75 mL of a saturated aqueous solution of KPF_6. The precipitate was retrieved using vacuum filtration.

Purification of this trimetallic was accomplished using adsorption alumina chromatography. The column was prepared using 2:1 (vol./vol.) toluene/acetonitrile. A typical stationary phase height in a 48 cm × 2.2 cm (I.D.) column was 20 cm. Approximately 5 mL of a highly concentrated solution of crude product in the mobile phase was loaded onto the column. The first band to elute was yellow, which was followed by a blue band. The second band was collected and evaporated to dryness using rotoevaporation. The complex was diluted in 5 mL of acetone and flash precipitated using 100 mL of diethyl ether. This blue solid product was generally produced in 65% yield.

$\{[(bpy)_2Ru(dpp)]_2Ru(CH_3CN)_2\}(PF_6)_{(6-x)}(BF_4)_x$. To synthesize this solvato complex, $\{[(bpy)_2Ru(dpp)]_2RuCl_2\}(PF_6)_4$ (0.10 g, 0.043 mmol) and $AgBF_4$ (0.0250 g, 0.130 mmol) were heated at reflux for 2 hours in a minimal amount of acetonitrile (10 mL). The cooled reaction mixture was run through a short (2 in.) adsorption alumina column, to remove any residual $AgBF_4$ and the AgCl precipitate. The alumina column was loaded with acetonitrile, and the maroon band was eluted in 1:1 (vol./vol.) acetonitrile/methanol. A typical stationary phase height in a 48 cm × 2.2 cm (I.D.) column was 20 cm. Approximately 5 mL of a concentrated solution of crude product in the mobile phase was loaded onto the column. This band was collected and rotory evaporated to dryness. The solid was dissolved in 5 mL of acetone and flash precipitated in diethyl

ether. This maroon solid was produced in a 93% yield, based on the assumption that the product was only a PF_6^- salt.

{[(bpy)$_2$Ru(dpp)]$_2$RhCl$_2$}(PF$_6$)$_5$. $RhCl_3 \cdot xH_2O$ (0.050 g, 0.24 mmol) and $[Ru(bpy)_2dpp](PF_6)_2$ (0.36 g, 0.38 mmol) were refluxed in a minimal amount of 2:1 (vol./ vol.) ethanol/water (15 mL) for 1 hour.[64] The product was precipitated in 100 mL of saturated KPF_6. To purify the berry-red solid, the complex was metathesized to the Cl^- salt. The solid was washed three times with 5 mL of acetone. The chloride salt was metathesized back to the KPF_6 salt and washed three times with 5 mL of deionized water. This procedure was repeated a second time. The purpose of metathesis to the chloride salt, and subsequent washing of the chloride salt, was to remove the ruthenium monometallic impurity. The final solid was dissolved in a minimal amount of acetonitrile and flash precipitated in diethyl ether. A typical reaction yield for this complex was 90%. Purity of the complex was determined by electronic absorption spectroscopy and cyclic voltammetry.

{[(bpy)$_2$Ru(dpp)]$_2$Rh^I}(PF$_6$)$_5$. An attempted synthesis of this Rh^I trimetallic complex was undertaken through the combination of $[Rh(C_2H_4)_2Cl]_2$ (0.05 g, 0.1 mmol) in 20 mL of acetonitrile with $TlPF_6$ (0.102 g, 0.258 mmol) in 3 mL of acetonitrile. Burdick and Jackson spectral grade acetonitrile was used. Prior to use this acetonitrile was passed through activated adsorption alumina under inert atmosphere conditions. The acetonitrile was passed through three separate syringe filters in order to remove any trace amounts of alumina that may have been present. The solvent was stored for a short time in a Schlenk flask while awaiting use. The Rh^I dimer and $TlPF_6$ starting materials were allowed to stir

for 20 minutes under nitrogen. At this time a white solid appeared in the reaction vessel with the yellow-brown solution. The ruthenium monometallic, $[Ru(bpy)_2(dpp)](PF_6)_2$ (0.48 g, 0.52 mmol), was added to the mixture and heated at reflux for 30 minutes. Cyclic voltammetry, electronic absorption spectroscopy, emission spectroscopy, and FAB mass spectroscopy all aided in the determination of the products identity. The product, from analysis of these techniques, appears to be the Rh^I trimetallic, although this conclusion needs further evidence.

CHAPTER 3.

SYNTHESIS AND CHARACTERIZATION OF SUBSTITUTED 2,3-(BIS(2-PYRIDYL)QUINOXALINE BRIDGING LIGANDS AND THEIR RUTHENIUM(II) MONO- AND BI-METALLIC COMPLEXES.

Introduction.

The quest for photochemical molecular devices (PMDs) has led researchers to focus their attention on specific active components of these supramolecular arrays. An example of such an active component is a photosensitizer. As an active component of a PMD, the photosensitizer performs the function of absorbing light and then transferring energy, or an electron, to another component of the PMD. There are some general criteria that the photosensitizer's physical characteristics must meet. Three of these general criteria are: (1) absorb light efficiently within the visible region of the electromagnetic spectrum; (2) have a sufficient excited state lifetime; (3) transfer energy or an electron. The photosensitizer needs a suitable excited state energy and/or redox properties to perform its function.

A transition metal complex that has been widely studied as a photosensitizer is $[Ru(bpy)_3]^{2+}$.[31-34] This Ru^{II} complex has been widely studied as a photosensitizer due to its excited state lifetime, redox properties, and electron transfer ability. Although $[Ru(bpy)_3]^{2+}$ has been employed in numerous electron transfer schemes, the complex requires some alteration prior to becoming a part of supramolecular architecture.

The $[Ru(bpy)_3]^{2+}$ complex may be modified in a way that will maintain the desirable photosensitizing characteristics, but make it able to be connected to other parts

of a supramolecular assembly. The transformation of $[Ru(bpy)_3]^{2+}$ to the $[Ru(bpy)_2(BL)]^{2+}$ (where BL is a bidentate bridging ligand) type complexes were discussed in Chapter 1. Even though the incorporation of the BL into the $Ru(bpy)_3^{2+}$ moiety alters the chromophore's characteristics, many of the desirable characteristics remain intact.

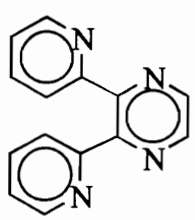

dpp

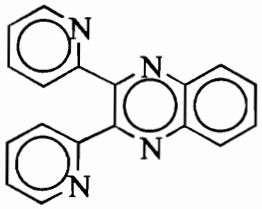

dpq

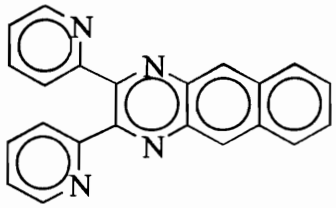

dpb

The previously prepared complexes $[Ru(bpy)_2(dpp)]^{2+}$,[36-38] $[Ru(bpy)_2(dpq)]^{2+}$,[39-42] and the herein synthesized $[Ru(bpy)_2(dpb)]^{2+}$, (dpp = 2,3-bis(2-pyridyl)pyrazine, dpq = 2,3-bis(2-pyridyl) quinoxaline, and dpb = 2,3-bis(2-pyridyl)benzoquinoxaline) exhibit a varying $Ru(d\pi) \rightarrow BL(\pi^*)$ charge transfer (MLCT) energies. Through the dpp, dpq, and dpb bridging ligand series, one can see a stepwise structural transformation. A benzene ring has been fused to the dpp pyrazine ring to produce dpq. The fusing of an additional benzene ring to the dpq produces dpb. The aim behind sequential variation of the bridging ligand is the tuning of the photosensitizer's photophysical properties. This alteration of the bridging ligand is a major step in tuning the light absorbing and redox properties of the photosensitizer. Further tuning of this series of chromophores may be achieved through the addition of substituent groups to individual bridging ligands.

To explore this approach to tuning the characteristics of these $[Ru(bpy)_2(BL)]^{2+}$ systems, the dpq (2,3-bis(2-pyridyl)quinoxaline) bridging ligand was chosen to be modified. The type of substituents, and location on the BL, called for cautious deliberation. If the substituents are placed at the 6 and 7 positions, the symmetry of the newly created ligand, X_2dpq (where X represents a substituent), will be the same as the parent ligand.

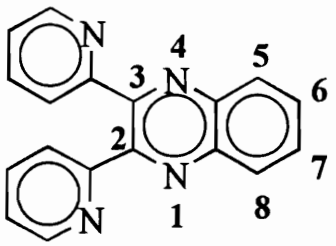

2,3-bis(2-pyridyl)quinoxaline

The occupation of positions 5 and 8 will have the same effect. If the substituents are placed in these locations, they could sterically interfere with metal binding. For reasons of maintaining the symmetry of the parent ligand and not interfering with metal binding, the substituents were placed at positions 6 and 7.

To achieve the desired tuning affect, the type of substituent to place on the bridging ligand needed to be considered. It has been noted in the literature that electron withdrawing substituents stabilize the π^* orbital, while electron donating substituents destabilize the π^* orbital.[35] For this reason, one electron withdrawing and electron donating substituent were chosen. The lowest lying λ_{max}^{abs} for this series of complexes corresponds to a $Ru(d\pi) \rightarrow BL(\pi^*)$ CT transition. Therefore, the Ru^{II} photosensitizers constructed from these ligands will be tuned by the alteration of the bridging ligand's

acceptor orbital energy. The specific substituents chosen for this study were methyl groups and chlorides.

The substituted dpq bridging ligands were synthesized and their structure was verified through infrared spectroscopy and ^{13}C nuclear magnetic resonance (NMR) spectroscopy. The ligands were further characterized using electrochemistry, electronic absorption spectroscopy, and emission spectroscopy. The next step in the investigation was the synthesis and characterization of the ruthenium mono- and bimetallic complexes. The study of these ruthenium complexes would further elucidate the effects of the substituted bridging ligands on the $[Ru(bpy)_2(BL)]^{2+}$ photosensitizers.

The Modification of the 2,3-bis(2-pyridyl)quinoxaline Bridging Ligand.

Synthesis.

The substituted 2,3-bis(2-pyridyl)quinoxaline ligands were synthesized and investigated.[60] A pictorial representation of the synthesis of these ligands is shown in Figure 12. In general, the diketone, 2,2'-pyridyl, was reacted with the disubstituted *o*-phenylenediamine in a Schiff base condensation to produce the substituted 2,3-bis(2-pyridyl)quinoxaline (X_2dpq). After the substituted ligands were synthesized, analysis by infrared spectroscopy determined the absence of any 2,2'-pyridyl starting material by the absence of a C=O stretch 1670 cm^{-1}.

NMR Spectroscopy.

^{13}C NMR spectroscopy was conducted on the substituted and unsubstituted dpq bridging ligands. (It should be noted here that dpq has been fully characterized by

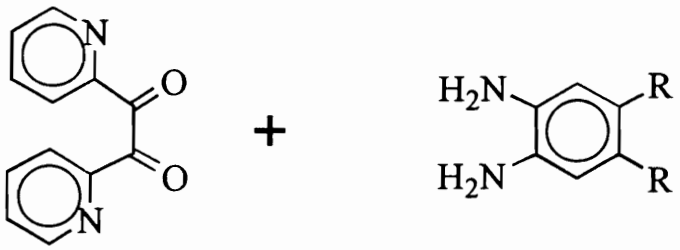

2,2'-pyridyl

R = CH_3: 4,5-dimethyl-1,2-phenylenediamine
R = Cl: 4,5-dichloro-1,2-phenylenediamine

Ethanol
Δ 8 hrs.

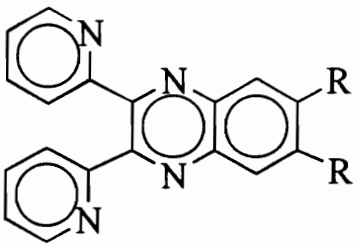

R = CH_3: 6,7-dimethyl-2,3-bis(2-pyridyl)quinoxaline (Me_2dpq)
R = Cl: 6,7-dichloro-2,3-bis(2-pyridyl)quinoxaline(Cl_2dpq)

Figure 12. *Synthesis of the Substituted 2,3-bis(2-pyridyl)quinoxaline Bridging Ligands.*

electronic absorption spectroscopy,[40] cyclic voltammetry,[40] infrared spectroscopy,[58] ^{13}C NMR,[46] and x-ray diffraction[44] by other researchers.) The ^{13}C chemical shifts and their assignments are presented in Table 7. Assignments made in this study agree with Murphy and co-workers independent work and assessment of the dpq ligand,[46] although under their conditions, C_e and C_f were not observed. Assignments of the substituted ligands were made based on comparison to the established assignments of the unsubstituted ligand.

Electrochemistry.

The results of the cyclic voltammetric analysis of the substituted 2,3-bis(2-pyridyl)quinoxaline ligands are presented in Table 8.[60] As is evident by the potentials listed, the Cl_2dpq, which contains the electron withdrawing substituent, reduces more easily than dpq by 0.25 V. The Me_2dpq, which contains the electron donating group, is more difficult to reduce by 0.12 V in comparison to dpq. The cyclic voltammetric data for the ligands shows that the addition of the two electron donating methyl groups produces a ligand that is harder to reduce than the original dpq ligand, and the two electron withdrawing chlorides produce a ligand that is easier to reduce. It is interesting to note that the $E_{1/2}^{red}$ values for the ligand series, dpp < Me_2dpq < dpq < Cl_2dpq < dpb, has created an incremental variation in the ligand π^* orbital energy spanning 0.66 V.

Electronic Absorption Spectroscopy.

Electronic absorption spectral data for the substituted dpq ligands' are summarized in Table 9 and shown in Figure 13.[60] A variation in the energy of the lowest lying optical transition is observed. This $n \rightarrow \pi^*$ absorption of the bridging ligand decreases in energy

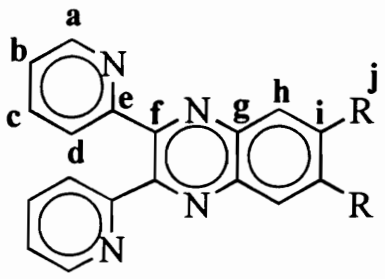

R= H, Cl, or CH_3

Table 7. ^{13}C Chemical Shifts (ppm)[a] and Assignments for a Series of Polypyridyl Bridging Ligands. (dpq = 2,3-bis(2-pyridyl)quinoxaline, Me_2dpq = 6,7-dimethyl-2,3-bis(2-pyridyl)quinoxaline, and Cl_2dpq = 6,7-dichloro-2,3-bis(2-pyridyl)quinoxaline.)[b]

Carbon	Chemical Shift (ppm)		
	dpq	Cl_2dpq	Me_2dpq
a	148.6	148.6	148.6
b	123.0	123.3	122.8
c	136.7	136.8	136.7
d	124.2	124.2	124.2
e	152.5	153.5	151.5
f	157.4	156.9	157.7
g	141.1	139.9	140.1
h	130.5	130.0	128.4
i	120.4	135.1	141.2
j			20.5

[a] All spectra were obtained on a Varian Unity-500 spectrophotometer. The solvent used in each case was $CDCl_3$ and the ppm shifts reported are versus TMS (tetramethylsilane).
[b] Reference 60.

Table 8. Cyclic Voltammetric Data[a] for a Series of Polypyridyl Bridging Ligands. (dpp = 2,3-bis(2-pyridyl)pyrazine, dpq = 2,3-bis(2-pyridyl)quinoxaline, Me_2dpq = 6,7-dimethyl-2,3-bis(2-pyridyl)quinoxaline, Cl_2dpq = 6,7- dichloro-2,3-bis(2-pyridyl)quinoxaline, and dpb = 2,3-bis(2-pyridyl)benzoquinoxaline.)[b]

LIGAND	Reduction
	$E_{1/2}$ (V)
dpp	-1.80
Me_2dpq	-1.55
dpq	-1.43
Cl_2dpq	-1.18
dpb	-1.14

[a] All cyclic voltammetric data was taken in room temperature spectral grade acetonitrile at a scan rate of 200 mV/s with 0.1 M Bu_4NPF_6 as the supporting electrolyte. The electrodes employed were a platinum working electrode, a platinum wire auxiliary electrode, and a Ag/AgCl reference electrode (0.29 vs. NHE).

[b] Reference 60.

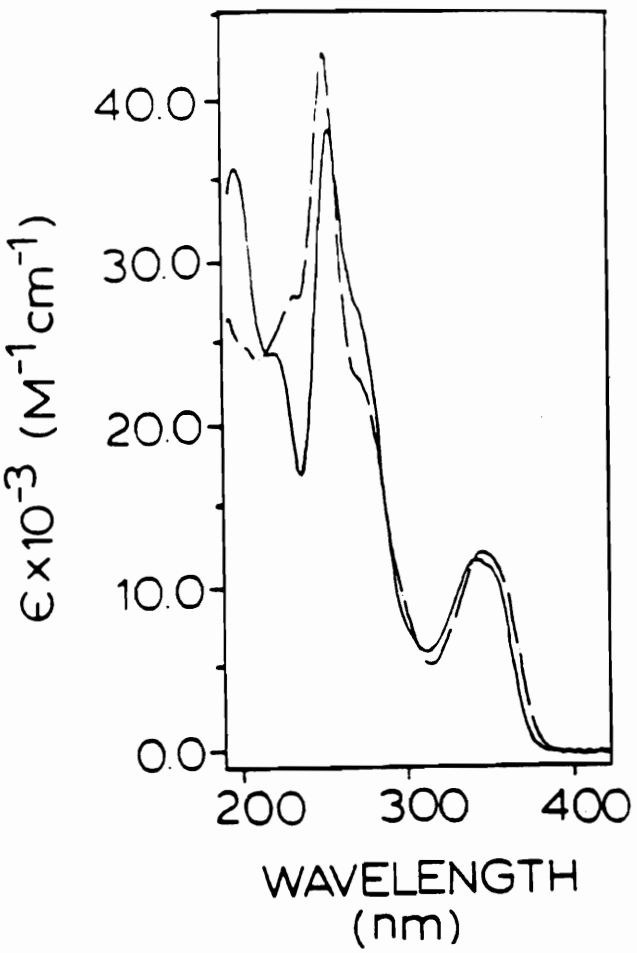

Figure 13. *Electronic Absorption Spectra for the Polypyridyl Bridging Ligands Me_2dpq [—]: 6,7-dimethyl-2,3-bis(2-pyridyl)quinoxaline and Cl_2dpq [— • —]: 6,7-dichloro-2,3-bis(2-pyridyl)quinoxaline.* All spectra were recorded in room temperature spectral grade acetonitrile.[a]

[a] Reference 60.

Table 9. Photochemical Data[a] for a Series of Polypyridyl Bridging Ligands.(dpp = 2,3-bis(2-pyridyl)pyrazine, dpq = 2,3-bis(2-pyridyl)quinoxaline, Me_2dpq = 6,7-dimethyl-2,3-bis(2-pyridyl)quinoxaline, Cl_2dpq = 6,7- dichloro-2,3-bis(2-pyridyl)quinoxaline, and dpb = 2,3-bis(2-pyridyl)benzoquinoxaline.)[b]

LIGAND	λ_{max} (nm)	
	Absorption[c]	Emission
dpp	284	402
Me_2dpq	341	404
dpq	332	410
Cl_2dpq	354	411
dpb	378	492

[a]All spectra were recorded in room temperature spectral grade acetonitrile.
[b]Reference 60.
[c]The lowest energy absorption maxima for the ligand.

through the series dpp > Me_2dpq > dpq > Cl_2dpq > dpb. The decrease in this absorption energy is observed as the bridging ligand's π^* orbital energy decreases. The non-bonding orbitals will not appreciably change in energy as the bridging ligand is transformed through the series. Therefore, the decrease in the $n \rightarrow \pi^*$ absorption energy is attributed to the decrease in the π^* orbital energy.

The energy of the emissive state varies through the same series of ligands in a similar manner to the absorption energy. The decreasing energy of emission in the series, dpp > Me_2dpq > dpq > Cl_2dpq > dpb, is another indication of the decreasing π^* orbital energy. The electronic absorption spectroscopy and emission spectroscopy trends, therefore, illustrate the stabilizing/destabilizing effects of the chloro- and methyl substituents.

Investigation of the Ruthenium Monometallic Complexes Containing the Substituted 2,3-bis(2-pyridyl)quinoxaline Bridging Ligands.

Synthesis.

The monometallic ruthenium complexes $[Ru(bpy)_2(BL)](PF_6)_2$ (BL = dpp, Me_2dpq, dpq, Cl_2dpq or dpb) were synthesized.[36-42, 60] Synthesis of the monometallics, which is discussed in depth above in the experimental section, was accomplished through the reaction of $[Ru(bpy)_2Cl_2]$ with the appropriate ligand in a 1.5:1 ratio (Figure 14). Previous to the work accomplished herein, the dpp and dpq systems appeared in the literature.[36-42] They were prepared herein to make comparisons of the properties of these complexes more valid. Characterization of a series of five complexes was achieved

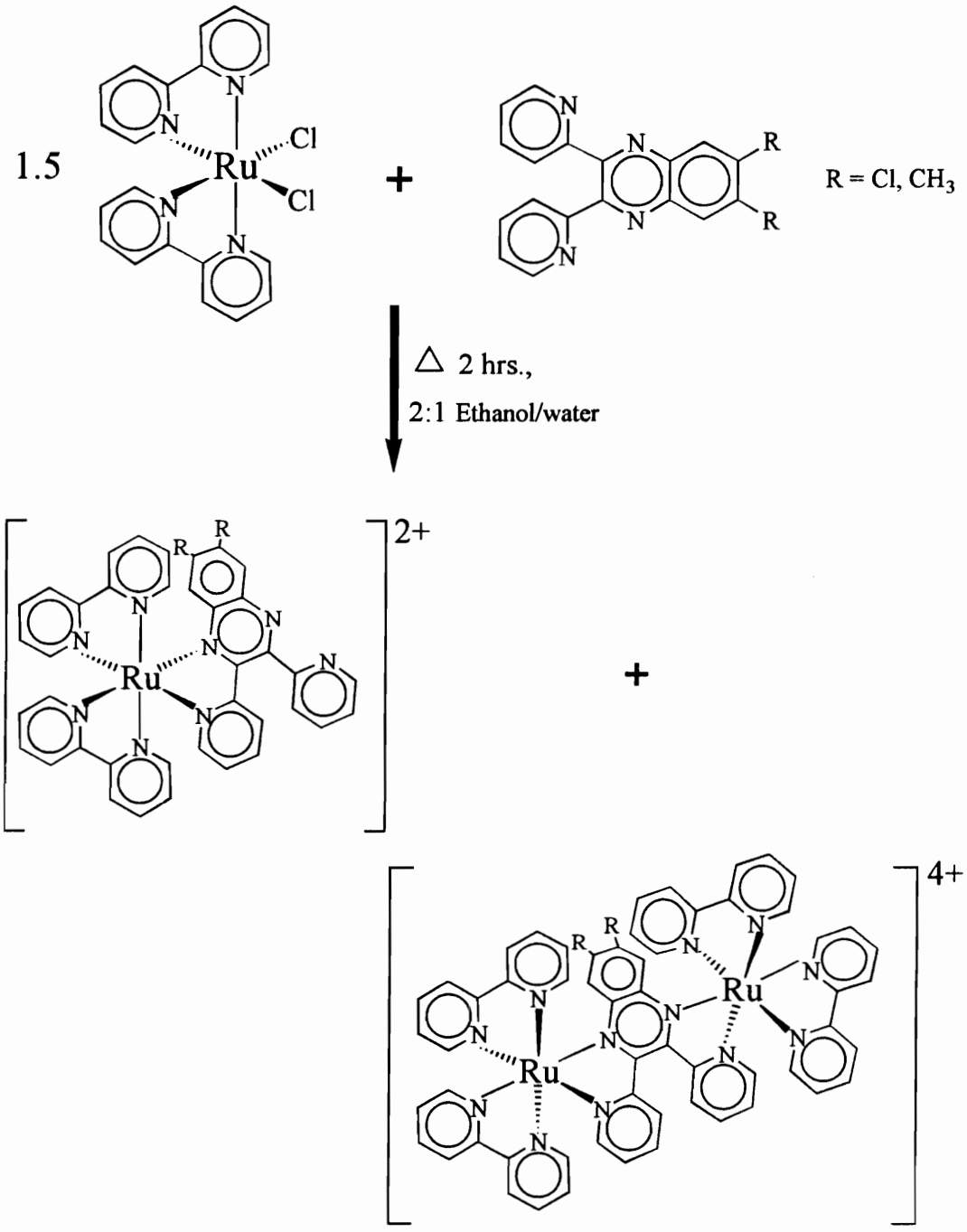

Figure 14. *Synthesis of the Ruthenium Monometallic and Bimetallic Complexes Containing Substituted 2,3-bis(2-pyridyl)quinoxaline Bridging Ligands, $[Ru(bpy)_2(BL)]^{2+}$ and $[Ru(bpy)_2(BL)]_2^{4+}$ (bpy = 2,2'-bipyridine and BL = Me_2dpq, R = CH_3; and Cl_2dpq, R = Cl).*

through the use of electrochemistry, electronic absorption spectroscopy, and emission spectroscopy.

Electrochemistry.

The cyclic voltammetric data for the monometallic complexes $[Ru(bpy)_2(BL)](PF_6)_2$ is summarized in Table 10 and shown in Figure 15.[60] The electrochemistry for the dpp and dpq ruthenium complexes has been previously reported.[36-42] The data presented are the cyclic voltammetric results measured under identical experimental conditions for the entire monometallic series utilizing the dpp, Me_2dpq, dpq, Cl_2dpq and dpb bridging ligands. Each system exhibits one reversible oxidation and three reversible reductions in the acetonitrile electrochemical window. Using the established electrochemical assignments of the analogous dpq monometallic complex, [39] the oxidation is assigned as a Ru^{II}/Ru^{III} couple, and the three reductions assigned as BL/BL^-, bpy/bpy^- and bpy/bpy^- couples, respectively.

In the monometallic series, the reversible ruthenium oxidation increased in potential slightly upon going from dpp to Me_2dpq to dpq to Cl_2dpq to dpb. The π^* orbital energy of the bridging ligand not only affects the potentials of the bridging ligand reductions, but the metal centered oxidations as well. The π-accepting ability of the bridging ligand increases through the series, dpp < Me_2dpq < dpq < Cl_2dpq < dpb. This creates a more positively charged ruthenium metal center in the $[Ru(bpy)_2(BL)]^{2+}$ complexes. This more positive ruthenium metal center is more difficult to oxidize, giving rise to the observed shift in the $E_{1/2}^{oxd}$.

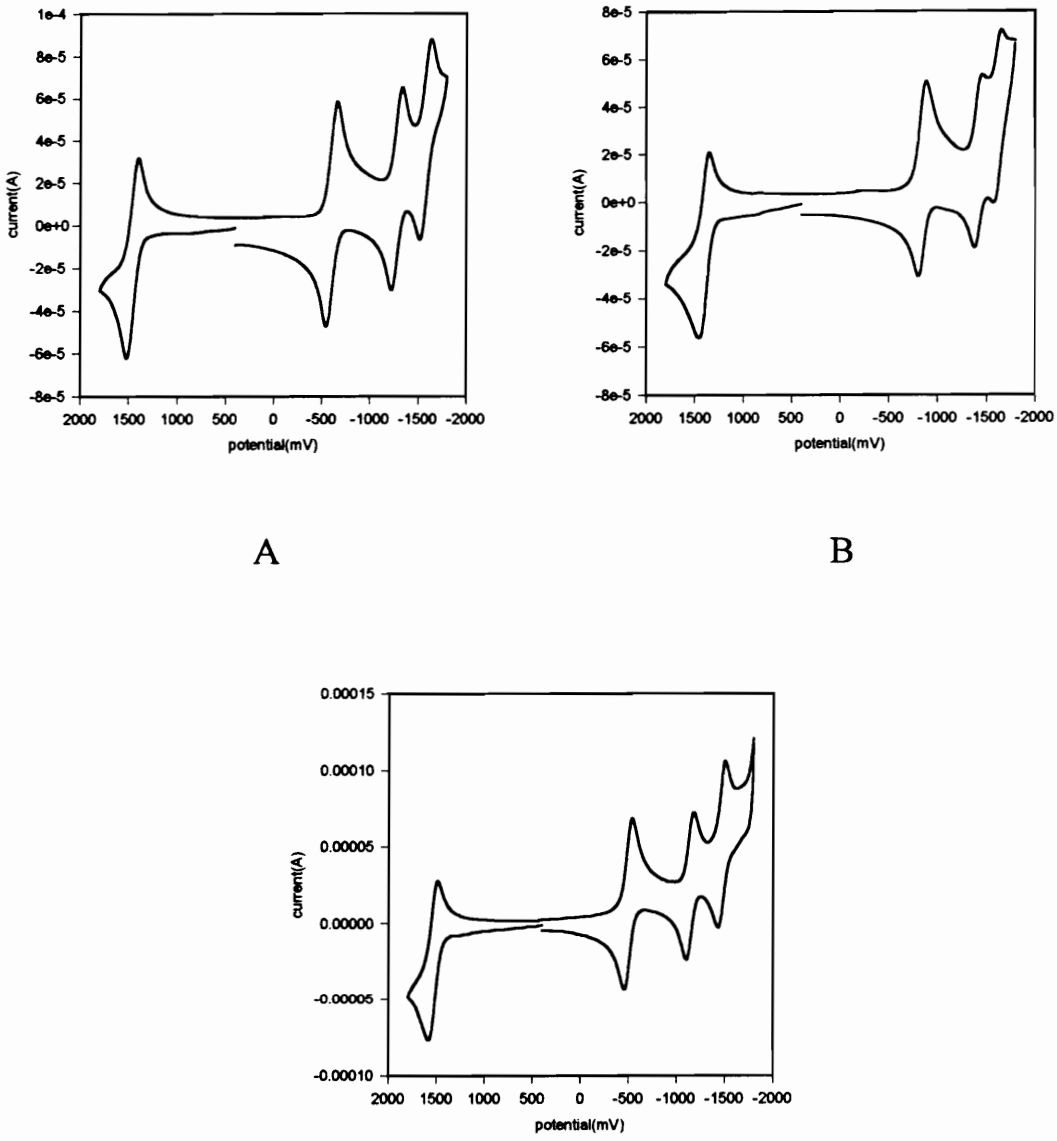

Figure 15. *Cyclic Voltammograms of* $[(bpy)_2Ru(BL)](PF_6)_2$, *bpy = 2,2'-bipyridine and BL =* Cl_2*dpq [A]: 6,7- dichloro-2,3-bis(2-pyridyl)quinoxaline;* Me_2*dpq [B]: 6,7-dimethyl-2,3-bis(2-pyridyl) quinoxaline; and dpb [C]: 2,3-bis(2-pyridyl)benzo quinoxaline.* All cyclic voltammetric data was taken in room temperature spectral grade acetonitrile at a scan rate of 200 mV/s with 0.1 M Bu_4NPF_6 as the supporting electrolyte. The electrodes employed were a platinum working electrode, a platinum wire auxiliary electrode, and a Ag/AgCl reference electrode (0.29 vs. NHE).[a]

[a] Reference 60.

Table 10. Cyclic Voltammetric Data[a] for a Series of Ruthenium Monometallic Complexes Containing Polypyridyl Bridging Ligands. (bpy = 2,2'-bipyridine, dpp = 2,3-bis(2-pyridyl)pyrazine, dpq = 2,3- bis(2-pyridyl)quinoxaline, Me_2dpq = 6,7-dimethyl-2,3-bis(2-pyridyl)quinoxaline, Cl_2dpq = 6,7- dichloro-2,3-bis(2-pyridyl)quinoxaline, and dpb =2,3-bis(2-pyridyl)benzoquinoxaline.)[b]

COMPLEX	Oxidation		Reductions	
	$E_{1/2}$(V)	Assignment	$E_{1/2}$(V)	Assignment
$[(bpy)_3Ru]^{2+}$	+1.36	Ru^{II}/ Ru^{III}	-1.30	bpy,bpy,bpy / bpy,bpy,bpy^-
			-1.49	bpy,bpy,bpy^-/ bpy,bpy^-,bpy^-
			-1.72	bpy,bpy^-,bpy^-/ bpy^-,bpy^-,bpy^-
$[(bpy)_2Ru(dpp)]^{2+}$	+1.38	Ru^{II}/ Ru^{III}	-1.01	dpp / dpp^-
			-1.46	bpy, bpy / bpy^-, bpy
			-1.67	bpy^-, bpy / bpy^-, bpy^-
$[(bpy)_2Ru(Me_2dpq)]^{2+}$	+1.40	Ru^{II}/ Ru^{III}	-0.84	Me_2dpq / Me_2dpq^-
			-1.43	bpy, bpy / bpy^-, bpy
			-1.64	bpy^-, bpy / bpy^-, bpy^-
$[(bpy)_2Ru(dpq)]^{2+}$	+1.47	Ru^{II}/ Ru^{III}	-0.72	dpq / dpq^-
			-1.40	bpy, bpy / bpy^-, bpy
			-1.62	bpy^-, bpy / bpy^-, bpy^-
$[(bpy)_2Ru(Cl_2dpq)]^{2+}$	+1.48	Ru^{II}/ Ru^{III}	-0.63	Cl_2dpq / Cl_2dpq^-
			-1.32	bpy, bpy / bpy^-, bpy
			-1.62	bpy^-, bpy / bpy^-, bpy^-
$[(bpy)_2Ru(dpb)]^{2+}$	+1.48	Ru^{II}/ Ru^{III}	-0.62	dpb / dpb^-
			-1.26	bpy, bpy / bpy^-, bpy
			-1.60	bpy^-, bpy / bpy^-, bpy^-

[a] All cyclic voltammetric data was taken in room temperature spectral grade acetonitrile at a scan rate of 200 mV/s with 0.1 M Bu_4NPF_6 as the supporting electrolyte. The electrodes employed were a platinum working electrode, a platinum wire auxiliary electrode, and a Ag/AgCl reference electrode (0.29 vs. NHE).

[b] Reference 60.

The first reductive process exhibits a major variation in potential as the BL is varied. This bridging ligand based reduction shows a much larger shift than the Ru or bipyridine based couples.[36-42] As the bridging ligand is varied, the first reduction shifts to a more positive potential with the dpp, Me_2dpq, dpq, Cl_2dpq, dpb series, corresponding to stabilization of the π^* orbital energy in the free ligands. The bridging reduction potentials also exhibit a shift upon incorporation into the $[Ru(bpy)_2(BL)]^{2+}$ monometallic complexes. The bridging ligand reductions shift to a more positive potential in the monometallic complexes relative to the free ligands, indicative of a stabilization of the π^* orbital.

The second and third reductions correspond to the bpy/bpy$^-$ couples. It is interesting to note that each bipyridine of the $[Ru(bpy)_2(BL)]^{2+}$ monometallic complexes reduces at a different potential. This indicates that the bipyridines are electronically coupled through the ruthenium center.[33, 65] The bipyridine reductions shift slightly to more positive potential through the series, dpp < Me_2dpq < dpq < Cl_2dpq < dpb. The shift in bipyridine reduction couples in the monometallic complexes is not as dramatic as the shift in the potentials for the BL reduction couples. This shift in potential reflects the increase in the π-accepting ability of the bridging ligand and the increasing positive charge on the ruthenium metal center. The more positive metal center leads to a decrease in the energy of the bipyridine π^* orbital and giving rise to a more easily reduced ligand.

The cyclic voltammetry demonstrates how the substituted 2,3-bis(2-pyridyl)quinoxaline can tune the redox properties of the ruthenium chromophore. The

localization of the first oxidation and reduction in these systems identifies the site of localization of the highest-occupied molecular orbital (HOMO) and lowest-unoccupied molecular orbital (LUMO), respectively. In this series of $[Ru(bpy)_2(BL)](PF_6)_2$ complexes, the HOMO is Ru(dπ) based and the LUMO is BL(π*) based. The HOMO-LUMO gap decreases in energy in the series of complexes where the BL is varied from dpp to Me_2dpq to dpq to Cl_2dpq to dpb. This electrochemically measured energy gap is a measure of the predicted relative energy of the lowest lying optical transition, i.e. the Ru(dπ) → BL(π*) CT band.[3]

Electronic Absorption Spectroscopy.

The absorption and emission spectroscopy of the monometallics show how the light absorbing properties of these chromophores have been tuned (Table 11 and Figure 16).[60] The $[Ru(bpy)_2(Me_2dpq)]^{2+}$ and $[Ru(bpy)_2(Cl_2dpq)]^{2+}$ monometallic complexes exhibit remarkably similar electronic absorption spectra.[60]

The assignments for the electronic absorption spectra of $[Ru(bpy)_2(Me_2dpq)]^{2+}$ and $[Ru(bpy)_2(Cl_2dpq)]^{2+}$ can be made by referencing the established spectrum of the parent complex, $[Ru(bpy)_2(dpq)]^{2+}$.[39, 60] The parent complex has six major peaks in its electronic absorption spectrum. These peaks appear at 284, 325, 350, 391, 426, and 517 nm. The two highest energy peaks of this series are assigned as π → π* intraligand absorptions. The next two highest energy absorptions are assigned as Ru(dπ) → BL(π*) CT and Ru(dπ) → bpy(π*) CT bands, respectively. The final two peaks at 517 and 426 nm are attributed to the Ru(dπ) → BL(π*) CT and Ru(dπ) → bpy(π*) CT, respectively.

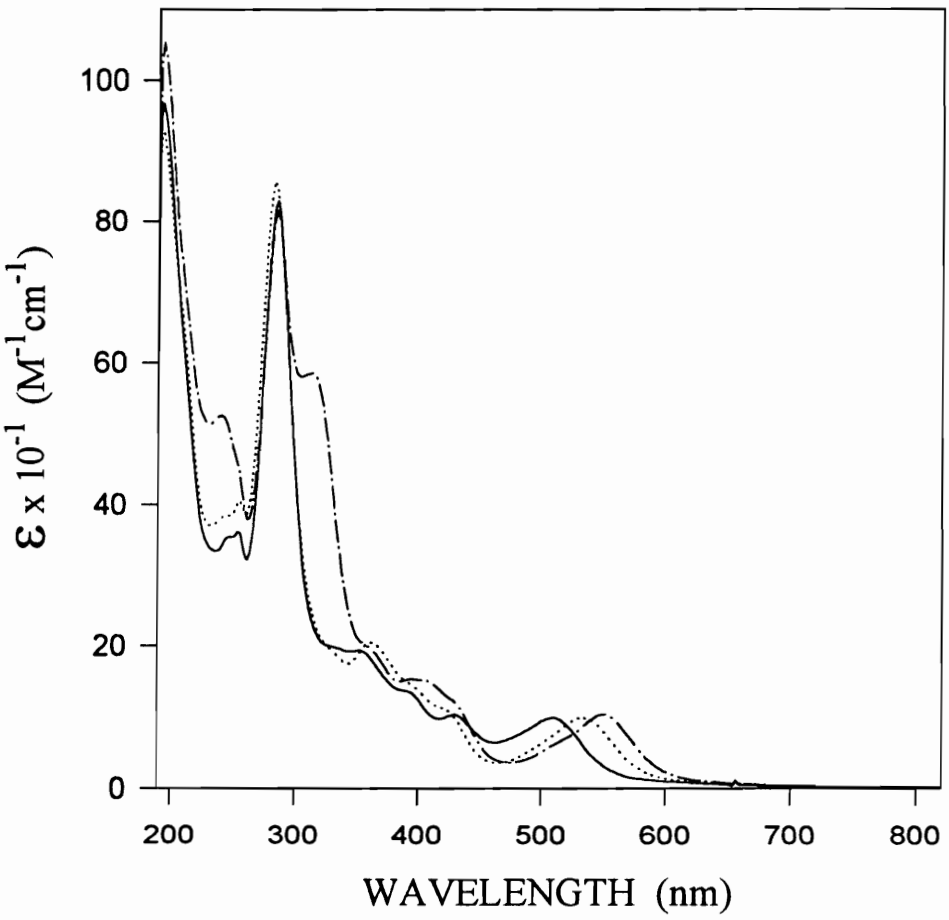

Figure 16. *Electronic Absorption Spectra of the $[Ru(bpy)_2(BL)](PF_6)_2$, bpy = 2,2'-bipyridine and BL = Me_2dpq [—]: 6,7-dimethyl-2,3-bis(2-pyridyl)quinoxaline; Cl_2dpq [• • • •]: 6,7- dichloro-2,3-bis(2-pyridyl)quinoxaline; and dpb [— • —]: 2,3-bis(2-pyridyl)benzoquinoxaline.* All spectra were recorded in room temperature spectral grade acetonitrile.[a]

[a] Reference 60.

Table 11. Electronic Absorption Spectral Data for a Series of Ruthenium Monometallic Bipyridyl Complexes Containing Polypyridyl Bridging Ligands. (bpy = 2,2'-bipyridine, Me_2dpq = 6,7-dimethyl-2,3-bis(2-pyridyl)quinoxaline, Cl_2dpq = 6,7-dichloro-2,3-bis(2-pyridyl)quinoxaline, and dpb = 2,3-bis(2-pyridyl)benzoquinoxaline.)[b]

Complex	λ(nm)[a]	Assignments
$[(bpy)_2Ru(Me_2dpq)]^{2+}$	286	$n \rightarrow \pi^*, \pi \rightarrow \pi^*$ (bpy)
	352	$\pi \rightarrow \pi^*$ (Me_2dpq)
	390	$Ru(d\pi) \rightarrow Me_2dpq(\pi^*)$ CT
	430	$Ru(d\pi) \rightarrow bpy(\pi^*)$ CT
	510	$Ru(d\pi) \rightarrow Me_2dpq(\pi^*)$ CT
$[(bpy)_2Ru(Cl_2dpq)]^{2+}$	284	$n \rightarrow \pi^*, \pi \rightarrow \pi^*$(bpy)
	362	$\pi \rightarrow \pi^*$ (Cl_2dpq)
	396	$Ru(d\pi) \rightarrow Cl_2dpq(\pi^*)$ CT
	422	$Ru(d\pi) \rightarrow bpy(\pi^*)$ CT
	534	$Ru(d\pi) \rightarrow Cl_2dpq(\pi^*)$ CT
$[(bpy)_2Ru(dpb)]^{2+}$	286	$n \rightarrow \pi^*, \pi \rightarrow \pi^*$(bpy)
	320	$\pi \rightarrow \pi^*$ (dpb)
	362	$Ru(d\pi) \rightarrow dpb(\pi^*)$ CT
	430	$Ru(d\pi) \rightarrow bpy(\pi^*)$ CT
	550	$Ru(d\pi) \rightarrow dpb(\pi^*)$ CT

[a]All spectra were recorded in room temperature spectral grade acetonitrile.
[b]Reference 60.

The newly constructed ruthenium monometallics have electronic absorption spectra that contain 5 major peaks. (A sixth peak may be discerned in the 330 nm region, but is not well defined.) The highest energy peak (at 286, 284, and 286 nm in the $[Ru(bpy)_2(Me_2dpq)]^{2+}$, $[Ru(bpy)_2(Cl_2dpq)]^{2+}$ and $[Ru(bpy)_2(dpb)]^{2+}$, respectively) is assigned as a $\pi \rightarrow \pi^*$ bpy intraligand absorption. The peaks that appear at 352 nm in $[Ru(bpy)_2(Me_2dpq)]^{2+}$, 362 nm in $[Ru(bpy)_2(Cl_2dpq)]^{2+}$, and 320 nm in $[Ru(bpy)_2(dpb)]^{2+}$ correspond to BL $\pi \rightarrow \pi^*$ intraligand bands. The next highest energy peak, at 390, 396, and 362 nm in the $[Ru(bpy)_2(Me_2dpq)]^{2+}$, $[Ru(bpy)_2(Cl_2dpq)]^{2+}$ and $[Ru(bpy)_2(dpb)]^{2+}$, respectively, is attributed to $Ru(d\pi) \rightarrow BL(\pi^*)$ charge transfer transitions. The last two peaks of the spectra appear at 430 and 510 nm for $[Ru(bpy)_2(Me_2dpq)]^{2+}$, 422 and 534 nm for $[Ru(bpy)_2(Cl_2dpq)]^{2+}$, and 430 and 550 nm for $[Ru(bpy)_2(dpb)]^{2+}$. In each case the 420 - 430 nm region peak corresponds to a $Ru(d\pi) \rightarrow bpy(\pi^*)$ CT, and the lowest energy absorption is assigned as a $Ru(d\pi) \rightarrow BL(\pi^*)$ CT.

In viewing the electronic absorption spectral data for these ruthenium monometallic complexes, some interesting trends appear. The energy of the lowest lying transition decreases as the π^* orbital energy on the BL is decreased. The cyclic voltammetric data for these monometallic complexes tells us that the $Ru(d\pi)$ HOMO to $BL(\pi^*)$ LUMO gap decreases within the series, dpp > Me_2dpq > dpq > Cl_2dpq > dpb. One thus expects that the λ_{max}^{abs} for this MLCT would decrease as the energy of the gap decreases through the series. This trend in the HOMO-LUMO energy gap should apply to emission spectroscopy as well.

Since the HOMO-LUMO gap decreases in the series of dpp > Me_2dpq > dpq > Cl_2dpq > dpb, the λ_{max}^{em} should exhibit a similar trend. As seen in Table 12, the trend in emission energies for these complexes does indeed follow the same trend. The λ_{max}^{em} of these complexes is at a lower energy than the λ_{max}^{abs}. The absorption value results from a transition from a ground state singlet to an excited state singlet. The emission, however, is an excited state triplet to a ground state singlet. Since the triplet excited state is lower in energy than the excited state singlet, the emission is red-shifted relative to the absorption.[3]

The rate of decay of the excited state depends on the energy of this state and hence the HOMO-LUMO gap. The energy gap law states that as the energy gap between the emissive initial and final state increases, the rate of nonradiative decay of the excited state will likewise increase.[66, 67] In other words, a larger HOMO-LUMO gap should correspond to a longer excited state lifetime, presuming a relative constant k_{rad}. In the case of $[Ru(bpy)_2(dpp)]^{2+}$, $[Ru(bpy)_2(dpq)]^{2+}$ and $[Ru(bpy)_2(dpb)]^{2+}$, this correlation appears valid.[37, 42, 60] Relative to these complexes, the newly prepared monometallics, however, do not possess the expected lifetimes in accordance with the energy gap law. The lifetime of $[Ru(bpy)_2(Me_2dpq)]^{2+}$ should fall between $[Ru(bpy)_2(dpp)]^{2+}$ and $[Ru(bpy)_2(dpq)]^{2+}$. Likewise, the lifetime for $[Ru(bpy)_2(Cl_2dpq)]^{2+}$ would be predicted to fall between $[Ru(bpy)_2(dpq)]^{2+}$ and $[Ru(bpy)_2(dpb)]^{2+}$. Although these new chromophores will still be useful in a covalently attached photosensitizing scheme, the Me_2dpq and Cl_2dpq complexes exhibit lifetimes lower than predicted. This decrease in the excited state

Table 12. Photochemical Data for a Series of Ruthenium Monometallic Bipyridyl Complexes Containing Polypyridyl Bridging Ligands. (bpy = 2,2'-bipyridine, dpp = 2,3-bis(2-pyridyl)pyrazine, dpq = 2,3-bis(2-pyridyl)quinoxaline, Me_2dpq = 6,7-dimethyl-2,3-bis(2-pyridyl)quinoxaline, Cl_2dpq = 6,7- dichloro-2,3-bis(2-pyridyl)quinoxaline, and dpb = 2,3-bis(2-pyridyl)benzoquinoxaline.)[a]

COMPLEX	λ_{max} (nm)[b]		τ (ns)[d]
	Absorption[c]	Emission	
$[(bpy)_3Ru]^{2+}$	450	603	850
$[(bpy)_2Ru(dpp)]^{2+}$	464	660	230
$[(bpy)_2Ru(Me_2dpq)]^{2+}$	508	750	20
$[(bpy)_2Ru(dpq)]^{2+}$	517	766	70
$[(bpy)_2Ru(Cl_2dpq)]^{2+}$	534	800	10
$[(bpy)_2Ru(dpb)]^{2+}$	550	810	60

[a]Reference 60.
[b]All spectra were recorded in room temperature spectral grade acetonitrile.
[c]The lowest energy absorption maxima for the complex.
[d]The lifetime of the complex, τ , was recorded at room temperature in deoxygenated spectral grade acetonitrile.

lifetimes could be attributed to the increased vibrational contribution resulting in an enhanced nonradiative decay constant.

Now that both the electrochemical and spectroscopic data are in hand, the two measurements of the HOMO-LUMO energy gap can be correlated. As noted by other authors,[68, 69] the electrochemical energy gap and spectroscopic energy gap can be correlated if the orbitals involving the electrochemical processes corresponds to the spectroscopic process. In the case of this series of monometallic complexes, the first oxidation is ruthenium and first reduction process is BL based, therefore a correlation to the Ru(dπ) →BL(π*) CT can be drawn.

The correlation between the optical and electrochemical measurement of the HOMO-LUMO energy gap is shown below [68, 69]

$$E_{abs} = \Delta E_{1/2} + \chi_i + \chi_o + Q + \Delta\Delta G_s + \Delta(sol)$$

χ_i and χ_o are the vibrational (inner) and solvation (outer) reorganization energies. The free energy constant Q takes into consideration electron transfer from the reduced to oxidized species. $\Delta\Delta G_s = 2\,\Delta G_s - \Delta G_s^{+} - \Delta G_s^{-}$, where ΔG_s is the solvation free energy for the ground state; ΔG_s is the solvation free energy of the oxidized ground state; ΔG_s^{-} is the solvation free energy of the reduced ground state. Finally, Δ(sol) defines the difference in the solvation free energy of the ground and excited state. This equation can be shortened to a more manageable size of $E_{abs} = m\Delta E_{1/2}$ + constant, presuming that χ_i,

χ_o, Q, $\Delta\Delta G_s$ and Δ(sol) do not change within a series of similar complexes. This is a mathematical formula for a straight line.

This relationship can yield interesting information about a series of similar complexes.[68, 69] The *y*-intercept is a conglomeration of all the solvation and reorganization factors. The slope of the line, *m*, may not be equal to one, depending on whether χ_i, χ_o, Q, $\Delta\Delta G_s$ or Δ(sol) have a dependence on $\Delta E_{1/2}$, the electrochemical potential involved in the relationship. The correlation coefficient of the least-squares fit to the data is also important. The amount of scatter in the data is dependent on the variation in the χ_i and χ_o, reorganization energies, as well as the solvation energy. Therefore, the fit of the data to a straight line can aide in forcasting spectral data from electrochemical data, or vice versa. It can also lend insight into other factors that limit the application of this relationship.

Figure 17 shows a plot of E_{abs}(MLCT) versus $\Delta E_{1/2}$ (where $\Delta E_{1/2} = E_{1/2}(Ru^{II}/Ru^{III}) - E_{1/2}(BL/BL^-)$).[60] This data yields a straight line with a correlation coefficient of 0.99, a *y*-intercept of -0.53, and a slope of 1.34. From these values one can see that the electrochemical and spectroscopic data do not give the same values for the HOMO-LUMO energy gap. The non-zero *y*-intercept can be attributed to the differences of timescale for the two means of measurement. The optical transition occurs too quickly for the internuclear distances to adjust to the new electronic configuration or the flipping of the electron's spin. Since the slope of the line is not equal to one, the parameters χ_i, χ_o, Q, $\Delta\Delta G_s$ or Δ(sol) may have some dependence on the $\Delta E_{1/2}$. The correlation coefficient

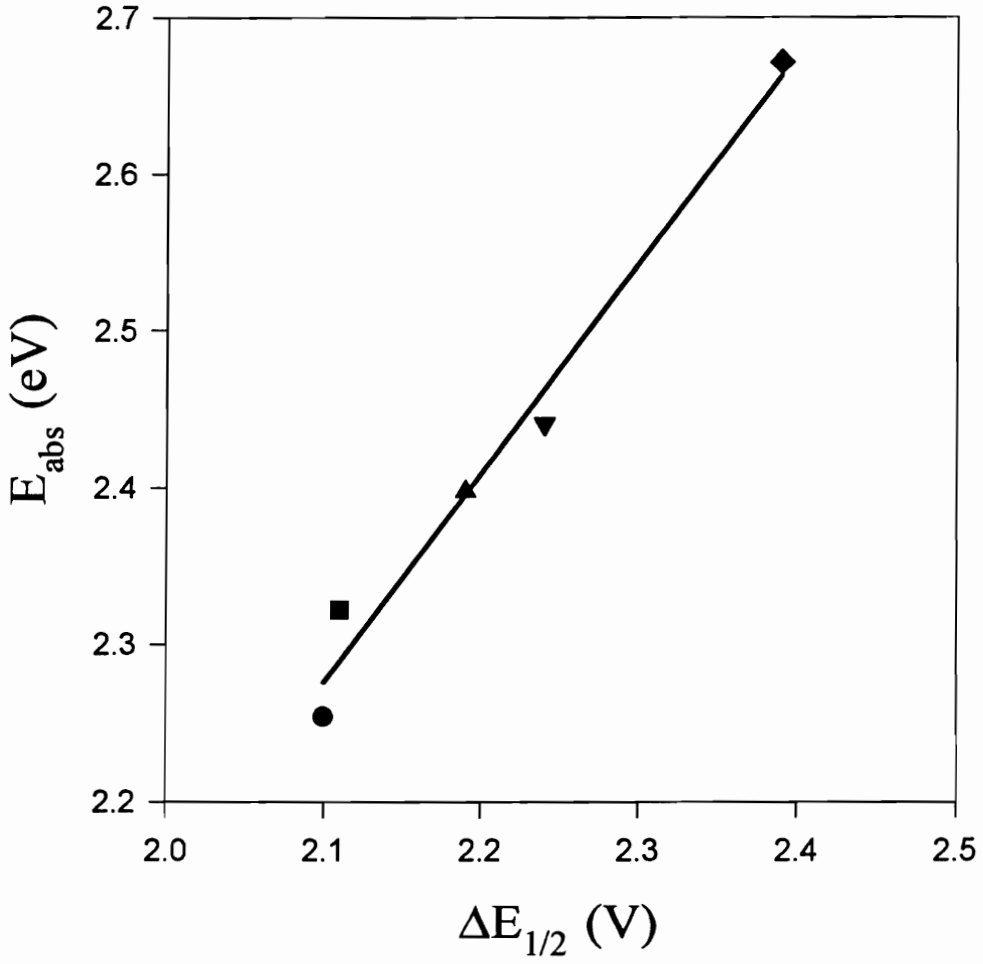

Figure 17. *Plot of E_{abs}(Ru(dπ) → π*(BL) CT)) versus $\Delta E_{1/2}$ ($\Delta E_{1/2} = E_{1/2}(Ru^{II}/Ru^{III}) - E_{1/2}(BL/BL^{-})$) for a Series of Ruthenium Monometallic Complexes Containing Polypyridyl Bridging Ligands, $[Ru(bpy)_2(BL)](PF_6)_2$ (bpy = 2,2'bipyridine and BL= dpp [◆]: 2,3-bis(2-pyridyl)pyrazine; Me_2dpq [▼]: 6,7-dimethyl-2,3-(2-pyridyl)quinoxaline; dpq [▲]: 2,3-bis(2-pyridyl)quinoxaline; Cl_2dpq [■]: 6,7-chloro-2,3-(2-pyridyl)quinoxaline and dpb [●]: 2,3-bis(2-pyridyl)benzoquinoxaline.)*[a]
[a]Reference 60.

of 0.99 corresponds to little scattering of the data around the best fit line. Therefore, the inner and reorganization energies do not appear to vary with $\Delta E_{1/2}$, and so it would seem that the remaining parameters have a dependence of $\Delta E_{1/2}$.

Investigation of the Ruthenium(II) Bimetallic Complexes Containing the Substituted 2,3-bis(2-pyridyl)quinoxaline Bridging Ligands.

Synthesis.

The bimetallic complexes of the substituted 2,3-bis(2-pyridyl)quinoxaline and dpb were synthesized and characterized. The systems, $\{[(bpy)_2Ru]_2(Me_2dpq)\}(PF_6)_4$, $\{[(bpy)_2Ru]_2(Cl_2dpq)\}(PF_6)_4$, and $\{[(bpy)_2Ru]_2(dpb)\}(PF_6)_4$ were synthesized in hopes of elucidating the effects a second metal center on the properties of these complexes. The bimetallic and monometallic complexes were both products of one reaction. After this series of complexes was synthesized each complex was characterized with cyclic voltammetry, electronic absorption spectroscopy, emission spectroscopy, and excited state lifetime measurements.

Electrochemistry.

The cyclic voltammograms of the bimetallic systems are shown in Figure 18 and their data is summarized in Table 13.[60] Each voltammogram exhibits two reversible oxidations and four reversible reductions between -2.0 and 2.0 V vs Ag/AgCl. The two oxidations of the bimetallic complexes correspond to the sequential oxidation of the two equivalent ruthenium metal centers. As in the monometallic systems, the ruthenium metal centers become harder to oxidize as the bridging ligand becomes more π-accepting.

Table 13. Cyclic Voltammetric Data[a] for a Series of Ruthenium Bimetallic Bipyridyl Complexes Containing Polypyridyl Bridging Ligands. (bpy = 2,2'-bipyridine, dpp = 2,3-bis(2-pyridyl)pyrazine, dpq = 2,3- bis(2-pyridyl)quinoxaline, Me_2dpq = 6,7-dimethyl-2,3-bis(2-pyridyl)quinoxaline, Cl_2dpq = 6,7-dichloro-2,3-bis(2-pyridyl)quinoxaline, and dpb = 2,3-bis(2-pyridyl)benzoquinoxaline.)[b]

COMPLEX	Oxidations		Reductions	
	$E_{1/2}$(V)	Assignment	$E_{1/2}$(V)	Assignment
$\{[(bpy)_2Ru]_2(dpp)\}^{4+}$	+1.43	Ru^{II}/Ru^{III}	-0.61	dpp/dpp^-
	+1.61	Ru^{II}/Ru^{III}	-1.09	dpp^-/dpp^{2-}
$\{[(bpy)_2Ru]_2(Me_2dpq)\}^{4+}$	+1.48	Ru^{II}/Ru^{III}	-0.41	Me_2dpq/Me_2dpq^-
	+1.65	Ru^{II}/Ru^{III}	-1.15	Me_2dpq^-/Me_2dpq^{2-}
$\{[(bpy)_2Ru]_2(dpq)\}^{4+}$	+1.52	Ru^{II}/Ru^{III}	-0.32	dpq/dpq^-
	+1.67	Ru^{II}/Ru^{III}	-1.10	dpq^-/dpq^{2-}
$\{[(bpy)_2Ru]_2(Cl_2dpq)\}^{4+}$	+1.53	Ru^{II}/Ru^{III}	-0.20	Cl_2dpq/Cl_2dpq^-
	+1.72	Ru^{II}/Ru^{III}	-0.89	Cl_2dpq^-/Cl_2dpq^{2-}
$\{[(bpy)_2Ru]_2(dpb)\}^{4+}$	+1.52	Ru^{II}/Ru^{III}	-0.22	dpb/dpb^-
	+1.70	Ru^{II}/Ru^{III}	-0.87	dpb^-/dpb^{2-}

[a] All cyclic voltammetric data was taken in room temperature spectral grade acetonitrile at a scan rate of 200 mV with 0.1 M Bu_4NPF_6 as the supporting electrolyte. The electrodes employed were a platinum working electrode, a platinum wire auxiliary electrode, and a Ag/AgCl reference electrode (0.29 vs. NHE).

[b] Reference 60.

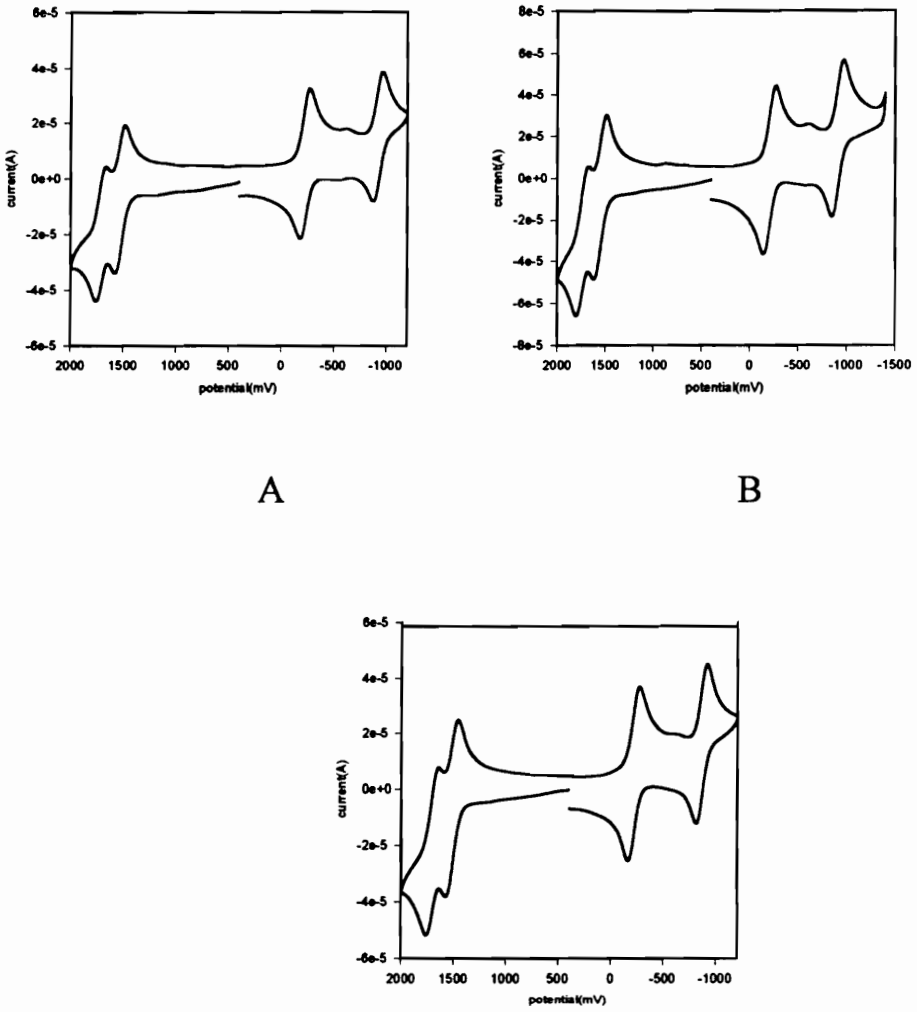

Figure 18. *Cyclic Voltammograms of $\{[(bpy)_2Ru]_2(BL)\}(PF_6)_4$, bpy = 2,2'-bipyridine and BL = Me_2dpq [A]: 6,7-dimethyl-2,3-bis(2-pyridyl)quinoxaline; Cl_2dpq [B]: 6,7-dichloro-2,3-bis(2-pyridyl)quinoxaline, and dpb [C]: 2,3-bis(2-pyridyl)benzoquinoxaline.* All cyclic voltammetric data was taken in room temperature spectral grade acetonitrile at a scan rate of 200 mV/s with 0.1 M Bu_4NPF_6 as the supporting electrolyte. The electrodes employed were a platinum working electrode, a platinum wire auxiliary electrode, and a Ag/AgCl reference electrode (0.29 vs. NHE).[a]

[a] Reference 60.

In general, both metal centers of the bimetallic systems are more difficult to oxidize than the monometallic metal centers. This may be attributed to the effect that the presence of the second metal center has on the system.

The two ruthenium metal centers oxidize at different potentials due to the fact that they are electronically coupled through the bridging ligand. The degree of metal-metal communication can be determined by investigating the stability of the mixed-valence Ru^{II}, Ru^{III} system.

$$(Ru^{II}, Ru^{II})^{4+} + (Ru^{III}, Ru^{III})^{6+} \underset{}{\overset{K_{com}}{\rightleftharpoons}} 2(Ru^{II}, Ru^{III})^{5+}$$

The comproportionation of a mixed-valence complex can be evaluated with the comproportionation constant K_{com}, which is calculated with the use of $\Delta E_{1/2}$ ($\Delta E_{1/2} = E_{1/2}^{oxid(1)} - E_{1/2}^{oxid(2)}$) in the equation $log\, K_{com} = (\Delta E_{1/2} / 0.059\ V)$.[70, 71] A large K_{com} value (if $K_{com} >> 4$)[70, 71] denotes a tendency for the equilibrium to favor the mixed-valence form. The values for the three newly synthesized bimetallic complexes and the dpq complex are: $K_{com}\{[(bpy)_2Ru]_2(Me_2dpq)\}(PF_6)_4] = 7.5\times10^2$; $K_{com}\{[(bpy)_2Ru]_2(Cl_2dpq)\}(PF_6)_4 = 1.7\times10^3$; $K_{com}\{[(bpy)_2Ru]_2(dpb)\}(PF_6)_4] = 1.1\times10^3$; and $K_{com}\{[(bpy)_2Ru]_2(dpq)\}(PF_6)_4 = 3.4\times10^2$. These K_{com} values are all very similar and indicate a large degree of stabilization of the mixed-valence species in these electronically coupled systems. The introduction of the second metal center has caused a general shift of the ruthenium metal center oxidation potentials in relation to the monometallic systems. In comparison to the monometallic systems, the oxidation potential of the bimetallic species have shifted to a more positive

potential. This results from an enhanced π-backbonding of the ruthenium metal centers to the more electron deficient BL.

The variation of the bridging ligand still has a slight effect on the oxidation potential of the ruthenium metal centers as observed in the monometallic complexes. The reductive electrochemistry in the bimetallic systems is drastically different from those of the monometallic systems. In the bimetallic complexes, the first two reductions are BL based,[36-42] the first reduction being assigned as BL/BL^-, and the second BL^-/BL^{2-}. This sequential placement of the first two electrons on the bridging ligand is in contrast to the monometallic systems. In the case of the monometallic complexes, the first electron is placed on the BL and the second on a bipyridine. This shift in order is due to the presence of the two positive metal centers. The result of the two coordinated metal centers is a dramatic stabilization of the BL based π* orbital. In general, both of the BL reductions shift to a more positive potential as the BL is varied from dpp to Me_2dpq to dpq to Cl_2dpq to dpb. This shift reflects the lower energy π* orbital of the BL through the series.

The HOMO in these bimetallic systems is Ru(dπ) based and the LUMO is BL(π*) based. In viewing the electrochemical data, the ruthenium oxidation potentials do not shift as drastically as the BL based reduction potentials upon variation of the BL. Thus, the energy of the Ru(dπ) orbital remains moderately constant, while the energy of the BL(π*) orbital varies to a greater degree. The significant change in the BL(π*) orbital energy allows for the systematic variation of the HOMO-LUMO energy gap. The

bimetallic systems exhibit a smaller HOMO-LUMO gap relative to the monometallic systems. Therefore, one would predict a red-shifted Ru(dπ) → BL(π*) CT in the bimetallic complexes in comparison to the monometallic complexes.

Electronic Absorption Spectroscopy.

The electronic absorption spectra of the newly synthesized bimetallic complexes, $\{[(bpy)_2Ru]_2(Me_2dpq)\}(PF_6)_4$, $\{[(bpy)_2Ru]_2(Cl_2dpq)\}(PF_6)_4$, and $\{[(bpy)_2Ru]_2(dpb)\}(PF_6)_4$ are shown in Figure 19 and summarized in Table 14.[60] These complexes exhibit similar electronic absorption spectra. Each spectrum contains six major characteristic peaks. These peaks can be assigned by comparing them to their monometallic counterparts, and making reference to the established spectrum of the parent complex, $\{[(bpy)_2Ru]_2(dpq)\}(PF_6)_4$.[39] The highest energy peak at 284 nm, for all three complexes, is assigned as bipyridine n → π* and π → π* intraligand absorptions. The BL π → π* intraligand absorptions appear at 316 nm for each substituted complex and 372 nm for the dpb complex. At 390, 394, and 410 nm for the methyl, chloro- and dpb complexes respectively, a higher energy Ru(dπ) → BL(π*) CT transition is observed. Another charge transfer absorption band is seen at 408 nm ($\{[(bpy)_2Ru]_2(Me_2dpq)\}^{4+}$), 412 nm ($\{[(bpy)_2Ru]_2(Cl_2dpq)\}^{4+}$), 424 nm ($\{[(bpy)_2Ru]_2(dpb)\}^{4+}$) and it is Ru(dπ) → bpy(π*) based. The lowest lying λ_{max}^{abs} of these systems is a Ru(dπ) → BL(π*) CT and appears at 596, 630, and 644 nm for the $\{[(bpy)_2Ru]_2(Me_2dpq)\}^{4+}$, $\{[(bpy)_2Ru]_2(Cl_2dpq)\}^{4+}$, and $\{[(bpy)_2Ru]_2(dpb)\}^{4+}$ complexes, respectively. The lowest energy MLCT band, corresponding to the Ru(dπ) → BL(π*) CT, decreases in energy

Table 14. Electronic Absorption Spectral Data[a] for a Series of Ruthenium Bimetallic Bipyridyl Complexes Containing Polypyridyl Bridging Ligands. (bpy = 2,2'-bipyridine, Me_2dpq = 6,7-dimethyl-2,3-bis(2-pyridyl)quinoxaline, Cl_2dpq = 6,7- dichloro-2,3-bis(2-pyridyl)quinoxaline, and dpb = 2,3-bis(2-pyridyl)benzoquinoxaline)[b]

Complex	λ(nm)[a]	Assignments
$\{[(bpy)_2Ru]_2(Me_2dpq)\}^{4+}$	284	$n \rightarrow \pi^*, \pi \rightarrow \pi^*$ (bpy)
	316	$\pi \rightarrow \pi^*$ (Me_2dpq)
	390	$Ru(d\pi) \rightarrow Me_2dpq(\pi^*)$
	408	$Ru(d\pi) \rightarrow bpy(\pi^*)$
	596	$Ru(d\pi) \rightarrow Me_2dpq(\pi^*)$
$\{[(bpy)_2Ru]_2(Cl_2dpq)\}^{4+}$	284	$n \rightarrow \pi^*, \pi \rightarrow \pi^*$ (bpy)
	316	$\pi \rightarrow \pi^*$ (Cl_2dpq)
	394	$Ru(d\pi) \rightarrow Cl_2dpq(\pi^*)$
	412	$Ru(d\pi) \rightarrow bpy(\pi^*)$
	630	$Ru(d\pi) \rightarrow Cl_2dpq(\pi^*)$
$\{[(bpy)_2Ru]_2(dpb)\}^{4+}$	284	$n \rightarrow \pi^*, \pi \rightarrow \pi^*$ (bpy)
	338	$n \rightarrow \pi^*, \pi \rightarrow \pi^*$ (bpy)
	372	$\pi \rightarrow \pi^*$ (dpb)
	410	$Ru(d\pi) \rightarrow dpb(\pi^*)$
	424	$Ru(d\pi) \rightarrow bpy(\pi^*)$
	644	$Ru(d\pi) \rightarrow dpb(\pi^*)$

[a]All spectra were recorded in room temperature spectral grade acetonitrile.
[b]Reference 60.

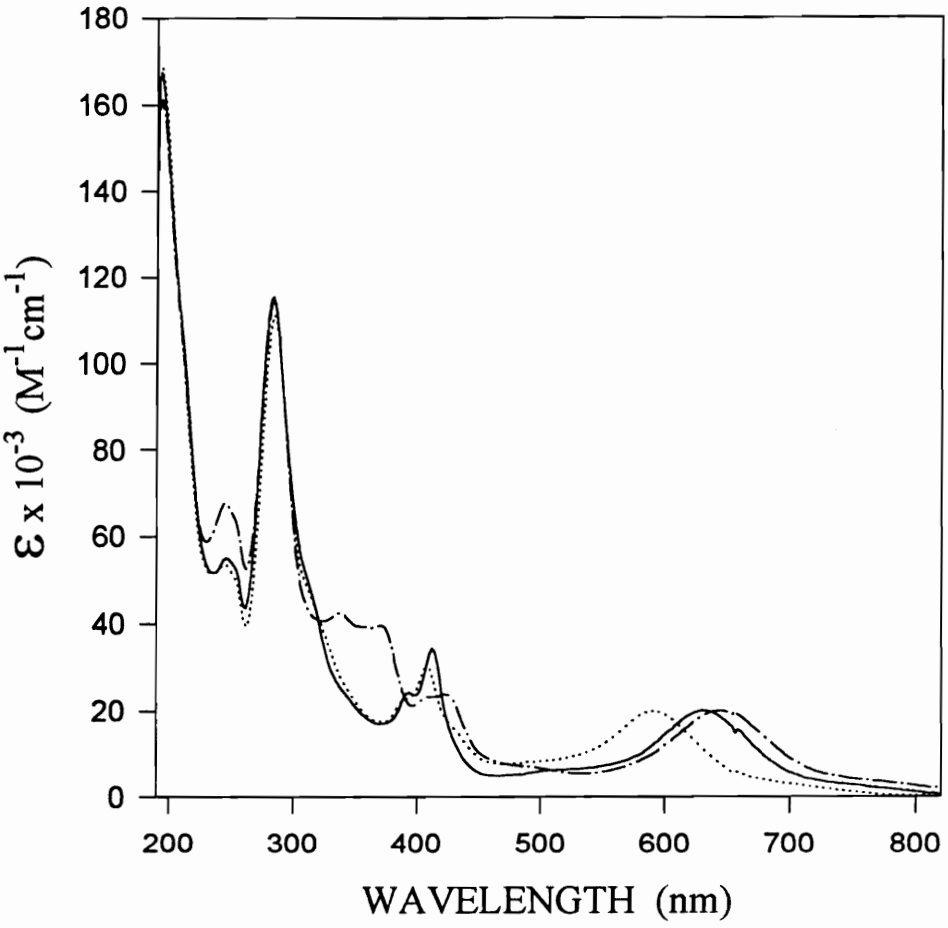

Figure 19. *Electronic Absorption Spectra of the {[(bpy)$_2$Ru]$_2$(BL)}(PF$_6$)$_4$, bpy = 2,2'-bipyridine and BL = Me$_2$dpq [• • • •]: 6,7-dimethyl-2,3-bis(2-pyridyl)quinoxaline; Cl$_2$dpq [—]: 6,7-dichloro-2,3-bis(2-pyridyl)quinoxaline, and dpb [— • —]: 2,3-bis(2-pyridyl)benzoquinoxaline.* All spectra were recorded in room temperature spectral grade acetonitrile.[a]

[a]Reference 60.

through the bimetallic series as the BL is varied from dpp to dpq to Cl_2dpq to Me_2dqq to dpb. After viewing the electrochemical data, one would expect this trend.

The lowest energy λ_{max}^{abs} of the bimetallic systems occurs at a lower energy in comparison to the monometallic systems. The electrochemical data shows that, in general, the BL(π^*) orbital energy is lower for the bimetallic systems versus the monometallic systems. Therefore, an overall shift of the λ_{max}^{abs} for the bimetallic complexes is seen since the Ru($d\pi$) does not drastically change with the addition of a second metal center.

The emission data for these bimetallic complexes is shown in Table 15.[60] The emission for the $\{[(bpy)_2Ru]_2(dpb)\}(PF_6)_4$ was not observed and, therefore, not reported. It is expected to occur in the near-IR region of the spectrum, which is beyond the detection limits of the fluorometer used. Since the emissive state involves the promotion of an electron from the HOMO to the LUMO, the emission data should show the same trend as for the λ_{max}^{abs} data. A stepwise decrease is seen in the emission energy for the bimetallic complexes upon changing the BL from dpp to Me_2dpq to dpq to Cl_2dpq to dpb. The alteration of the bridging has led to a sequential variation in the emission energy for these complexes.

As discussed in the section on their monometallic analogs, a correlation between the electrochemical and spectroscopic HOMO-LUMO energy gap may be drawn. A combined plot of both the mono- and bimetallic E_{abs} (MLCT) versus $\Delta E_{1/2}$ values can be made to correlate the electrochemical and spectroscopic energy gap. This is valid since both sets of systems are similar. Figure 20 shows the results of combining the mono- and

Table 15. Photochemical Data for a Series of Ruthenium Bimetallic Bipyridyl Complexes Containing Polypyridyl Bridging Ligands. (bpy = 2,2'-bipyrdine, dpp = 2,3-bis(2-pyridyl)pyrazine; dpq = 2,3- bis(2-pyridyl)quinoxaline; Me_2dpq = 6,7-dimethyl-2,3-bis(2-pyridyl)quinoxaline; Cl_2dpq = 6,7-dichloro-2,3-bis(2-pyridyl)quinoxaline; dpb = 2,3-bis 2-pyridyl)benzoquinoxaline.)[a]

COMPLEX	λ_{max} (nm)[b]	
	Absorption[c]	Emission
$\{[(bpy)_2Ru]_2(dpp)\}^{4+}$	525	755
$\{[(bpy)_2Ru]_2(Me_2dpq)\}^{4+}$	593	808
$\{[(bpy)_2Ru]_2(dpq)\}^{4+}$	603	822
$\{[(bpy)_2Ru]_2(Cl_2dpq)\}^{4+}$	635	860
$\{[(bpy)_2Ru]_2(dpb)\}^{4+}$	644	—

[a]Reference 60.
[b]All spectra were recorded in room temperature spectral grade acetonitrile.
[c]The lowest energy absorption maxima for the complex.

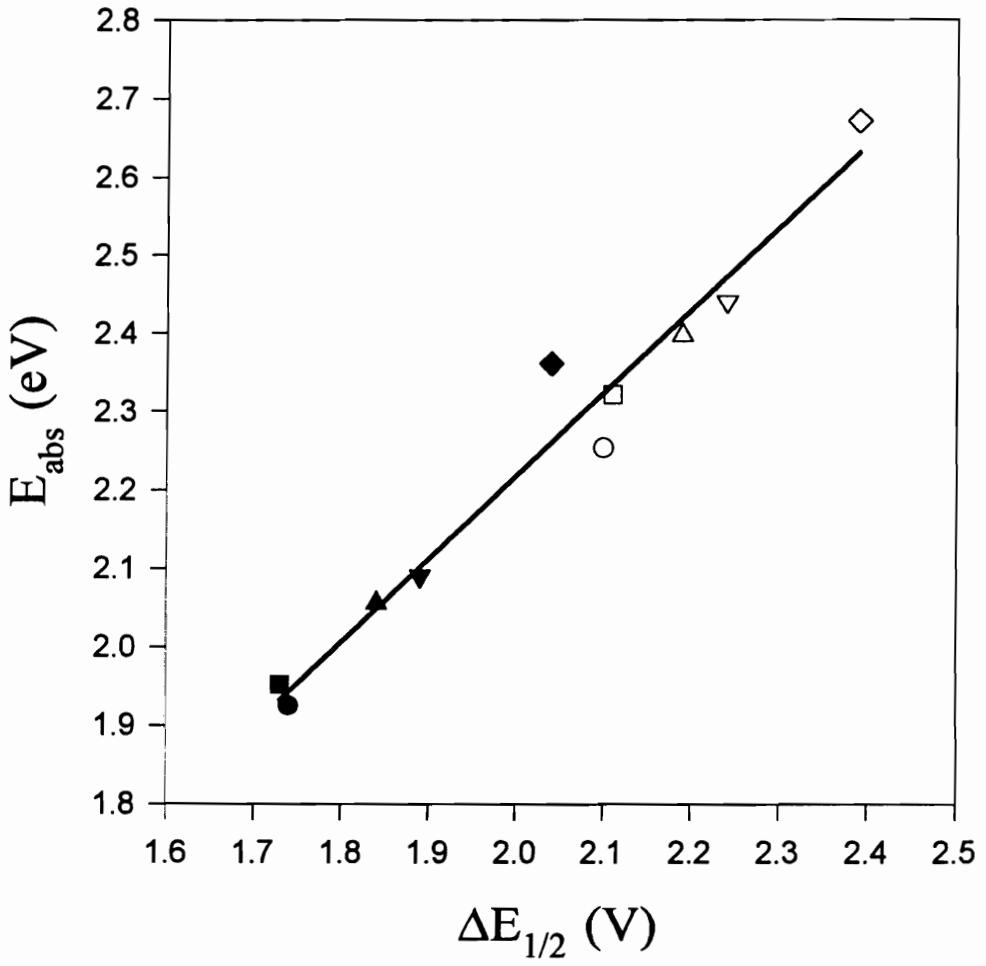

Figure 20. *Plot of E_{abs} (Ru(dπ) → π*(BL) CT) versus $\Delta E_{1/2}$ ($\Delta E_{1/2} = E_{1/2}(Ru^{II}/Ru^{III}) - E_{1/2}(BL/BL^{-})$) for a Series of Ruthenium Mono- and Bimetallic Complexes Containing Polypyridyl Bridging Ligands, $[Ru(bpy)_2(BL)](PF_6)_2$ and $[Ru(bpy)_2(BL)]_2(PF_6)_4$ (bpy = 2,2'-bipyridine and BL = dpp, Me_2dpq, dpq, Cl_2dp, and dpb).* For $[Ru(bpy)_2(BL)](PF_6)_2$, BL = dpp [◇]: 2,3-bis(2-pyridyl)pyrazine, Me_2dpq [▽]: 6,7-dimethyl-2,3-bis(2-pyridyl)quinoxaline, dpq [△]: 2,3-bis(2-pyridyl)quinoxaline, Cl_2dpq [□]: 6,7-chloro-2,3-bis(2-pyridyl)quinoxaline, and dpb [○]: 2,3-bis(2-pyridyl)benzoquinoxaline; for $[Ru(bpy)_2(BL)]_2(PF_6)_4$, BL = dpp [◆], Me_2dpq [▼], dpq [▲], Cl_2dpq [■], and dpb [●].[a]
[a]Reference 60.

bi- metallic data. The correlation coefficient for this graph is 0.981, a *y*-intercept of 0.106, and a slope of 1.1. The correlation coefficient does slightly deteriorate upon combination of the data, yet the *y*-intercept is closer to a zero value and the slope approaches 1. The slope approaching 1 is predicted and agrees that χ_i, χ_o, Q, $\Delta\Delta G_s$ and Δ(sol) do not vary within this series.

Conclusions.

The inclusion of methyl or chloro substituent groups and an aromatic ring into the dpq structure has been shown to tune the π^* orbital energy of the polypyridyl bridging ligand series. The synthesis and investigation of the mono- and bimetallic ruthenium systems have shown that the lowest lying electronic absorption is Ru(dπ) $\rightarrow$ BL(π^*) CT based. The $[Ru(bpy)_2(BL)]^{2+}$ chromophore, depending on the substituent of choice, can now be tuned to contain more widely varied photophysical characteristics. A correlation exists between the optical and electrochemical measurements of the HOMO-LUMO energy gap in these complexes, $[Ru(bpy)_2(BL)]^{2+}$ and $[Ru(bpy)_2(BL)]_2^{4+}$. The polypyridyl bridging ligand series may be further extended by the addition of various substituent groups onto the dpp and dpb structure as well. This would produce a vast series of ligands containing a wide range of π^* orbital energies. The inclusion of these ruthenium chromophores into supramolecular complexes will not only extend the tuning abilities photochemical molecular devices, but also aid in the elucidation of their complicated spectroscopy and photochemistry.

CHAPTER 4.

SYNTHESIS AND CHARACTERIZATION OF A SERIES OF MIXED-METAL Ir^{III}/Ru^{II} TRIMETALLIC COMPLEXES DEVELOPED FOR PHOTOINITIATED ELECTRON COLLECTION.

Introduction.

A main objective in designing a working photoinitiated electron collector (PIEC) is to use light energy to collect reducing equivalents. This requires a coupling of two light absorbers to an electron collector (Figure 1, p.3).[1] Many workers have postulated that simple bimetallics would perform this function.[36-42, 72, 73] Detailed analysis of the properties of typical polyazine bridged bimetallics clearly shows that the two LA are coupled and, thus, can not function independently. Consequently, an intervening spacer that can function as an electron collector is needed. The light absorbing moiety, $[(bpy)_2Ru(BL)]^{2+}$, of the photoinitiated electron collector has been discussed in Chapters 1 and 3. The electron collector fragment, $[Ir(BL)_2CL_2]^+$, has also been previously investigated as discussed in Chapter 1. The next step is to assemble the LA-EC-LA unit. This has been done in the synthesis of the $\{[(bpy)_2Ru(BL)]_2IrCl_2\}(PF_6)_5$ trimetallics.[62, 64, 74] These complexes have been synthesized in a building block approach.

As demonstrated in Figure 21, the two monometallic fragments are synthesized, purified, and characterized prior to the trimetallic synthesis. The ruthenium monometallic $[Ru(bpy)_2Cl_2]$ is combined with the $[Ir(BL)_2Cl_2]^+$ in a 2:1 ratio to produce $\{[(bpy)_2Ru(BL)]_2IrCl_2\}(PF_6)_5$ and purified using size-exclusion chromatography. This building block approach has been successfully implemented in the synthesis of other Ir^{III}

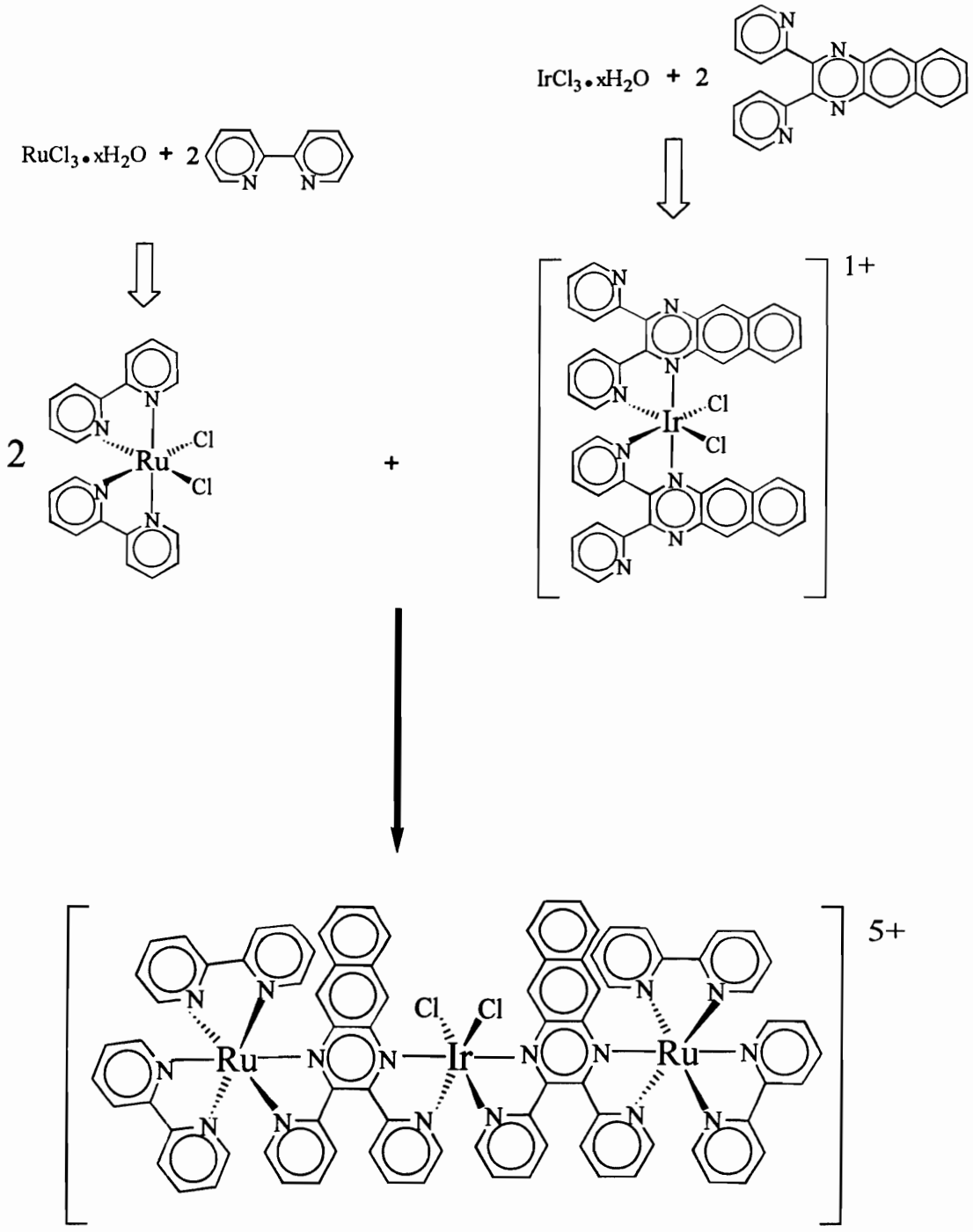

Figure 21. *The Building Block Approach to the Synthesis of the* $\{[(bpy)_2Ru(dpb)]_2IrCl_2\}(PF_6)_5$ *(bpy = 2,2'-bipyridine and dpb = 2,3-bis(2-pyridyl)benzoqunioxaline) Trimetallic Complex.*

systems (BL = dpp or dpq) as well as the $\{[(bpy)_2Ru(BL)]_2RhCl_2\}(PF_6)_5$[64] and $\{[(bpy)_2Ru(BL)]_2OsCl_2\}(PF_6)_5$[75] trimetallic series. This series of nine mixed-metal trimetallics, which vary the central metal and BL, make it possible to elucidate the complicated spectroscopy and electrochemistry of these systems through this application of synthetic modification.[62, 64, 74, 75]

Electrochemistry

The electrochemical data for the $\{[(bpy)_2Ru(BL)]_2IrCl_2\}(PF_6)_5$ trimetallic series is summarized in Table 16.[62] Figure 22 shows cyclic voltammograms of the dpq and dpb trimetallic complexes. The presentation of the two voltammograms visually illustrates the similarity and differences of the trimetallics' electrochemistry. The cyclic voltammograms exhibit one oxidation and seven reductions within the +1.80 to -1.80 V electrochemical window. Figure 23 shows a general electrochemical scheme for this trimetallic series.

The ruthenium based oxidation, $Ru^{II/III}$, remains unchanged at the same potential throughout the series. As one can see from Table 16, the oxidation potential of the ruthenium metal centers is the same, 1.56 V, for all three trimetallic complexes. This oxidation is reversible with a ΔE_p ($\Delta E_p = E_p^a - E_p^c$) of 100 mV and represents two closely spaced $1e^-$ oxidations of the two equivalent ruthenium centers. The overlapping nature of the metal centered oxidations indicates that the ruthenium metal centers do not have any appreciable degree of electronic communication within the trimetallic framework. This is a critical point in the design of our systems. The lack of significant electronic coupling allows each of the two ruthenium chromophores to function independently.

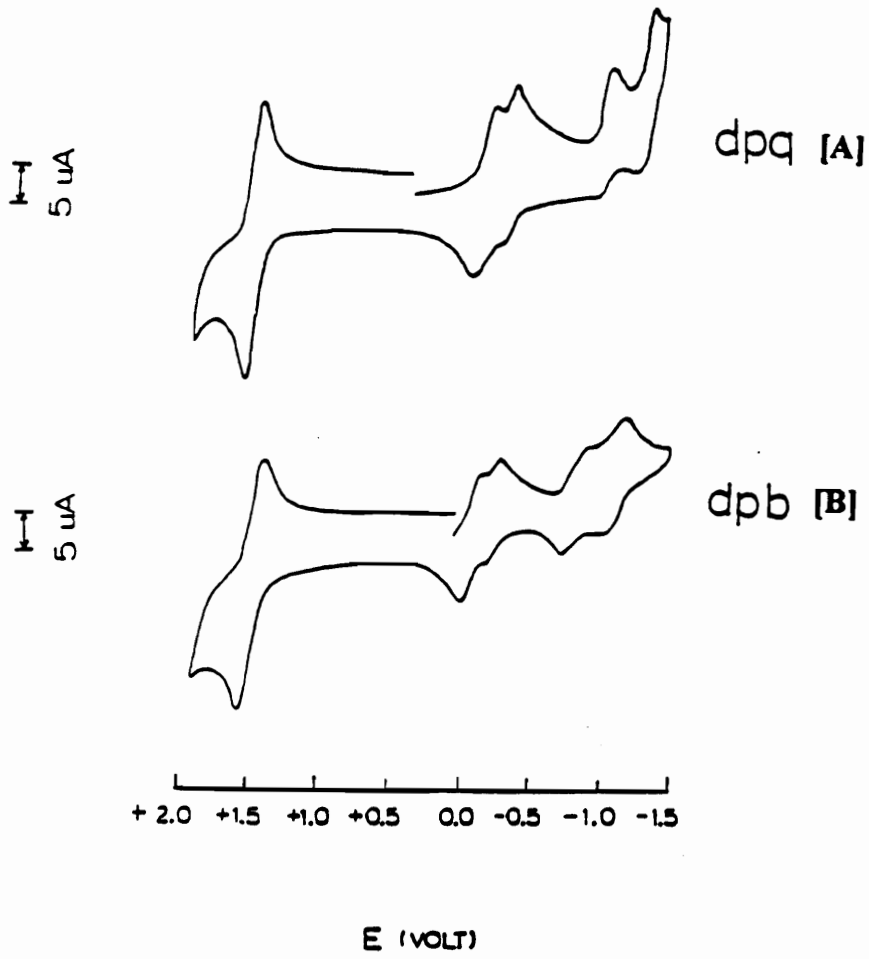

Figure 22. *Cyclic Voltammograms of Ir^{III}/Ru^{II} Mixed-Metal Trimetallic Complexes Containing Polypyridyl Bridging Ligands.* These voltammograms were taken at a scan rate of 200 mV/s, in acetonitrile with 0.1 M Bu_4NPF_6, with a platinum working electrode, a platinum wire auxiliary electrode, and a Ag/AgCl reference electrode (0.29 vs. NHE). [A] $\{[(bpy)_2Ru(dpq)]_2IrCl_2\}(PF_6)_5$ (bpy = 2,2'-bipyridine and dpq = 2,3-bis(2-pyridyl)quinoxaline), and [B] $\{[(bpy)_2Ru(dpb)]_2IrCl_2\}(PF_6)_5$ (dpb = 2,3-bis(2-pyridyl)benzoquinoxaline).[a]

[a]Reference 62.

Table 16. Cyclic Voltammetric Data[a] for a Series of Ir^{III}/ Ru^{II} Mixed-Metal Trimetallic Complexes Containing Polypyridyl Bridging Ligands. (bpy = 2,2'-bipyridine, dpp = 2,3-bis(2-pyridyl)pyrazine, dpq = 2,3- bis(2-pyridyl) quinoxaline, and dpb = 2,3-bis(2-pyridyl) benzoquinoxaline.)[b]

COMPLEX	Oxidations		Reductions	
	$E_{1/2}$(V)	Assignment	$E_{1/2}$(V)	Assignment
$\{[(bpy)_2Ru(dpp)]_2IrCl_2\}^{5+}$	+1.56	Ru^{II}/ Ru^{III}	-0.39	dpp, dpp /dpp, dpp^-
			-0.54	dpp, dpp^- /dpp^-, dpp^-
			-1.06	dpp^-, dpp^- /dpp^-,dpp^{2-}
			-1.22	dpp^-, dpp^{2-} /dpp^{2-}, dpp^{2-}
$\{[(bpy)_2Ru(dpq)]_2IrCl_2\}^{5+}$	+1.56	Ru^{II}/ Ru^{III}	-0.12	dpq, dpq /dpq, dpq^-
			-0.26	dpq, dpq^- /dpq^-, dpq^-
			-0.90	dpq^-, dpq^- /dpq^-, dpq^{2-}
			-1.22	dpq^-, dpq^{2-} /dpq^{2-}, dpq^{2-}
			-1.39	(bpy, bpy),(bpy, bpy) / (bpy^-, bpy),(bpy^-, bpy)
			-1.56	(bpy^-, bpy),(bpy^-, bpy)/ (bpy^-, bpy^-),(bpy^-, bpy^-)
			-1.70	Ir^{III}/ Ir^{I}
$\{[(bpy)_2Ru(dpb)]_2IrCl_2\}^{5+}$	+1.56	Ru^{II}/ Ru^{III}	0.03	dpb,dpb/dpb,dpb^-
			-0.12	dpb, dpb^- /dpb^-, dpb^-
			-0.71	dpb^-, dpb^- / dpb^-, dpb^{2-}
			-0.98	dpb^-, dpb^{2-} /dpb^{2-}, dpb^{2-}
			-1.44	(bpy, bpy),(bpy, bpy) / (bpy^-, bpy),(bpy^-, bpy)
			-1.70	Ir^{III}/ Ir^{I}
			-1.60	(bpy^-, bpy),(bpy^-, bpy)/ (bpy^-, bpy^-),(bpy^-, bpy^-)

[a]All cyclic voltammetric data was taken in room temperature spectral grade acetonitrile with 0.1 M Bu_4NPF_6 as the supporting electrolyte and a scan rate of 200 mV/s. The electrodes employed were a platinum working electrode, a platinum wire auxiliary electrode, and a Ag/AgCl reference electrode (0.29 vs. NHE).
[b]Reference 50, 62.

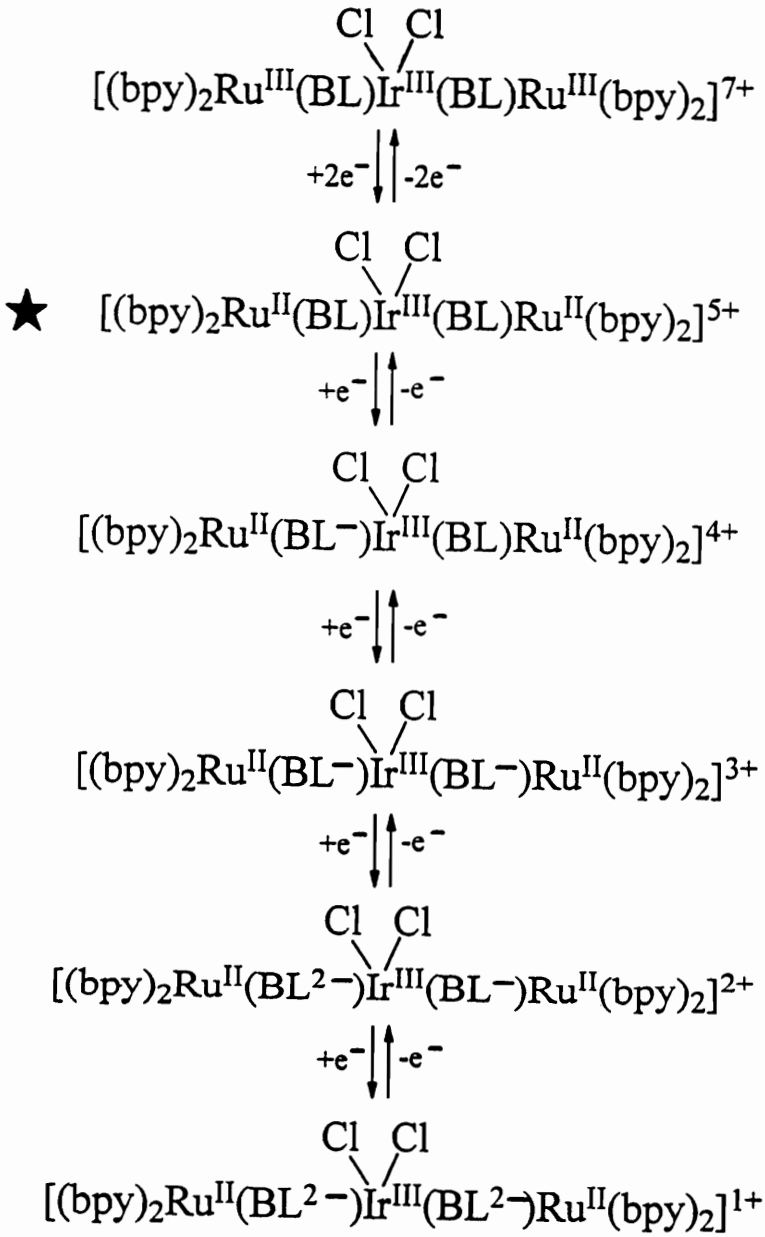

Figure 23. *General Electrochemical Scheme for the {[(bpy)$_2$Ru(BL)]$_2$IrCl$_2$}(PF$_6$)$_5$ (bpy = 2,2'-bipyridine and BL = dpq: 2,3-bis(2-pyridyl)quinoxaline and dpb: 2,3-bis(2-pyridyl)benzoquinoxaline Trimetallic Complexes.* The '★' indicates the synthesized oxidation state.

The reductive portion of the cyclic voltammograms for these trimetallic complexes is more complex. The seven reduction couples can be grouped into three segments. The first segment contains the first four reductive couples, which correspond to the BL reductions. In viewing the electrochemical data for these reduction couples, a shift to more positive potentials occurs upon going from dpp to dpq to dpb. This shift corresponds to the stabilization of the BL π^* orbital. Such a shift is expected due to the stabilizing affect of the addition of the aromatic rings on the π^* orbital energy of the bridging ligand. It is also interesting to note that the two equivalent bridging ligands in each trimetallic reduce at different potentials. The fact that they do not reduce at the same potential indicates that the two BLs are electronically coupled through the central iridium. In these polymetallic systems, the BL^{-}/BL^{2-} reductions occur before the bpy/bpy^{-} reduction couples indicative of a bridged system.[38, 43]

Reduction of the complexes past the fourth wave gives rise to couples that involve the two reversible bipyridine reduction couples and the irreversible Ir^{III} reduction couple. These bipyridine reductions are closely spaced two electron waves. This occurs since the two bpys bound to one ruthenium center are electronically coupled, whereas the bipyridines bound to the other ruthenium centers are not coupled to those on the remote ruthenium. Each wave represents the simultaneous reduction of one of the bpys bound to each ruthenium center. The Ir^{III} reduction is an irreversible two electron wave. In viewing the last three reductive couples, severe overlapping of waves obscures distinctive wave

couples and adsorption/desorption spikes appear. For this reason the values quoted for these half-wave potentials in Table 16 are approximations.

Understanding the electrochemistry of these trimetallic systems can aid in their electronic absorption spectroscopy assignments. The first electrochemical oxidation and reduction correspond to the site of localization of the HOMO and LUMO. Therefore, the HOMO is ruthenium($d\pi$) based and the LUMO is BL(π^*) based. The energy of the HOMO remains constant as the energy of the LUMO decreases in energy upon going from dpp to dpq to dpb based systems. The nature of the HOMO and LUMO would predict that a Ru($d\pi$) $\rightarrow$ BL(π^*) CT lowest lying spectroscopic transition would be present in the trimetallics. The varying energy of the LUMO would also predict a decrease in the energy of this MLCT upon going from dpp to dpq to dpb.

Electronic Absorption Spectroscopy.

Figure 24 shows the electronic absorption spectra for the series of trimetallics.[62] The electronic absorption data is also summarized in Table 17.[62] The two ruthenium light absorbing moieties play a dominating role in the electronic absorption spectra of the trimetallic complexes. Consequently, there are many spectral features common to all complexes. One of the most interesting observations of these systems is the lack of intense absorptions which involve the iridium metal center. Not a single iridium based transition is observed in the 190 to 820 nm range. This has been established through the synthesis of the rhodium analogs, $\{[(bpy)_2Ru(BL)]_2RhCl_2\}(PF_6)_5$.[64] The spectroscopy of the rhodium and iridium trimetallic complexes utilizing the same bridging ligand are

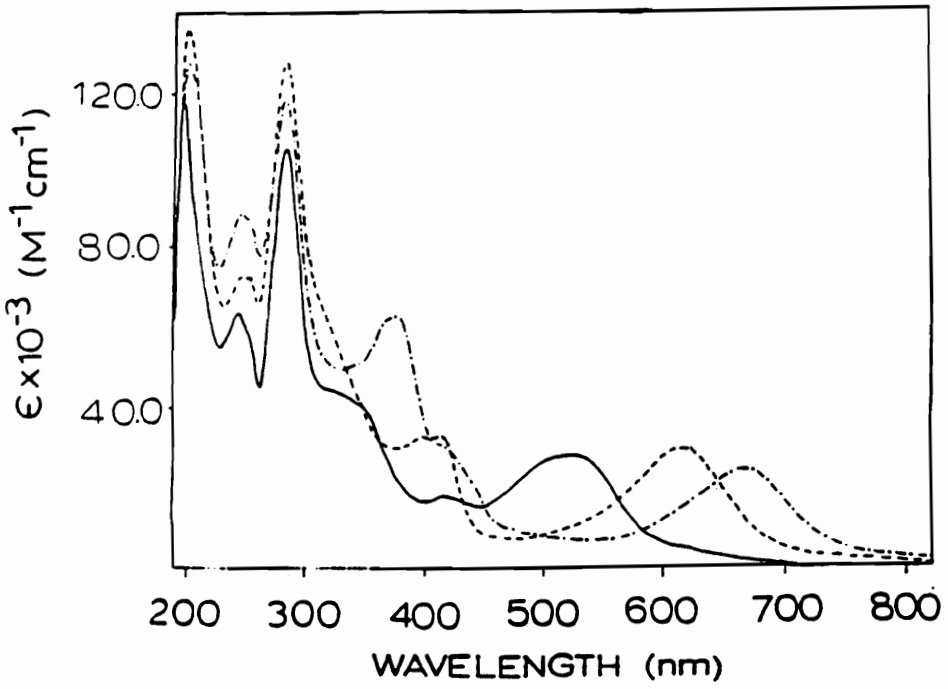

Figure 24. *Electronic Absorption Spectra of the {[(bpy)$_2$Ru(BL)]$_2$ IrCl$_2$}(PF$_6$)$_5$ (bpy = 2,2'-bipyridine and BL = dpp [—]: 2,3-bis(2-pyridyl)pyrazine; dpq [– – –]: 2,3-bis(2-pyridyl)quinoxaline, and dpb [—•—]: 2,3-bis(2-pyridyl)benzoquinoxaline) Complexes Containing Polypyridyl Bridging Ligand.* All spectra were taken in room temperature spectral grade acetonitrile.[a]

[a]Reference 62.

Table 17. Electronic Absorption Spectral Data [a] for a Series of Ir^{III}/Ru^{II} Mixed-Metal Trimetallic Complexes Containing Polypyridyl Bridging Ligands. (bpy = 2,2'-bipyridine, dpp = 2,3-bis(2-pyridyl) pyrazine, dpq = 2,3- bis(2-pyridyl)quinoxaline, and dpb = 2,3-bis(2-pyridyl)benzoquinoxaline.)[b]

COMPLEX	λ_{max} (nm) Absorption	$\varepsilon \times 10^{-3}$ ($M^{-1}cm^{-1}$)	Assignment
$\{[(bpy)_2Ru(dpp)]_2IrCl_2\}^{5+}$	284	106	$n \rightarrow \pi^*$, $\pi \rightarrow \pi^*$(bpy)
	326(sh)	43.5	Ru $\rightarrow$ bpy CT
	344(sh)	40.4	$\pi \rightarrow \pi^*$(dpp)
	416	18.0	Ru $\rightarrow$ bpy CT
	522	27.9	Ru $\rightarrow$ dpp CT
$\{[(bpy)_2Ru(dpq)]_2IrCl_2\}^{5+}$	284	128	$n \rightarrow \pi^*$, $\pi \rightarrow \pi^*$(bpy)
	324(sh)	58.2	Ru $\rightarrow$ bpy CT
	350(sh)	38.5	$\pi \rightarrow \pi^*$(dpq)
	396	33.2	Ru $\rightarrow$ dpq CT
	414	33.6	Ru $\rightarrow$ bpy CT
	616	30.2	Ru $\rightarrow$ dpq CT
$\{[(bpy)_2Ru(dpb)]_2IrCl_2\}^{5+}$	284	118	$n \rightarrow \pi^*$, $\pi \rightarrow \pi^*$(bpy)
	336(sh)	50.3	Ru $\rightarrow$ bpy CT
	374	63.5	$\pi \rightarrow \pi^*$(dpb)
	416(sh)	30.7	Ru $\rightarrow$ bpy CT
	442(sh)	20.3	Ru $\rightarrow$ dpb CT
	666	24.8	Ru $\rightarrow$ dpb CT

[a] All spectral data was obtained in room temperature spectral grade acetonitrile.
[b] Reference 62.

virtually superimposable, providing evidence that the spectroscopy is dominated by the two ruthenium chromophores.

Although the visible region of the electronic absorption spectra for $\{[(bpy)_2Ru(BL)]_2IrCl_2\}^{5+}$ is distinctive for each individual trimetallic complex, striking similarities exist in the ultraviolet region. Between approximately 190 and 300 nm the absorption peaks of all three complexes are similar. Each trimetallic exhibits a $n \rightarrow \pi^*$, $\pi \rightarrow \pi^*$ (bpy) based intraligand transition absorption band at 284 nm. At approximately 326 (dpp), 324 (dpq), and 336 nm (dpb) a high energy $Ru(d\pi) \rightarrow$ bpy (π^*) CT is seen. Another transition seen in all three complexes is the BL $\pi \rightarrow \pi^*$ intraligand transiton at 344 (dpp), 350 (dpq), and 374 nm (dpb). This transition will be discussed later in the text.

The visible region contains the most notable differences between the $\{[(bpy)_2Ru(BL)]_2IrCl_2\}^{5+}$ complexes. The pronounced difference is in the lowest energy band that shifts to the red in going from dpp to dpq to dpq. This transition is assigned as a $Ru(d\pi) \rightarrow BL(\pi^*)$ CT and is also present at higher energy in the monometallic systems, $[Ru(bpy)_2(BL)]^{2+}$.[59] When placed into the trimetallic framework, this transition of the $Ru^{II}(bpy)_2(BL)$ moiety shifts to lower energy. This shift to lower energy is seen when a second metal is bridged in the homobimetallic systems $\{[(bpy)_2Ru]_2(BL)\}^{4+}$.[60] In the trimetallic systems, a more drastic shift is seen and is due to the Ir^{III} center. The increased positive charge on Ir^{III}, versus Ru^{II}, has stabilized the π^* orbital of the bridging ligand to a greater degree. This causes the observed red shift of the $Ru(d\pi) \rightarrow BL(\pi^*)$ CT band.

Amidst the peaks in the visible region, there is one band that is common to all three systems. Through all three spectra a peak is present at approximately 414 nm. This peak occurs in electronic absorption spectra of the monometallic analogs and is attributed to a $Ru(d\pi) \rightarrow bpy(\pi^*)$ CT.[60]

The incorporation of the bridging ligands into the trimetallic framework has altered their π^* orbital energy and given rise to peaks shifts relative to their ruthenium monometallic analog. The coordination of the bridging ligand to the Ir^{III} metal center has further stabilized its π^* orbital. This should lead to a red shift of the BL ($\pi \rightarrow \pi^*$) based bands. The BL $\pi \rightarrow \pi^*$ intraligand transitions occur at 344, 350, and 374 nm for the dpp, dpq and dpb trimetallic complexes, respectively.

Both the electrochemistry and electronic absorption spectroscopy have provided the value for the energy gap between the HOMO and LUMO of each trimetallic. In the electrochemistry, the HOMO correspond to the first oxidation and the LUMO to the first reduction. It has been established that the first oxidation is $Ru(d\pi)$ based and the first reduction is BL(π^*) based. The lowest lying λ_{max}^{abs} is a $Ru(d\pi) \rightarrow \pi^*$(BL) CT, which involves the HOMO and LUMO. Since an optical and electrochemical measure of the HOMO-LUMO energy gap are both available, a correlation between the two may be drawn.[68, 69] A plot of E_{abs} ($Ru(d\pi) \rightarrow \pi^*$(BL) CT) versus $\Delta E_{1/2}$ ($\Delta E_{1/2} = E_{1/2}(Ru^{II}/Ru^{III}) - E_{1/2}(BL/BL^-)$) is shown in Figure 25. The correlation coefficient of this graph is 0.998, with a slope of 1.24 and a y-intercept of -0.04. For this series of complexes, it appears

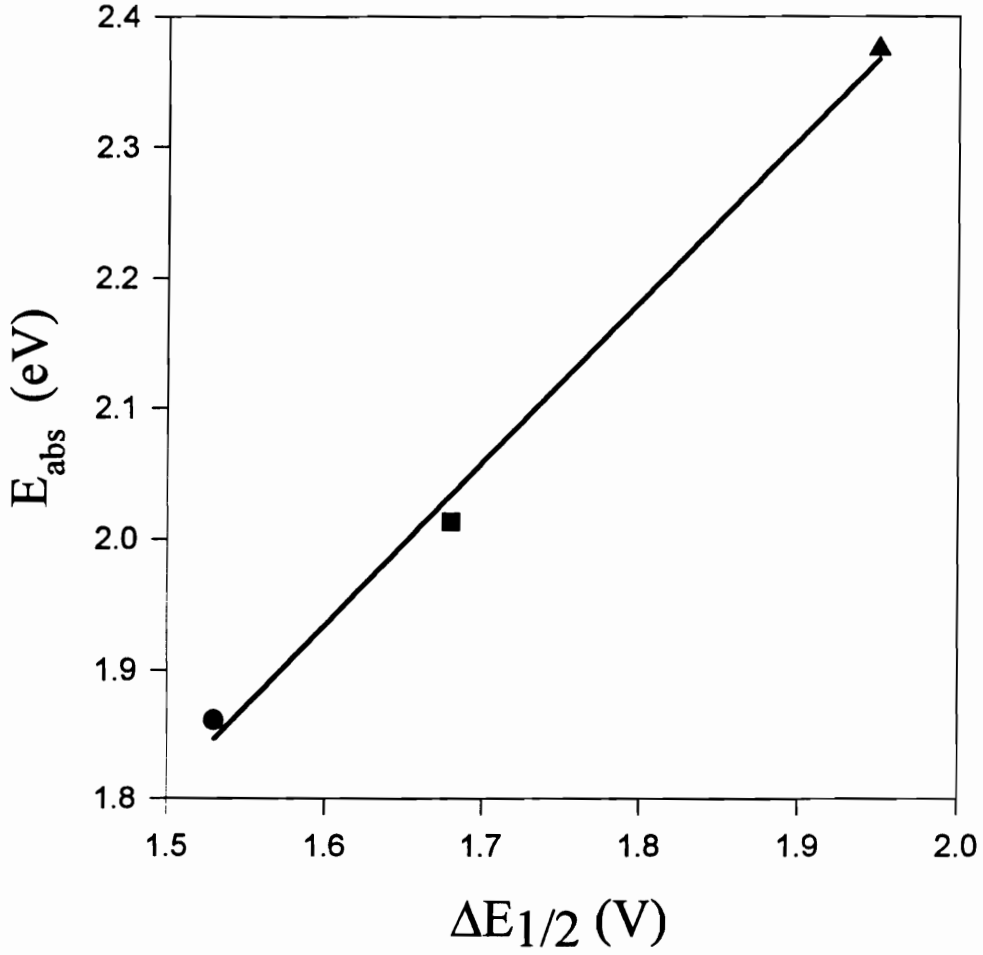

Figure 25. *Plot of E_{abs} ($Ru(d\pi) \rightarrow \pi^*(BL)$ CT) versus $\Delta E_{1/2}$ ($\Delta E_{1/2} = E_{1/2}(Ru^{II}/Ru^{III}) - E_{1/2}(BL/BL^-)$) for the Trimetallic Complexes Containing Polypyridyl Bridging Ligands, $\{[(bpy)_2Ru(BL)]_2IrCl_2\}(PF_6)_5$ (bpy = 2,2'-bipyridine and BL = dpp [▲]: 2,3-bis(2-pyridyl)pyrazine, dpq [■]: 2,3-bis(2-pyridyl)quinoxaline and dpb [●]: 2,3-bis(2-pyridyl)benzoquinoxaline).*[a]

[a]Reference 62.

that there exists a linear correlation between the electrochemical and spectroscopic measurement of the HOMO-LUMO energy gap.

This series of trimetallic complexes contain the same chromophore as the $[Ru(bpy)_2(BL)]^{2+}$ and $\{[Ru(bpy)_2]_2(BL)\}^{4+}$ complexes discussed in Chapter 3. The similarity of all three sets of complexes permits the incorporation of all the systems into a correlation of E_{abs} and $\Delta E_{1/2}$. A plot of E_{abs} ($Ru(d\pi) \rightarrow \pi^*(BL)$ CT) versus $\Delta E_{1/2}$ ($\Delta E_{1/2} = E_{1/2}(Ru^{II}/Ru^{III}) - E_{1/2}(BL/BL^-)$) which incorporates the complexes: $[Ru(bpy)_2(BL)]^{2+}$ and $\{[Ru(bpy)_2]_2(BL)\}^{4+}$ (BL = dpp, Cl_2dpq, dpq, Me_2dpq, and dpb) as well as $\{[(bpy)_2Ru(BL)]_2IrCl_2\}(PF_6)_5$, (BL = dpp, dpq, and dpb) is shown in Figure 26. The correlation coefficient of this plot is 0.95, with a slope of 0.93 and *y*-intercept of 0.40. Considering the diversity of the ligand set both correlation coefficient and slope are surprisingly very close to unity. The scatter of the line, with respect to the $[Ru(bpy)_2(BL)]^{2+}$ and $\{[Ru(bpy)_2]_2(BL)\}^{4+}$ line scatter, or the $\{[(bpy)_2Ru(BL)]_2IrCl_2\}(PF_6)_5$ line scatter, has increased. This result along with the slight deviation of the slope from 1.0 and the y-intercept from 0, leads one to the conclusion that there exists some dependence of χ_i, χ_o, Q, $\Delta\Delta G_s$ or Δ(sol) on $\Delta E_{1/2}$ in these widely varied complexes.[68, 69]

Emission Spectroscopy and Excited State Lifetimes.

Two of the trimetallic complexes, $\{[(bpy)_2Ru(BL)]_2IrCl_2\}(PF_6)_5$, (BL = dpp, dpq, and dpb), display detectable emission at room temperature in deoxygenated acetonitrile, and these complexes have been characterized with emission spectroscopy and excited state

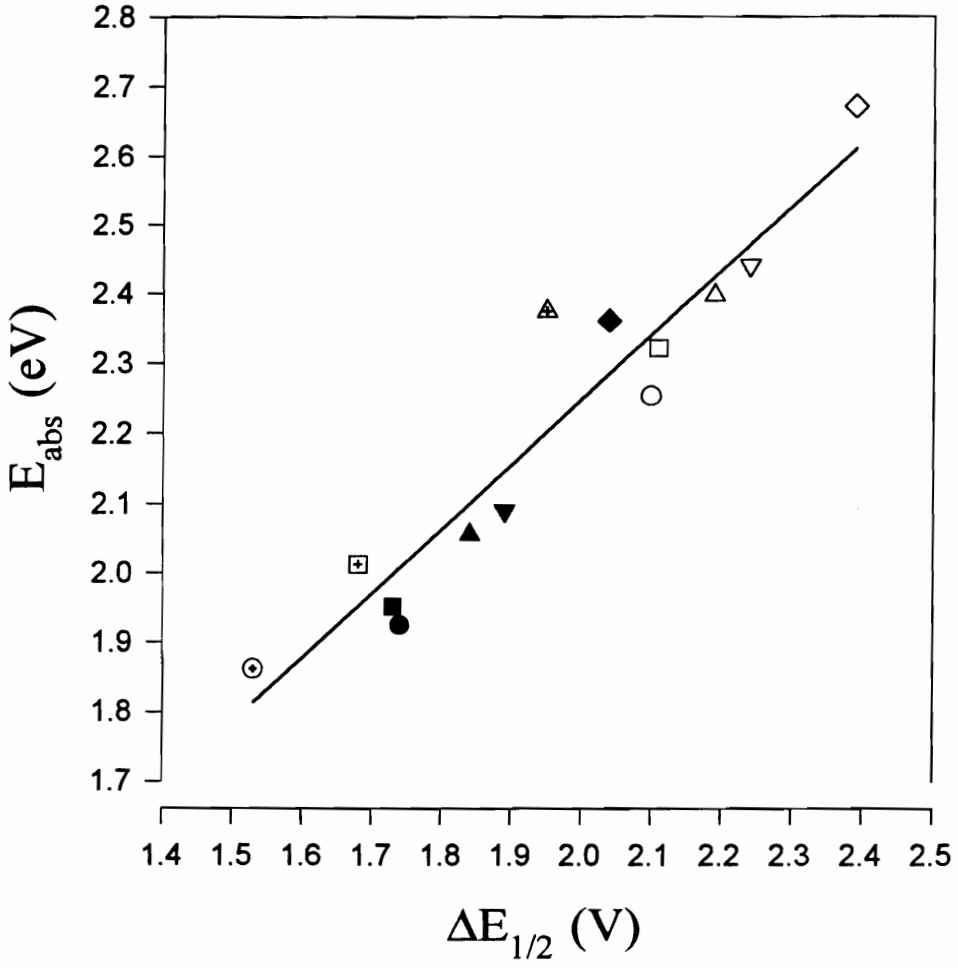

Figure 26. *Plot of E_{abs} ($Ru(d\pi) \rightarrow \pi^*(BL)$ CT) versus $\Delta E_{1/2}$ ($\Delta E_{1/2} = E_{1/2}(Ru^{II}/Ru^{III}) - E_{1/2}(BL/BL^-)$) for the Bipyridyl Complexes of the form: $[Ru(bpy)_2(BL)]^{2+}$, $\{[Ru(bpy)_2]_2(BL)\}^{4+}$, and $\{[(bpy)_2Ru(BL)]_2IrCl_2\}(PF_6)_5$, for $\{[Ru(bpy)_2](BL)\}^{2+}$, bpy = 2,2'-bipyridine and BL = dpp [◇]: 2,3-bis(2-pyridyl)pyrazine, Me_2dpq [▽]: 6,7-dimethyl-2,3-bis(2-pyridyl)quinoxaline, dpq [△]: 2,3-bis(2-pyridyl)quinoxaline, Cl_2dpq [□]: 6,7-dichloro-2,3-bis(2-pyridyl)quinoxaline and dpb [○]: 2,3-bis(2-pyridyl)benzoquinoxaline. For $\{[Ru(bpy)_2]_2(BL)\}^{4+}$, BL = dpp [◆], Me_2dpq [▼], dpq [▲], Cl_2dpq [■] and dpb [●]. For$\{[(bpy)_2Ru(BL)]_2IrCl_2\}(PF_6)_5$, BL = dpp [⧋], dpq [⊞] and dpb [⊕].*[a]

[a]Reference 60, 62.

lifetime measurements. The emission maxima of the trimetallic complex decreases in energy when the bridging ligand is changed from dpp to dpq, 794 and 866 nm, respectively. The dpb emission could not be detected by the system utilized. This inability to obtain data is due to the emission being red shifted beyond the detection limits of the photomultiplier tube utilized within the system. The excited state lifetime ($\tau = 1/k$) for the emissive complexes was determined in fluid solution at room temperature. The lifetimes of the dpp and dpq systems were 32 ns and 5 ns. Glen Jensen,[74] a member of the Brewer group, attempted to determine the excited state lifetime of the dpb trimetallic using a transient absorbance system. No data was obtained for the complex. Therefore, the lifetime is probably $\leq$ 5 ns, given the pulse width (~5ns of the Nd-YAG laser used in the experimental system).

Spectroelectrochemistry.

For the series of $\{[(bpy)_2Ru(BL)]_2IrCl_2\}(PF_6)_5$ (BL = dpp, dpq, and dpb) trimetallic complexes, the two electron oxidized species were electrogenerated and characterized via electronic spectroscopy. The two and four electron reduced species for the dpq and dpb complexes were also electrogenerated. For the $\{[(bpy)_2Ru(dpp)]_2IrCl_2\}(PF_6)_5$ complex, electrogeneration of reduced species was not possible. The system decomposed upon bulk electrolysis to the two electron reduced species. This decomposition has been seen in other complexes containing the dpp bridging ligand.[43, 64]

The lack of stability of the reduced dpp bridged complexes has been related to the nature of the π^* acceptor orbital. When the $\{[(bpy)_2Ru(dpp)]_2IrCl_2\}(PF_6)_5$ trimetallic

complex is reduced by two electrons, the dpp ligand accepts the electrons. Occupation of this LUMO has repercussions that are different from the dpq and dpb bridging ligands. With the use of ESR, Wertz and co-workers[43] determined that the LUMO of the dpq bridging ligand is quinoxaline based. In the one electron reduction of $\{[(bpy)_2Ru]_2(dpp)\}^{4+}$, the electron resides on the pyridyl and pyrazine portion of the bridging ligand. In the case of the $\{[(bpy)_2Ru]_2(dpq)\}^{4+}$, the electron resides on the quinoxaline portion of the BL. The instability of the the two electron reduced form of $\{[(bpy)_2Ru]_2(dpp)\}^{4+}$ complex is attributed to this pyridine contribution to the LUMO. Movement of the electron localization to the quinoxaline portion of the ligand in the dpq results in no pyridyl contribution to the π^* LUMO. Occupation of the dpq (and dpb) LUMO will, therefore, not promote Ru-N bond cleavage and allow for a more stable complex. An interesting point to note about the $\{[(bpy)_2Ru(dpp)]_2IrCl_2\}(PF_6)_5$ trimetallic is that fragmentation occurs via the delegation of the BL from the central Ir^{III}.[62, 64] This assertion comes from the fact that upon a two-electron reduction, the electronic absorption spectrum resembles the independently synthesized $[(bpy)_2Ru(dpp)]^{2+}$ fragment.

The oxidative and reductive spectroelectrochemistry experiments on $\{[(bpy)_2Ru(dpq)]_2IrCl_2\}^{5+}$ have validated the various individual spectral and electrochemical assignments (Figure 27).[62] The dpq trimetallic has absorption maxima at 284, 324(sh), 350(sh), 396, 414, and 616 nm. Upon a two electron oxidation (to generate two Ru^{III}), and a two or four electron reduction (to generate reduced BLs), the lowest lying absorption band, at 616 nm, is lost. These results, along with the high ε value, are consistent with the band assignment of $Ru(d\pi) \rightarrow dpq(\pi^*)$ CT. Loss of the absorption

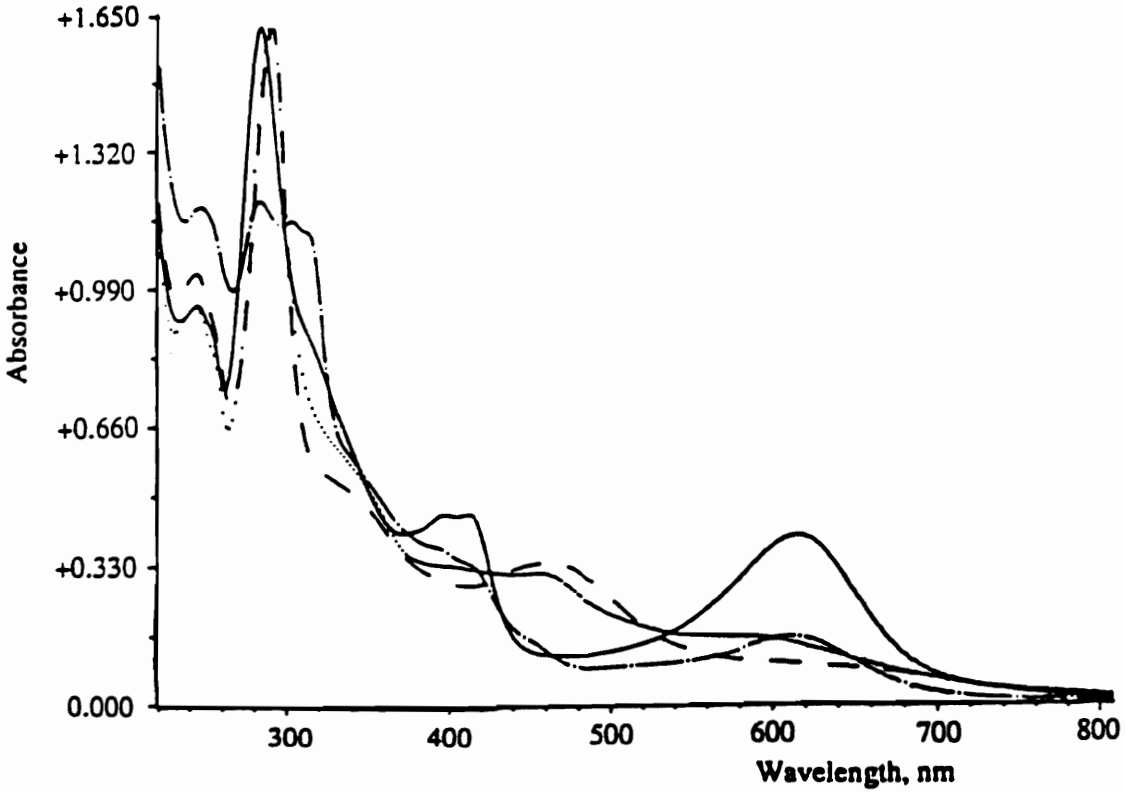

Figure 27. *Electronic Absorption Spectra for* $\{[(bpy)_2Ru(dpq)]_2IrCl_2\}^{n+}$ *(bpy = 2,2'-bipyridine and dpq = 2,3-(2-pyridyl)quinoxaline): n = 5 [—], 3 [• • •], 1[- - -], 7 [—•—].* All spectra were taken in room temperature acetonitrile containing 0.1 M Bu_4NPF_6.[a]

[a]Reference 62.

band at 616 nm upon oxidation of both ruthenium metal centers would imply that the absorption band does indeed involve the metal center. It must now be determined to which ligand the absorption occurs. The first four electron reductions are bridging ligand based. Reduction of the dpq gives rise to the loss of the peak at 616 nm. Since this MLCT is lost when either the ruthenium is oxidized or the dpq is reduced, one would deduce that it is a Ru($d\pi$) $\rightarrow$ dpq(π^*) CT transition. Other verified MLCT absorptions occur at 324 nm Ru($d\pi$) $\rightarrow$ bpy(π^*) CT, 396 nm Ru($d\pi$) $\rightarrow$ dpq(π^*) CT, and 414 nm Ru($d\pi$) $\rightarrow$ bpy(π^*) CT. The two closely spaced peaks around 400 nm have been distinguished as two different MLCT bands. Upon a two-electron oxidation of the complex, both the 414 and 396 nm peaks are lost. This verifies the ruthenium metal center involvement with these transitions. The 414 nm peak shifts to lower energy upon a 1, 2, 3 or 4 electron reduction. This has been noted before in the reduced forms of the homobimetallic ruthenium complexes of the form $\{[(bpy)_2Ru]_2(dpq)\}^{4+}$.[43] A shift to lower energy can be accounted for by the destabilization of the Ru($d\pi$) orbital upon dpq reduction. Reduction of the bridging ligand causes a decrease in its π-accepting ability and, consequently, induces the destabilization of the metal based orbital. This gives rise to a shift to lower energy of the 414 nm Ru($d\pi$) $\rightarrow$ bpy(π^*) CT transitions. In the case of the 396 nm peak, upon a two- or four-electron reduction, the peak is lost. The loss of this peak upon reduction denotes bridging ligand involvement in the transition, since the first four reductions are all bridging ligand based. The peak at 396 nm represents a higher energy Ru($d\pi$) $\rightarrow$ dpq (π^*) CT transition. The highest energy MLCT at observed 324 nm

is assigned as a Ru(dπ) → bpy(π*) CT. Upon the two electron oxidation the peak at 324 nm is lost. The disappearance of the shoulder in this region upon oxidation occurs in all three trimetallic complexes, and may be a high energy Ru(dπ) → bpy(π*) CT.

The shoulder at 350 nm in $\{[(bpy)_2Ru(dpq)]_2IrCl_2\}^{5+}$ is assigned as a dpq intraligand transition. Upon a two- and four-electron reduction the band is no longer present. When the complex is oxidized, the shoulder appears to shift to lower energy. Again, since the first four reductions are dpq based, the loss of the band denotes dpq involvement. The shift to lower energy upon the two-electron oxidation may be explained through the more positive metal centers being generated. More positive metal centers create a stabilizing affect on the dpq π* orbital due to Ru^{III} having less π backbonding ability than Ru^{II}. This is consistent with a dpq π → π * band at 350 nm.

The bipyridine intraligand transition assignments at 284 nm in $\{[(bpy)_2Ru(BL)]_2IrCl_2\}(PF_6)_5$ (BL = dpp, dpq, and dpb) have been validated with the use of spectroelectrochemistry. The peak at 284 nm, assigned as overlapping n → π* and π→ π* transitions, is very intense and remains unchanged in a two- and four-electron reduction. The two-electron oxidation of the complex, however, splits the peak into two components. This splitting behavior upon electrogeneration of the Ru^{III} species may be explained by overlapping transitions that separate upon ruthenium oxidation. One band appears to remain unchanged and the other appears to move to lower energy. Ligand based π→ π* bipyridine transitions have been shown to account for peaks in this region in other bipyridyl complexes.[4, 33] The two peaks that appear after the two electron oxidation

may be explained by two bipyridine intraligand transitions. The oxidation of the metal center should stabilize the π^* orbital on the bpy due to the increased electron withdrawing ability of the metal center, as well as the decreased π backbonding ability of the Ru^{III} as compared to the Ru^{II} center. An increase in positive charge on the metal center affects the energy of the nonbonding orbitals as well. The nonbonding orbitals on the Ru^{III} are stabilized in relation to the nonbonding orbitals on the Ru^{II} center. Figure 28 represents a comparative orbital energy diagram showing the affects of the metal oxidation. Since both nonbonding and π^* orbitals are stabilized to a similar degree, the energy of the $n \rightarrow \pi^*$ transition remains relatively unchanged upon metal oxidation. So, when the peak at 284 nm splits, the peak at higher energy, that remains relatively unchanged in energy upon oxidation, is the bpy $n \rightarrow \pi^*$ transition. The peak that shifts to a lower energy is assigned as the bpy $\pi \rightarrow \pi^*$ transition. The oxidation of the Ru^{II} center to Ru^{III} does not alter, to any large degree, the energy of the π orbitals on the bpy. Stabilization of π^* orbitals decreases the energy gap between the π and π^* orbitals. This decrease in the energy gap results in shifting the transition to a lower energy. The oxidative spectroelectrochemistry, therefore, establishes the presence of overlapping bipyridine $n \rightarrow \pi^*$ and $\pi \rightarrow \pi^*$ transitions in the 284 nm region of this complex.

Both oxidative and reductive spectroelectrochemistry were performed on the $\{[(bpy)_2Ru(dpb)]_2IrCl_2\}(PF_6)_5$ trimetallic (Figure 29).[62] This trimetallic exhibits peaks at 284, 336(sh), 374, 416(sh), 442(sh), and 666 nm. As in the dpq trimetallic complex, the lowest lying absorption is lost upon a two electron oxidation (generating a Ru^{III} center)

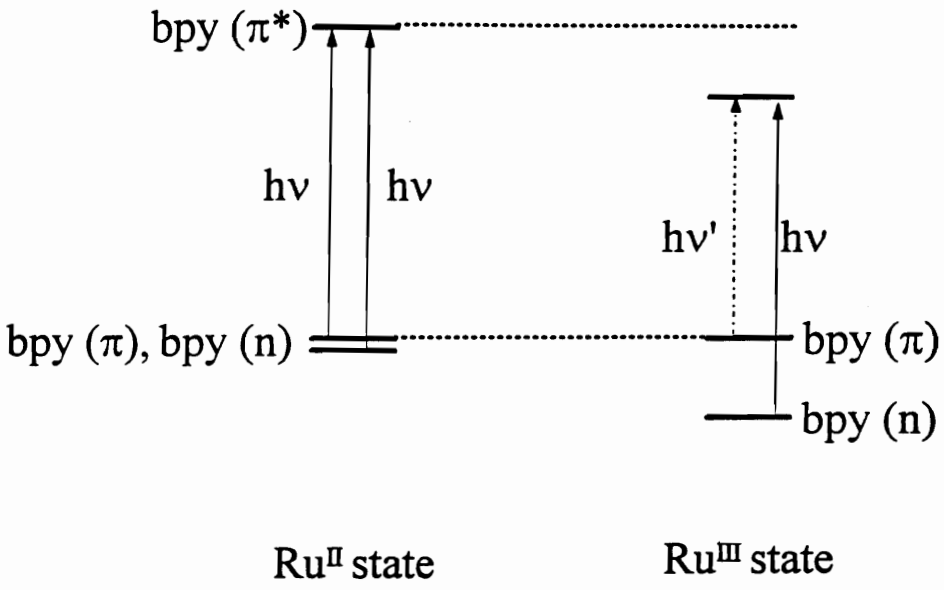

Figure 28. *A Representative Orbital Energy Diagram of the Parent and Oxidized Ruthenium Moiety in $\{[(bpy)_2Ru(BL)]_2IrCl_2\}(PF_6)_5$ (bpy = 2,2'-bipyridine and BL = dpp: 2,3-bis(2-pyridyl)pyrazine; dpq: 2,3-bis(2-pyridyl)quinoxaline or dpb: 2,3-bis(2-pyridyl)benzoquinoxaline).*

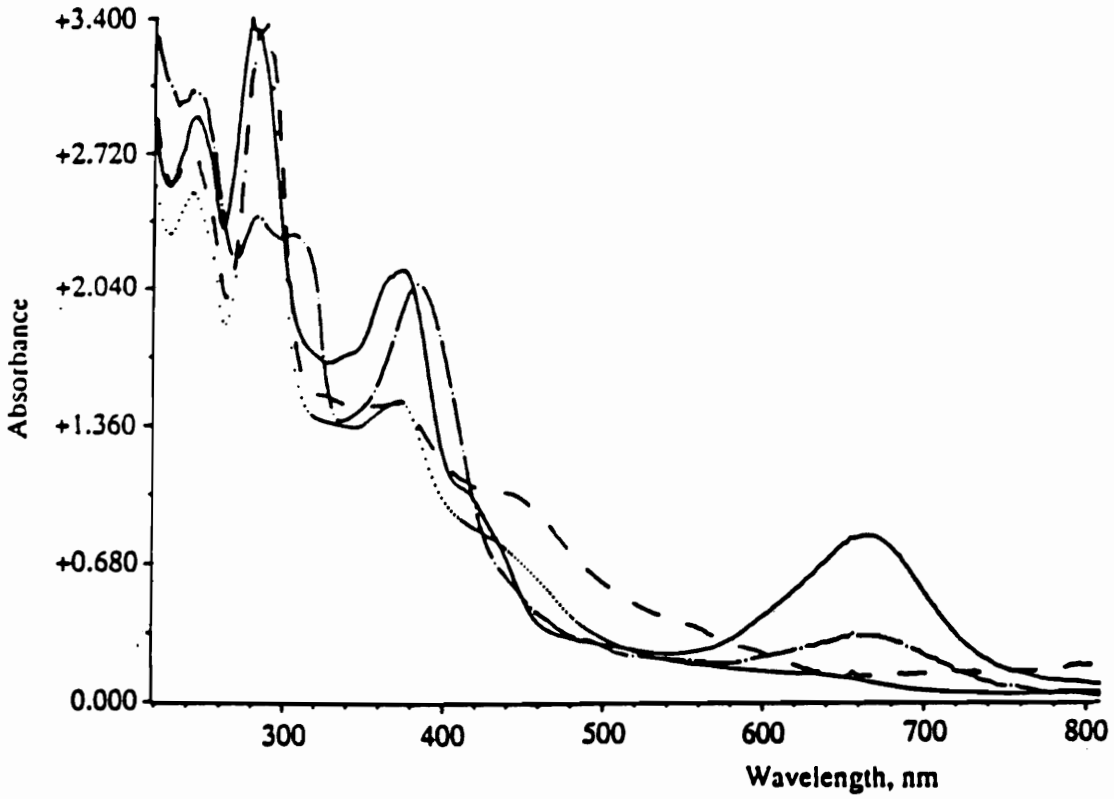

Figure 29. *Electronic Absorption Spectra for* $\{[(bpy)_2Ru(dpb)]_2IrCl_2\}^{n+}$ *(bpy = 2,2'-bipyridine and dpb = 2,3-(2-pyridyl)benzoquinoxaline): n = 5 (—), 3 (• • •), 1(- - -), 7 (—•—).* All spectra were taken in room temperature acetonitrile containing 0.1 M Bu_4NPF_6.[a]

[a]Reference 62.

and a two or four electron reduction (generating reduced dpb ligands). At this wavelength the molar extinction coefficient is high. Therefore, the band is assigned as a Ru(dπ) → dpb(π*) CT.

The next two higher energy peaks (416 and 442 nm) for $\{[(bpy)_2Ru(dpb)]_2IrCl_2\}(PF_6)_5$ for are both shoulders. When the two electron oxidized species is generated, both of the shoulders are lost. This would indicate involvement of the ruthenium metal center. If the complex is reduced by two or four electrons, reducing the dpb ligands, then one of the two peaks shifts to lower energy and the other is lost. A similar shift in the dpq has also been noted. Therefore, the peak at 416 nm is assigned as a Ru(dπ) → bpy(π*) CT. The disappearance of the 442 nm peak upon a two or four electron reduction, and a two electron oxidation, indicates that it is a Ru(dπ) → dpb(π*) CT.

The peak at 374 nm for $\{[(bpy)_2Ru(dpb)]_2IrCl_2\}(PF_6)_5$ is lost when the two or four electron reduced species is electrogenerated. When the two electron oxidized species is produced, the peak shifts to lower energy. The loss of this peak upon reduction is consistent with a dpb π → π* transition. The shift to lower energy after oxidation of the ruthenium metal centers is also consistent with a dpb transition. The electrogenerated Ru^{III} metal center stabilizes the dpb π* orbital to a greater degree than the Ru^{II} metal center does. This stabilization shifts the intraligand absorption to a lower energy.

The two highest energy peaks occur at 284 and 336 nm for $\{[(bpy)_2Ru(dpb)]_2IrCl_2\}(PF_6)_5$. The shoulder at 336 nm is lost upon oxidation and

thought to be a higher energy Ru(dπ) → bpy(π*) CT. The peak at 284 nm is divided into two components upon a two electron oxidation, yet remains undisturbed when the two or four electron reduced species is generated. This behavior is mirrored in the dpq trimetallic and is attributed to overlapping bpy based n → π* and π → π* intraligand absorptions.

The $\{[(bpy)_2Ru(dpp)]_2IrCl_2\}^{5+}$ does not generate a stable two or four electron reduced species. Therefore, only the oxidative spectroelectrochemistry was conducted on this particular system (Figure 30). The intensities and positioning of these peaks relative to the dpq and dpb analogs aided in their spectral assignments. Upon a two electron oxidation some interesting changes occur in the dpp trimetallic. The 284 nm peak splits into two peaks. The peaks at 326, 416 and 522 nm are lost. The striking change in the spectrum is the new transition at approximately 630 nm. The introduction of this new peak is also seen in the two electron oxidized Rh^{III} analog and is thought to be a dpp → Ru^{III} ligand-to-metal charge transfer band.[64]

Utilizing the electrochemistry and electronic absorption spectroscopy results for the $\{[(bpy)_2Ru(dpb)]_2IrCl_2\}(PF_6)_5$ trimetallic, an orbital energy diagram of the system can be derived (Figure 31). From these diagrams one can see how the trimetallic forms the basis of a MD for photoinitiated electron collection. This $\{[(bpy)_2Ru(dpb)]_2IrCl_2\}^{5+}$ trimetallic forms the LA-EC-LA core of the molecular device as depicted in Figure 1 (p.3). Given this diagram, the photochemistry of this complex in the presence of an electron donor looks promising.

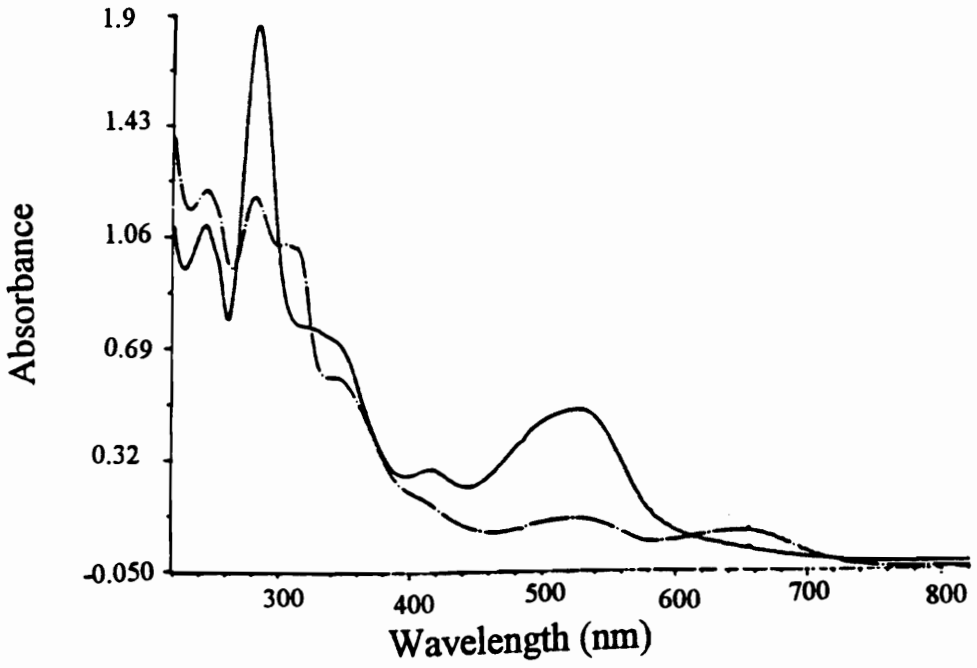

Figure 30. *Electronic Absorption Spectra for* $\{[(bpy)_2Ru(dpp)]_2IrCl_2\}^{n+}$ *(bpy = 2,2'-bipyridine and dpp = 2,3-bis(2-pyridyl)pyrazine): n = 5 (—) and 7 (—•—).* All spectra were taken in room temperature acetonitrilecontaining 0.1 M Bu_4NPF_6.[a]
[a]Reference 62.

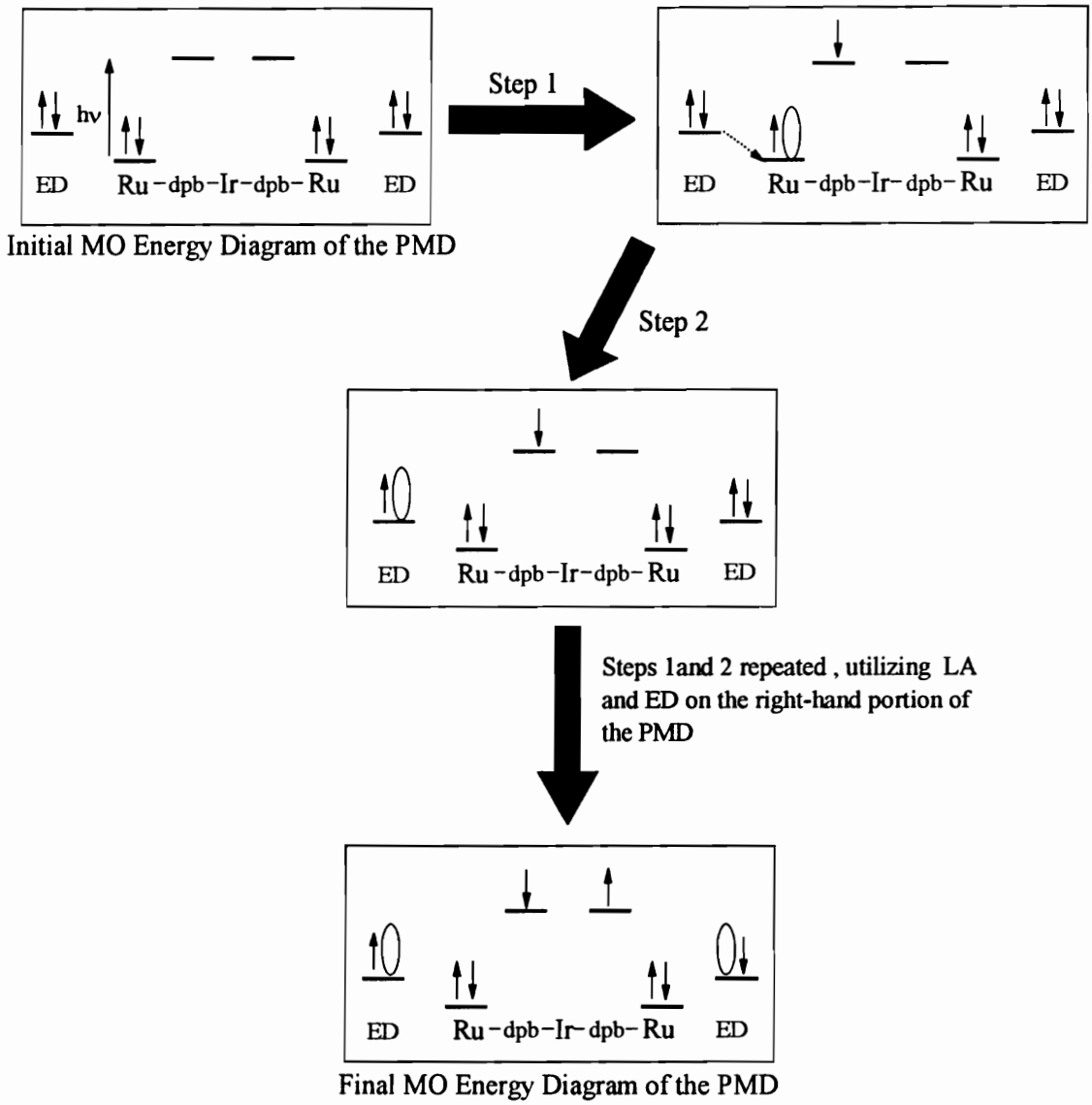

Figure 31. *Molecular Energy Orbital Diagram of the $\{[(bpy)_2Ru(dpb)]_2IrCl_2\}(PF_6)_5$ (bpy = 2,2'-bipyridine and dpb = 2,3-bis(2-pyridyl)benzoquinoxaline) Trimetallic Before and After Light Absorption.* Step 1 is light absorption by one of the Ru moieties; Step 2 is electron transfer from the ED to the Ru moiety, replacing the promoted electron in Step 1. Steps 1-2 are repeated utilizing the complimentary Ru and ED moieties, resulting is the final MO energy diagram.

Photolysis of $\{[(bpy)_2Ru(dpb)]_2IrCl_2\}(PF_6)_5$

The spectroscopic and electrochemical studies of the $\{[(bpy)_2Ru(dpb)]_2IrCl_2\}(PF_6)_5$ trimetallic shows that it possesses many of the desired qualities of a molecular device for photoinitiated electron collection. The photoinitiated electron collector's (PIEC) initiation step is the absorption of a photon and promotion of an electron to a central electron collector. The lowest lying excited state of the $\{[(bpy)_2Ru(dpb)]_2IrCl_2\}(PF_6)_5$ is a MLCT, which directs electron flow to the central $Ir^{III}(BL)_2Cl_2$ core, a $Ru(d\pi) \rightarrow dpb(\pi^*)$ CT. Additionally, the trimetallic complexes are stable with respect to a two-electron reduction. This two-electron reduced form has also been characterized with electronic absorption spectroscopy. With the use of spectroelectrochemistry, the assignments of the electronic spectroscopy and cyclic voltammetry have been validated. Now the ground work has been laid to test the functioning of the device as a PIEC.

Figure 32 shows the general scheme of events that are involved in the photochemical generation of the two electron reduced trimetallic complex. The first step is the excitation of one ruthenium chromophore by a photon of light. A sacrificial electron donor comes in contact with the excited trimetallic and undergoes excited-state electron transfer. Once an electron has been transfered from this quencher, a one electron reduced trimetallic and an oxidized electron donor is produced. Now that one electron has been successfully transfered, the process needs to be repeated. A second photon excites the other ruthenium chromophore of the now one electron reduced species. This critical step necessitates the independent functioning of each ruthenium chromophore. After this

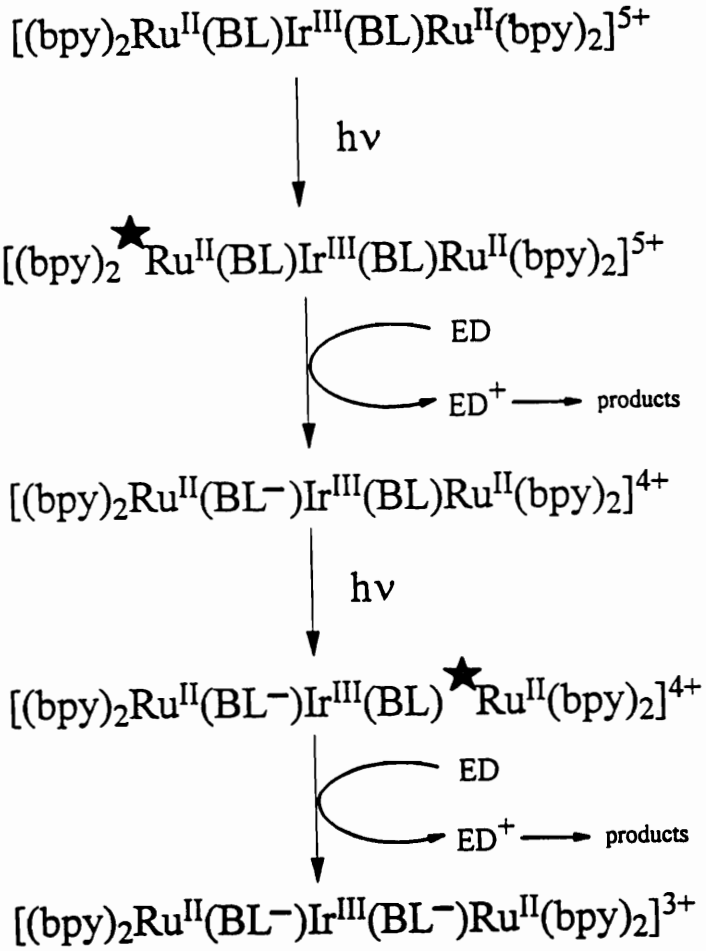

Figure 32. *Photolysis Scheme for the {[(bpy)$_2$Ru(BL)]$_2$IrCl$_2$}(PF$_6$)$_5$ (bpy = 2,2'-bipyridine and BL = dpq: 2,3-bis(2-pyridyl)quinoxaline or dpb: 2,3-bis(2-pyridyl)benzoquinoxaline.)Trimetallic Complexes Containing Polypyridyl Bridging Ligands.* In this photochemical scheme the absorption of light to produce an excited state of a given moiety is denoted by a '★'.

excited complex comes into contact with an electron donor in solution and undergoes excited-state electron transfer, the trimetallic will then be reduced by two electrons, thus functioning as a PMD for PIEC.

Since the reductive spectroelectrochemistry of these trimetallics has been conducted, the two electron reduced species are identified by electronic absorption spectroscopy. Most importantly, all seven stable oxidation states of $\{[(bpy)_2Ru(dpb)]_2IrCl_2\}^{5+}$ have characteristic electronic absorption spectra. Therefore, the one electron reduced species can be distinquished from the two electron species. The two electron reduced species is characterized by a loss of the $Ru(d\pi) \rightarrow dpb(\pi^*)$ CT band and a red shift of the $Ru(d\pi) \rightarrow bpy(\pi^*)$ CT. Comparison of the electrochemically reduced complex and the photoproduct will determine the photoproducts identity.

The sacrificial electron donor needs to be carefully chosen. An irreversible electron donor whose oxidized species will not react with the reduced trimetallic species is necessary. Another qualification is the electron donor not react with the trimetallic and transfer an electron in the ground state. The irreversible electron donor chosen was N, N-dimethylaniline ($(CH_3)_2NC_6H_5$). This amine oxidizes at +1.20 V vs. SCE. The oxidation products of dimethylaniline in acetonitrile, as reported by Hand and Nelson,[76] are varied with respect to the initial $(CH_3)_2NC_6H_5$ concentration. N,N,N',N'-tetramethylbenzidine (TMB) forms at low concentration, while at increased concentrations and electrolysis time, 4,4-methylenebis(N,N-dimethylaniline) and crystal violet in addition to TMB[76] are produced. This consideration is pertinent since even though the oxidized dimethylaniline concentration is low within the photochemical experiment, the concentration of

unoxidized dimethylaniline is high (0.035 M). For optimal correlation of the photochemical and electrochemical experiment, it would be ideal to have a low dimethylaniline concentration. In a combined photochemical and electrochemical experiment, a high concentration of dimethylaniline will be needed in order for the photochemical portion of the experiment to function. Ultimately, the electron donor concentration conflict will produce differences in the distribution of products from the oxidized electron donor. This issue will be verified later in the presentation of the photochemical experiments.

The photochemical generation of the two electron reduced trimetallic complex is monitored with electronic absorption spectroscopy. Under darkroom conditions, the trimetallic complex is dissolved in an acetonitrile solution of known electron donor concentration. An aliquot of the trimetallic and electron donor solution is placed in a cell with a 1 mm magnetic stir bar and deoxygenated. The sample cell is then irradiated at 660 nm. The irradiation wavelength should be at the 666 nm, corresponding to the $Ru(d\pi) \rightarrow dpb(\pi^*)$ CT band. Available filtering capabilities (a 660 nm narrow bandpass filter), however, restrict the irradiation wavelength to 660 nm. The progression of the photolysis is intermittently monitored by obtaining an UV-vis spectrum of the system. The changes over time in the visible spectrum can be seen in Figure 33. In this time progression, the $Ru(d\pi) \rightarrow dpb(\pi^*)$ CT at 666 nm is lost and the 416 nm peak shifts to lower energy. The spectroelectrochemistry of this complex shows quite similar behavior. The photolysis produces the same electronic absorption spectrum as the two electron reduced species.

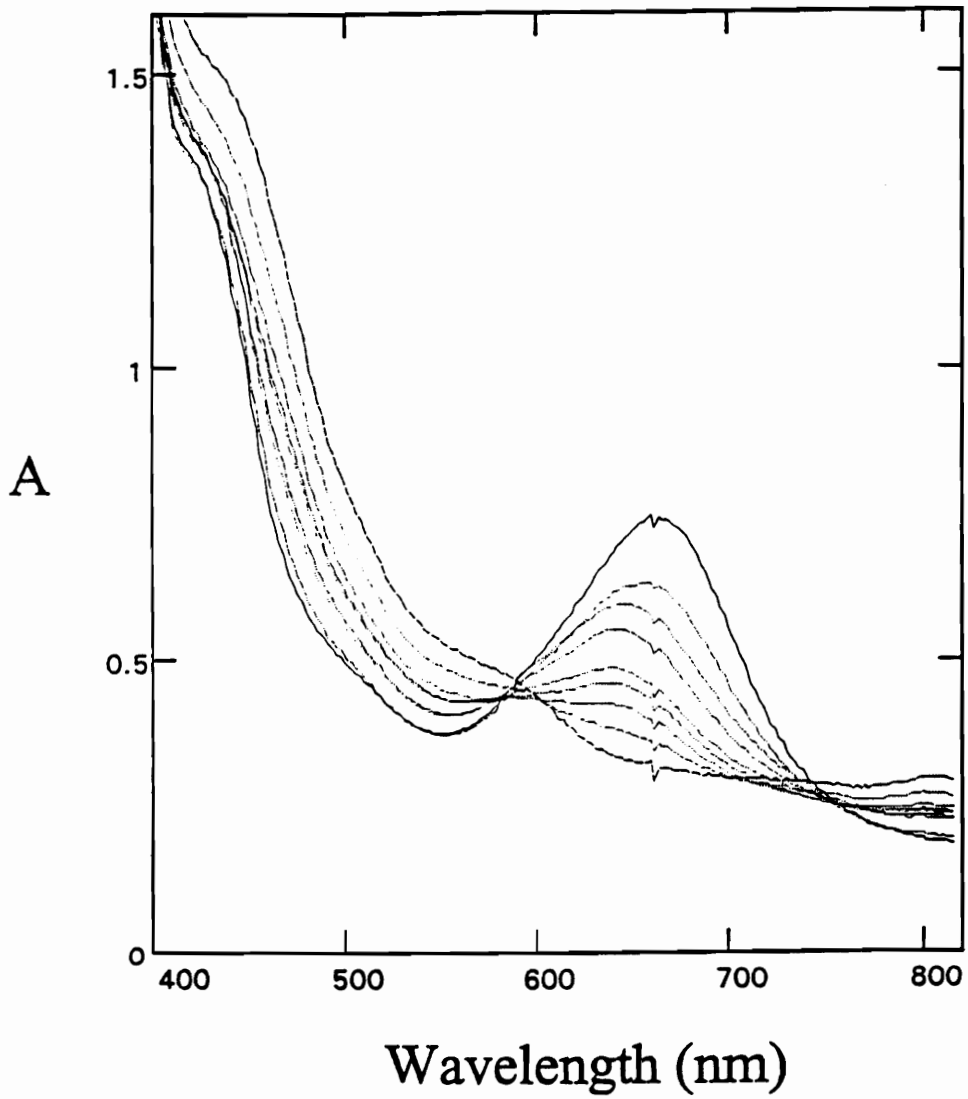

Figure 33. *Time Progression of a Photolysis of the {[(bpy)$_2$Ru(dpb)]$_2$IrCl$_2$}(PF$_6$)$_5$ (bpy = 2,2'-bipyridine and dpb= 2,3-bis(2-pyridyl)benzoquinoxaline) Trimetallic with an Electron Donor.* The (—) line represents zero time, the (• • •) lines are through the progression of time, ending in the final time of 30 minutes (- - -). The trimetallic complex (2.4×10^{-5} M) is in acetonitrile with the electron donor, 0.035 M dimethylaniline. The system was irradiated at 660 nm. All spectra were recorded at room temperature.[a]
[a]Reference 74.

No changes are observed in the UV-vis spectrum of $\{[(bpy)_2Ru(dpb)]_2IrCl_2\}^{5+}$ in this solvent electron donor mixture without exposure to light. No changes occurred in the spectrum of the $\{[(bpy)_2Ru(dpb)]_2IrCl_2\}^{5+}$ in the absence of the ED upon exposure to light. The changes in the $\{[(bpy)_2Ru(dpb)]_2IrCl_2\}^{5+}$ spectrum were only exhibited in the presence of both the ED and irradiation at 660 nm.

To further verify the production of the two electron species a combined experiment of spectroelectrochemistry and photolysis was conducted. An acetonitrile stock solution of the trimetallic complex, electrolyte, and sacrificial electron donor was made under dark room conditions. Spectroelectrochemistry was conducted on an aliquot of that solution to generate the two electron reduced complex in the presence of the ED. After the sample had been reduced by two electrons, it was re-oxidized to the original oxidation state. During this procedure, both reduction and re-oxidation, UV-vis spectra were taken, yet dark room conditions were maintained. After the $\{[(bpy)_2Ru(dpb)]_2IrCl_2\}^{5+}$ complex was regenerated, this electrolyzed solution was photolyzed, using a 660 nm 10 nm narrow bandpass filter. The irradiation wavelength should be at the 666 nm, corresponding to the $Ru(d\pi) \rightarrow dpb(\pi^*)$ CT band. Available filtering capabilities, however, restrict the irradiation wavelength to 660 nm. The results of these combined experiments are shown in Figures 34 and 35.

The combined spectroelectrochemical/photochemical experiment was conducted with two different sacrificial electron donors, triphenylamine and dimethylaniline. The solid line, in both cases, corresponds to the $\{[(bpy)_2Ru(dpb)]_2IrCl_2\}(PF_6)_5$ parent complex. The dotted lines are the electrogenerated two electron reduced species, and the

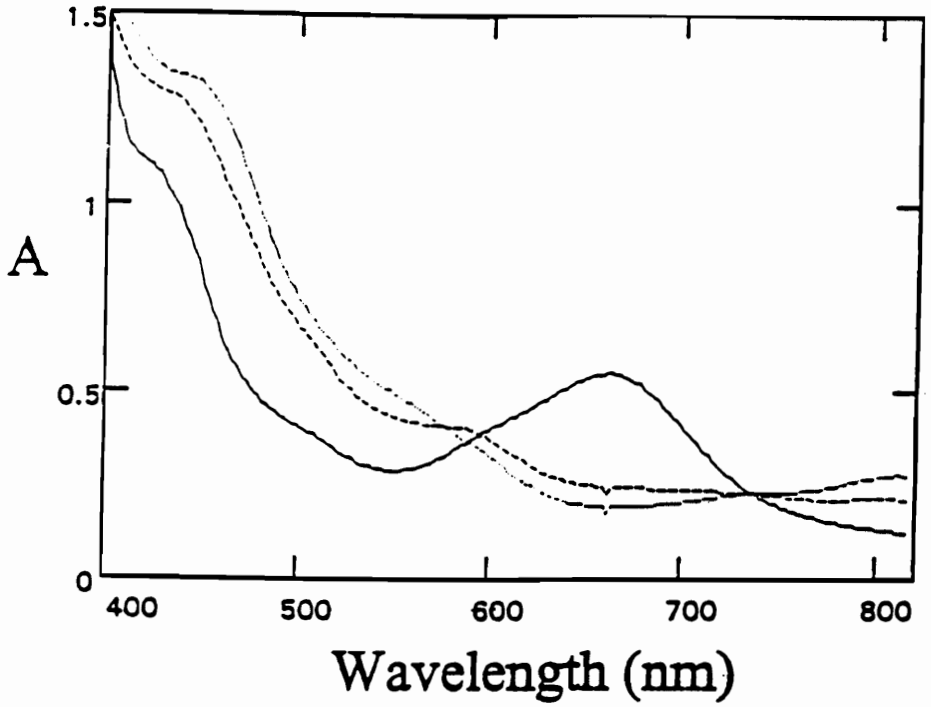

Figure 34. *Results of the Combination of Spectroelectrochemistry and Photochemistry of the {[(bpy)$_2$Ru(dpb)]$_2$IrCl$_2$}(PF$_6$)$_5$ (2,2'-bipyridine and dpb = 2,3-bis(2-pyridyl)benzoquinoxaline) Trimetallic with an Electron Donor.* [—] original trimetallic (2.4×10^{-5} M) in solution with dimethylaniline (0.035 M) and 0.1 M Bu_4NPF_6. [• • •] electrochemically generated two electron reduced trimetallic $\{[(bpy)_2Ru(dpb)]_2IrCl_2\}^{3+}$ and oxidized dimethylaniline. [- - -] after 30 minutes of 660 nm exposure to photochemically produce the $\{[(bpy)_2Ru(dpb)]_2IrCl_2\}^{3+}$. All spectra were recorded at room temperature.[a]

[a]Reference 74.

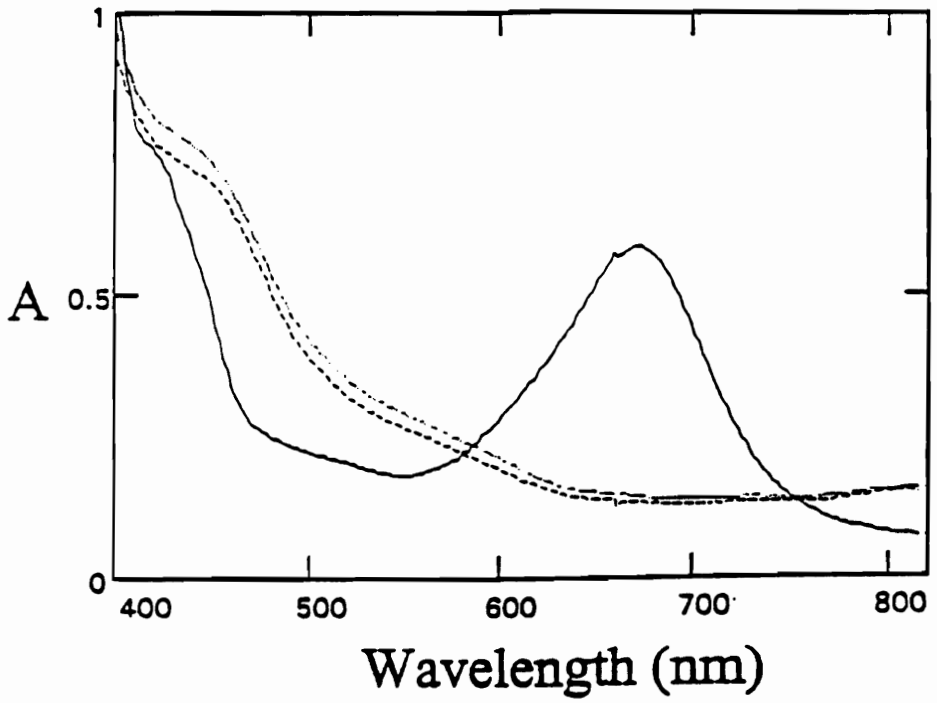

Figure 35. *Results of the Combination of Spectroelectrochemistry and Photochemistry of the {[(bpy)$_2$Ru(dpb)]$_2$IrCl$_2$}(PF$_6$)$_5$ (bpy = 2,2'-bipyridine and dpb = 2,3-bis(2-pyridyl)benzoquinoxaline) Trimetallic with an Electron Donor.* [—] = original trimetallic (2.8×10^{-5} M) in solution with triphenylamine (1.4×10^{-2} M) and 0.1 M Bu_4NPF_6. [• • •] = electrochemically generated two electron reduced trimetallic, $\{[(bpy)_2Ru(dpb)]_2IrCl_2\}^{3+}$. [- - -] 30 minutes of 660 nm exposure to photochemically produce the $\{[(bpy)_2Ru(dpb)]_2IrCl_2\}^{3+}$. All spectra were recorded at room temperature.[a]
[a]Reference 74.

dashed lines correspond to the photochemically generated two electron reduced species. In the case of dimethylaniline as the electron donor, the comparison to the photochemically and electrochemically produced reduced species shows some minor differences. This is due to the oxidized products of the dimethylaniline. A peak is produced at 590 nm. Hand and Nelson observed this peak in the oxidation of dimethylaniline.[76] It has been attributed to the crystal violet product. This same product also exhibits a broad, although less intense, peak at 700 nm. The introduction of the bands resulting from the oxidative product would explain the variance between the electrochemical and photochemical results in the region between approximately 550-800 nm. The use of an alternate electron donor, triphenylamine, in the photolysis of the trimetallic system yields less complicated spectroscopy and better overlap of the UV/vis spectra. This is due to no triphenylamine oxidative product being observed in the region of interest. A drawback of using this sacrificial electron donor is that this system has a much lower quantum yield for the product. In either event, with this experiment, the identity of the photolyzed species has been identified. The two electron reduced species of the trimetallic complex has been photochemically generated. This establishes that $\{[(bpy)_2Ru(dpb)]_2IrCl_2\}^{5+}$ is the first functioning molecular device for photoinitiated electron collection.

To determine the nature of the electron donor (ED) interaction with the trimetallic complex, Stern-Volmer quenching experiments were performed. The ED can quench the excited state of the trimetallic complex in two fashions. The quenching can be either dynamic or static. The difference between the two types of quenching is a matter of

determining if the ED interacted with the absorbing species prior to or after excitation. Static quenching implies a preassociation of the electron donor and the trimetallic prior to the excitation step. Dynamic quenching, on the other hand, assumes that interaction which leads to the desired photoproduct did not involve a preassociation of the ED and light absorber. Stern-Volmer quenching is a dynamic quenching kinetic scheme. As discussed in Chapter 2, the plot of the inverse of the quantum yield for product formation ($1/\Phi$) versus the concentration of the electron donor or quencher (1/[Q]) results in a straight line whose ratio of slope to intercept ratio yields the Stern-Volmer quenching constant (K_{SV}) . This constant's value is equal to the product of the light absorber's excited state lifetime (τ_A) and the quenching rate constant (k_q). The limiting quantum yield, at zero photolysis time, for the trimetallic complex was determined for varying electron donor concentrations. The quantum yield for production of product needed to be determined. At each concentration, a photolysis experiment was conducted that produced the reduced species. A plot of the quantum yield at each time interval versus the photolysis time was made. The extrapolation of this line back to zero time gives the limiting quantum yield of the trimetallic at that electron donor concentration. The inverse values for the quantum yields [$1/\Phi$] and the electron donor concentrations [1/Q] were plotted (Figure 36). This yields a value for the Stern-Volmer quenching constant (K_{SV}) of 85 M^{-1} ($K_{sv} = \tau_A k_q$). If one assumes a diffusional limit of for k_q ($1.9 \times 10^{10} M^{-1}s^{-1}$),[77] then one can calculate the lower limit for the trimetallic's excited state lifetime. This analysis gives $\tau_A > 4.5$ ns. The Stern-Volmer plot yielded a straight line but the τ_A value produced

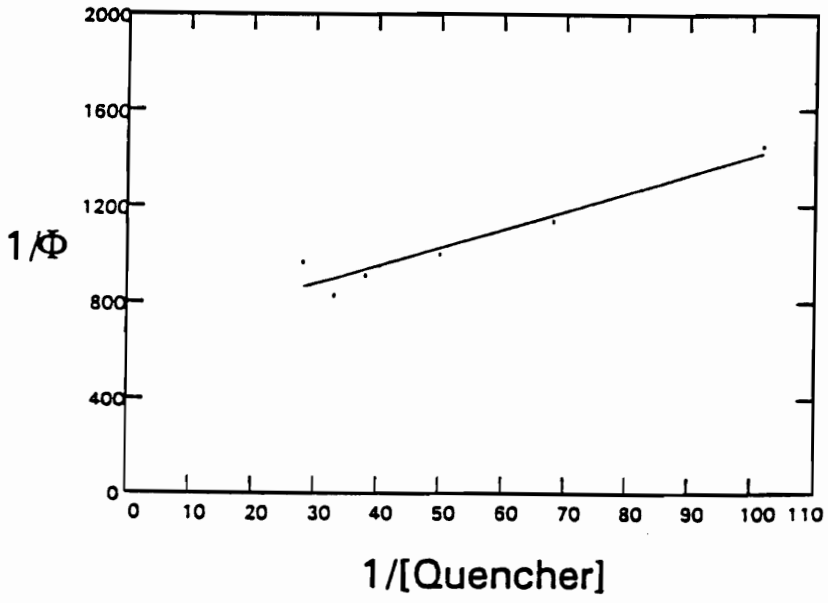

Figure 36. *Stern-Volmer Plot for the $\{[(bpy)_2Ru(dpb)]_2IrCl_2\}^{5+}$ (bpy = 2,2'-bipyridine and dpb = 2,3-bis(2-pyridyl)benzoquinoxaline) Trimetallic Complex with the Electron Donor Dimethylaniline.* This quenching plot for the photolysis of $\{[(bpy)_2Ru(dpb)]_2IrCl_2\}^{5+}$ has been produced by varying the concentration of the dimethylaniline electron donor while maintaining a constant 2.8×10^{-5} M $\{[(bpy)_2Ru(dpb)]_2IrCl_2\}^{5+}$ concentration. The limiting quantum yields were determine for each concentration and plotted versus concentration. The system was photolyzed at 650 nm and its spectra were recorded at room temperature in spectral grade acetonitrile.[a]
[a]Reference 74.

was not consistent with the predicted lifetime of the complex, $\tau < 5$ ns. In order for the Stern-Volmer dynamic quenching model to hold, the lifetime of the complex should be greater that 5 ns, since electron transfer quenching to produce observable product will not normally occur at a diffusion controlled rate. This data indicates that a dynamic model for the electron donor interaction with the trimetallic is not completely accurate, i.e, some static quenching is probably occurring.

Given the structure of the trimetallic and electron donor, one can see how the interaction may not be exclusively dynamic. The dpb trimetallic complex has an extending π system inherent to the dpb bridging ligand. It is plausible that the π system of the DMA electron donor has a preassocitation with the trimetallic prior to excitation. This is more likely due to the high concentration of electron donor in solution. A π-stacking interaction could be taking place between the electron donor and trimetallic before excitation. This assertion of a preassociation could lead to some degree of static quenching. The quenching scheme is probably quite complex, involving both a static and dynamic component.

Conclusions.

The synthesis of the $\{[(bpy)_2Ru(BL)]_2IrCl_2\}(PF_6)_5$ (where BL = dpp, dpq, and dpb) has produced the first functional photoinitiated electron collection device known in the literature.[74] The device has been designed, prepared, and studied. With the combination of two experiments, spectroelectrochemistry and photolysis, the device has been proven to perform its function. Although the great venture from drawing table to

reality of the first functioning photoinitiated electron collector has taken place, improvements can still be made.

The main pitfall of the $\{[(bpy)_2Ru(dpb)]_2IrCl_2\}(PF_6)_5$ trimetallic is its short excited state lifetime. The lifetime of less that 5 ns drastically limits the quantum yield for the functioning of this complex. Although it performs its electron collecting function, improvements in efficiency can be made. The direct association of the electron donor and the trimetallic will improve the quantum efficiency. The complexes will already be preassociated and will eliminate any need for diffusion of the electron donor to the trimetallic.

The direct association of the electron donor and trimetallic are underway with the incorporation of an inorganic electron donor into the trimetallic framework. Two $(bpy)_2Ru^{II}(dpp)$ moieties will be substituted for the bipyridine ligands on each LA of the PIEC core. This will create the heptametallic complex

$$\{[(bpy)_2Ru(dpp)]_2Ru(BL)IrCl_2(BL)Ru[(dpp)Ru(bpy)_2]_2\}^{13+}$$

Here, optical excitation will lead to an oxidized Ru on the periphery of the molecule and a reduced BL at the center. This charge separated state is spatially separated and will have a $\tau >> 5$ ns. This will drastically improve device functioning. The starting materials of this complex have already been synthesized. The $\{[(bpy)_2Ru(dpp)]_2RuCl_2\}^{4+}$ complex had previously been prepared in the literature,[63] but its synthesis has been modified. The bridging ligand complex

$\{[(bpy)_2Ru(dpp)]_2Ru(dpq)\}^{6+}$ has also been synthesized. Even though the first generation photoinitiated electron collectors have recently been developed, the second generation is already on its way.

CHAPTER 5.

SYNTHESIS AND INVESTIGATION OF A Rh^{III}/Ru^{II} MIXED-METAL TRIMETALLIC COMPLEX DESIGNED FOR PHOTOINITIATED ELECTRON COLLECTION.

Introduction.

Although further investigation and modifications of the Ir^{III}/Ru^{II} trimetallic are currently underway, synthesis and exploration of a Rh^{III}/Ru^{II} analog has ensued.[64] The trimetallic complex $\{[(bpy)_2Ru(dpp)]_2RhCl_2\}(PF_6)_5$, is similar in architecture to the iridium trimetallic complex, yet affords different spectroscopic and electrochemical properties. The rhodium trimetallic complex will function differently as a photoinitiated electron collection device. Photoinitiation will still occur at the ruthenium chromophore $Ru(d\pi) \rightarrow dpp\ (\pi^*)$ CT, but electron "storage" will be on the rhodium metal center instead of the bridging ligands.

Synthesis.

The rhodium trimetallic complex was synthesized in a building block manner, yet its purification was quite different from the iridium trimetallic.[62, 64] As depicted in Figure 37, the $[(bpy)_2Ru(dpp)](PF_6)_2$ was heated at reflux with $RhCl_3$ in a 2:1 ethanol/water for 2 hours. The purification of the iridium trimetallic was via size exclusion chromatography. For the rhodium trimetallic complex, however, no chromatography was needed. Instead, a series of metathesis steps back and forth between the PF_6^- salt and the Cl^- salt rids the system of the monometallic impurity. This made it possible to prepare large quantities of this complex quite easily.

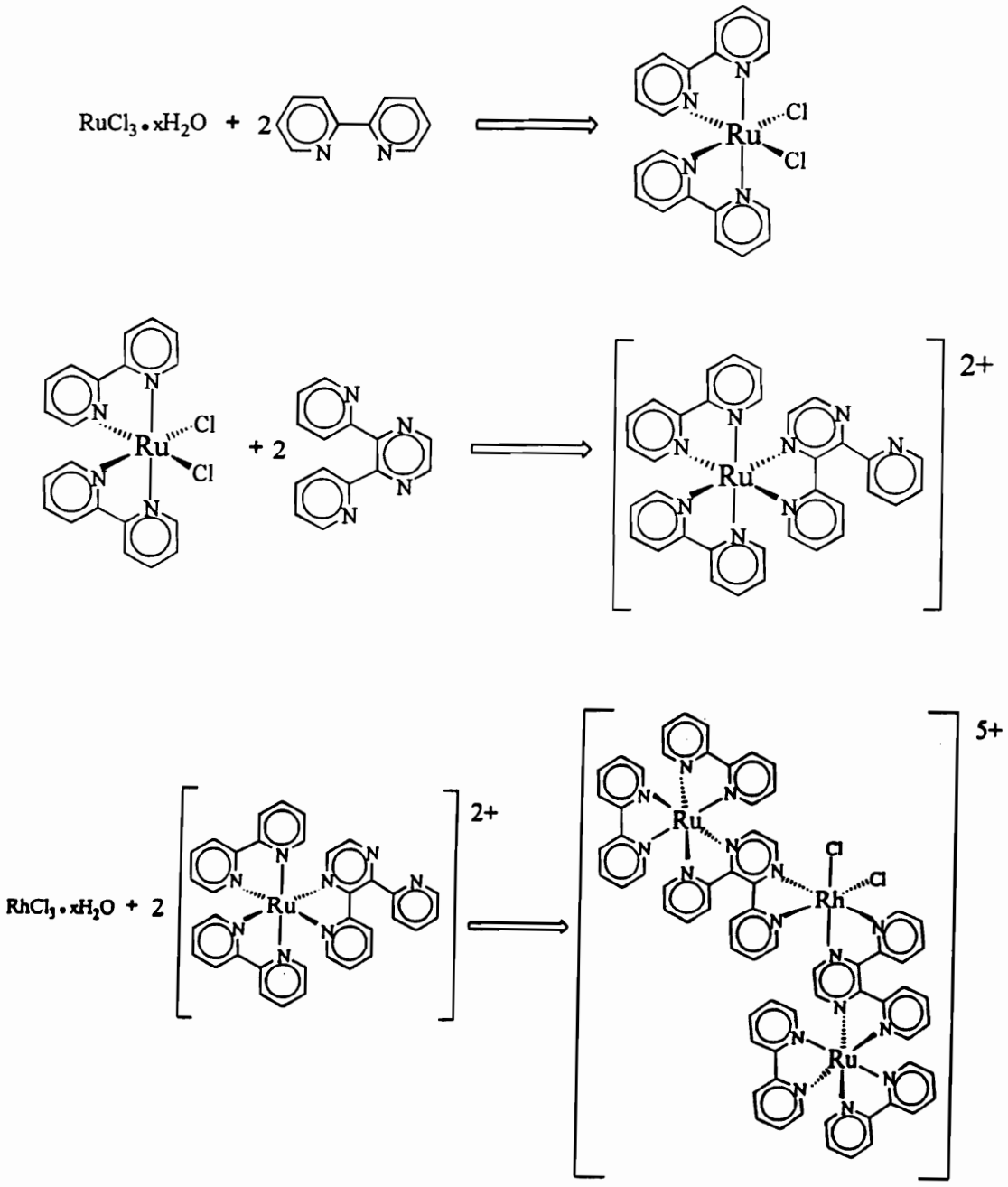

Figure 37. *Synthesis of the $\{[(bpy)_2Ru(dpp)]_2RhCl_2\}(PF_6)_5$ (bpy = 2,2'-bipyridine and dpp = 2,3-bis(2-pyridyl)pyrazine) Trimetallic Complex.*

Electrochemistry.

The cyclic voltammogram of $\{[(bpy)_2Ru(dpp)]_2RhCl_2\}(PF_6)_5$ is shown in Figure 38.[64] This trimetallic has one oxidation and three reductions. The oxidation is assigned as two closely spaced, one electron waves corresponding to the oxidation (Ru^{II}/Ru^{III}) of the two equivalent ruthenium centers and occurs at 1.50 V. The fact that the two $Ru^{II/III}$ oxidations are overlapping indicates that these metal centers are largely electronically uncoupled. Thus, the two chromophores will function independently. The first reduction in the cyclic voltammogram is irreversible and corresponds to a two electron reduction of the Rh^{III}. This Rh^{III}/Rh^{I} reduction appears at -0.40 V. The second and third reversible reductions are dpp based couples and occur at -0.62 V and -0.85V.

The electrochemical scheme of this system is quite interesting. As depicted in Figure 39, the $Rh^{III/I}$ reduction causes a structural change in the complex. Once the metal center has been reduced to Rh^{I}, the geometry around this metal center changes from octahedral to square planar. The now d^8 metal center prefers the square planar geometry. This promotes the loss of the two chlorides attached to the Rh^{I} center. This free Cl^- has been detected electrochemically (an irreversible $2Cl^-/Cl_2$ couple at +0.90 V vs. Ag/AgCl) and chemically (by addition of Ag^+ yielding a AgCl precipitate).

Electronic Absorption Spectroscopy.

The electronic absorption spectrum of the $\{[(bpy)_2Ru(dpp)]_2RhCl_2\}(PF_6)_5$ can be assigned with the use of the established spectrum of it iridium analog, previously discussed in Chapter 4.[64] The spectrum of the rhodium based system, Figure 40, has five

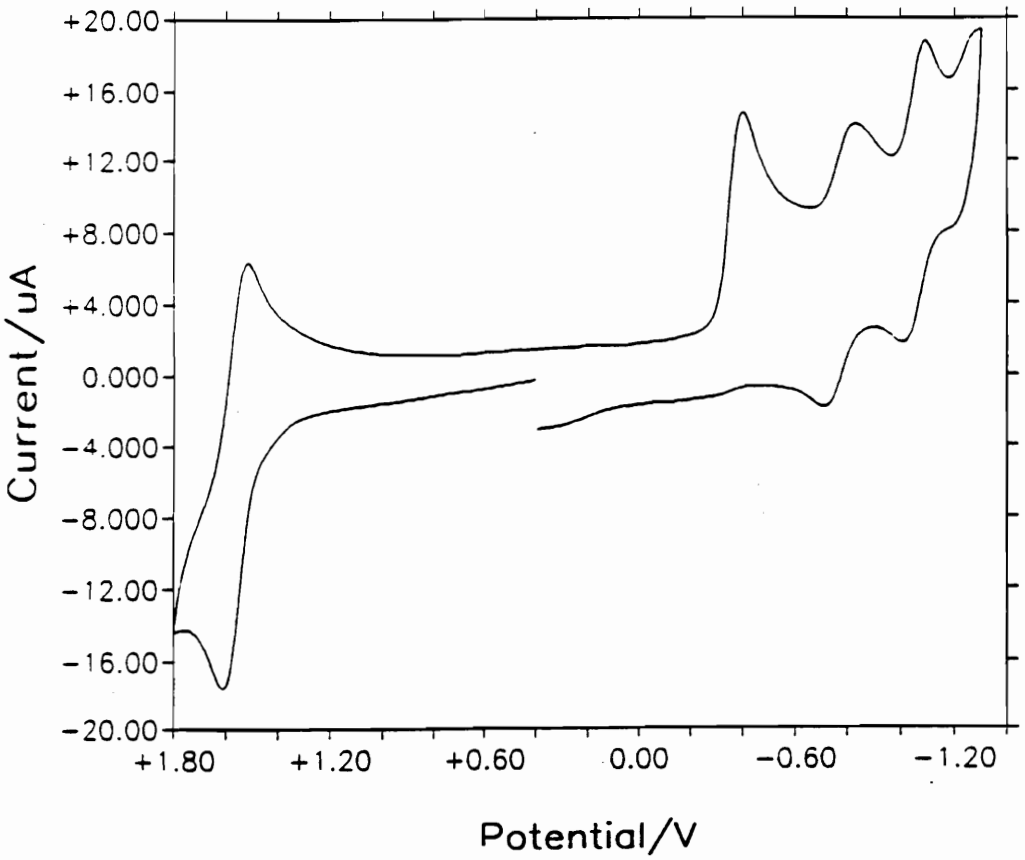

Figure 38. *Cyclic Voltammogram of $\{[(bpy)_2Ru(dpp)]_2RhCl_2\}(PF_6)_5$ (bpy = 2,2'-bipyridine and dpp = 2,3-bis(2-pyridyl)pyrazine).* This voltammogram was taken at RT, at a scan rate of 200 mV/s, in spectral grade acetonitrile with 0.1 M Bu_4NPF_6 as the supporting electrolyte. The electrodes utilized were a platinum disk working electrode, a platinum wire auxiliary electrode, and a Ag/AgCl gel reference electrode (0.29 V vs. NHE).[a]

[a]Reference 64.

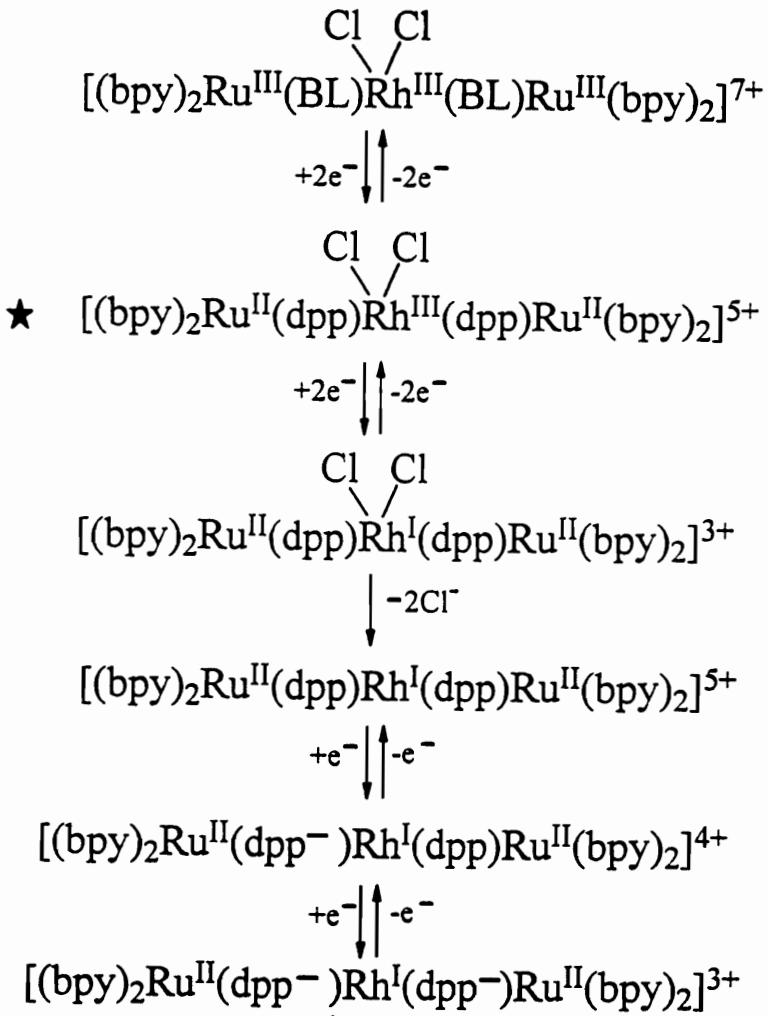

Figure 39. *The Electrochemical Scheme Corresponding to the Cyclic Voltammogram for the {[(bpy)$_2$Ru(dpp)]$_2$RhCl$_2$}(PF$_6$)$_5$ (bpy = 2,2'-bipyridine dpp = 2,3-bis(2-pyridyl)pyrazine).* The '★' denotes the synthesized oxidation state.

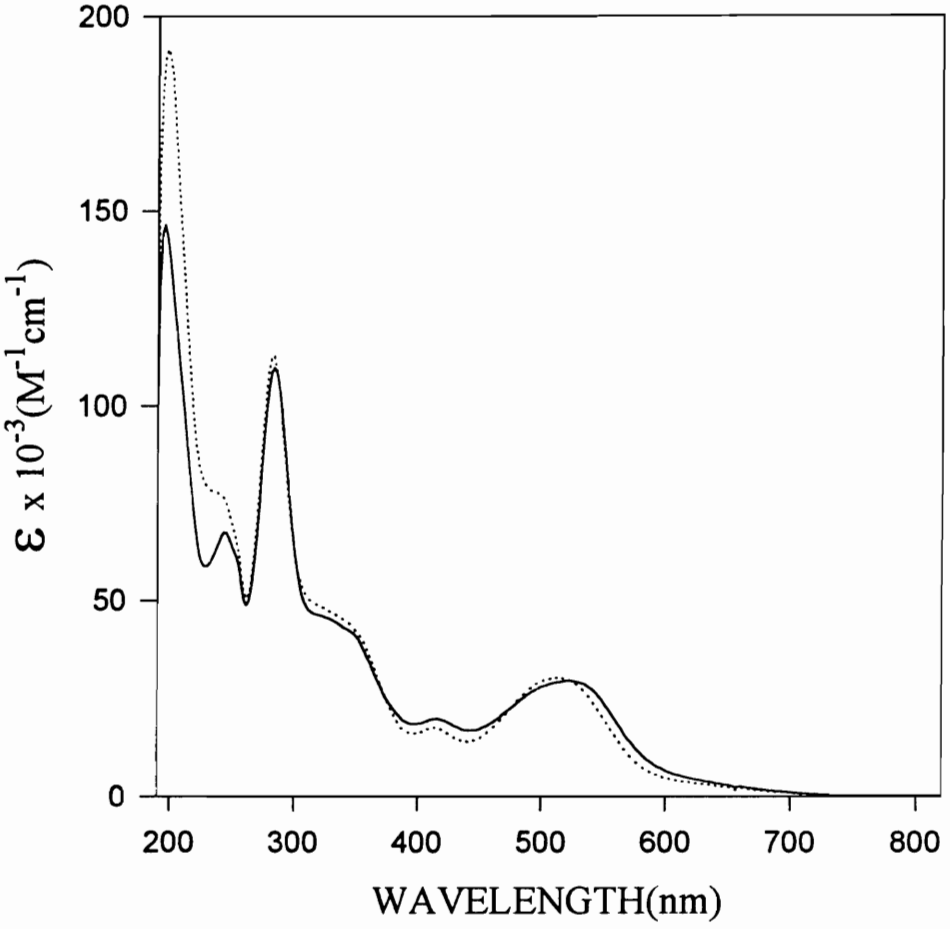

Figure 40. *Electronic Absorption Spectrum of* $\{[(bpy)_2Ru(dpp)]_2RhCl_2\}^{5+}$ *[—] and* $\{[(bpy)_2Ru(dpp)]_2IrCl_2\}^{5+}$ *[••••] (bpy = 2,2'-bipyridine and dpp = 2,3-bis(2-pyridyl)pyrazine).* These spectra were taken in room temperature spectral grade acetonitrile.[a]

[a]Reference 64.

characteristic peaks. The lowest lying peak is at 514 nm and corresponds to a Ru(dπ) → dpp(π*) CT transition. At 416 nm the characteristic Ru(dπ) → bpy(π*) CT transition is exhibited. The n → π*, π → π* intraligand transitions of the bpy ligands appears at 284 nm. Finally, two shoulders appear at 324 and 346 nm. As in the iridium trimetallic complex, these bands correspond to a Ru(dπ) → bpy(π*) CT and an intraligand dpp π→ π* transition. As exhibited by the overlaid spectra, the electronic absorption spectroscopy of $\{[(bpy)_2Ru(dpp)]_2IrCl_2\}(PF_6)_5$ and $\{[(bpy)_2Ru(dpp)]_2RhCl_2\}(PF_6)_5$ are virtually indistinguishable. This demonstrates the dominance of the ruthenium chromophores in the electronic absorption spectroscopy of these trimetallic systems.

Spectroelectrochemistry.

Figure 41 shows the spectroelectrochemistry results for the two electron reduced form of the rhodium trimetallic. Upon a two electron reduction, at -0.60 V, the Ru(dπ) → dpp(π*) CT is lost, as well as the two shoulders at 324 and 346 nm. Two peaks grow in at approximately 422 and 468 nm. In the case of the 422 nm peak, this could be interpreted as a shift of the Ru(dπ) → bpy(π*) CT. The exact nature of the bands is unclear. The reoxidation to generate the original trimetallic is not possible. This irreversible spectroelectrochemistry reproducibly generates the same species. The reproducibility is an indication that the same products of the two electron reduction are occurring each time. In other words, it appears that the product is not random fragmentation of the rhodium trimetallic upon generation of the Rh^I center. If random

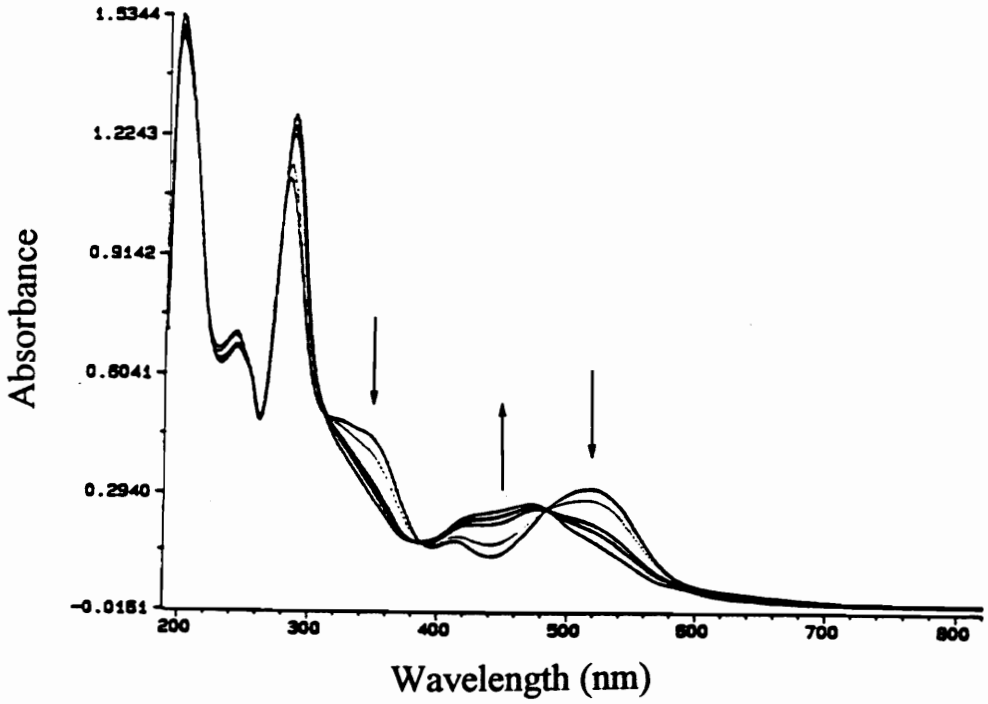

Figure 41. *Electronic Absorption Spectra of the* $\{[(bpy)_2Ru(dpp)]_2RhCl_2\}^{5+}$ *(bpy = 2,2'-bipyridine and dpp = 2,3-bis(2-pyridyl)pyrazine) and the Species Produced During and After a Two Electron Reduction.* All spectra were taken in room temperature spectral grade acetonitrile containing 0.1 M Bu_4NPF_6.

fragmentation was occurring, the spectroelectrochemistry of the two electron reduction would not be reproducible.

Bulk Electrolysis/Cyclic Voltammetry.

To further explore the products produced upon the two electron reduction of $\{[(bpy)_2Ru(dpp)]_2RhCl_2\}^{5+}$, a combined experiment of bulk electrolysis and cyclic voltammetry was conducted. The $\{[(bpy)_2Ru(dpp)]_2RhCl_2\}(PF_6)_5$ complex was dissolved in spectral grade acetonitrile with 0.1 M Bu_4NPF_6 and a cyclic voltammogram was taken. Next, the complex was reduced by two electrons, and then a cyclic voltammogram of the reduced species was taken. The results of this experiment are shown in Figure 42. The single ruthenium oxidation in the $\{[(bpy)_2Ru(dpp)]_2RhCl_2\}^{5+}$ complex has become two oxidations, the rhodium reduction has been lost, and a peak corresponding to $2Cl^-/Cl_2$ has now grown in at 0.90V. Chloride was also tested for, and found present, through the addition of $AgPF_6$ to the bulk electrolysis solution which produced a AgCl precipitate. All of these facts support the assumption that a Rh^I based trimetallic, of the form $\{[(bpy)_2Ru(dpp)]_2Rh^I\}(PF_6)_5$, is produced. This is consistent with the observed electrochemical behavior of $Rh^{III}(bpy)_2Cl_2$, which undergoes an irreversible $2e^-$ reduction followed by Cl^- loss to produce $[Rh^I(bpy)_2]^+$.[47]

Synthesis of the Rh^I Trimetallic.

In an attempt to verify the identity of the electrogenerated species, the Rh^I trimetallic was independently synthesized by reaction of the Rh^I dimer $[(C_2H_4)_2Rh^ICl]_2$ with two equivalents of the ruthenium monometallic, $[Ru(bpy)_2(dpp)](PF_6)_2$. The dimer

[A]

[B]

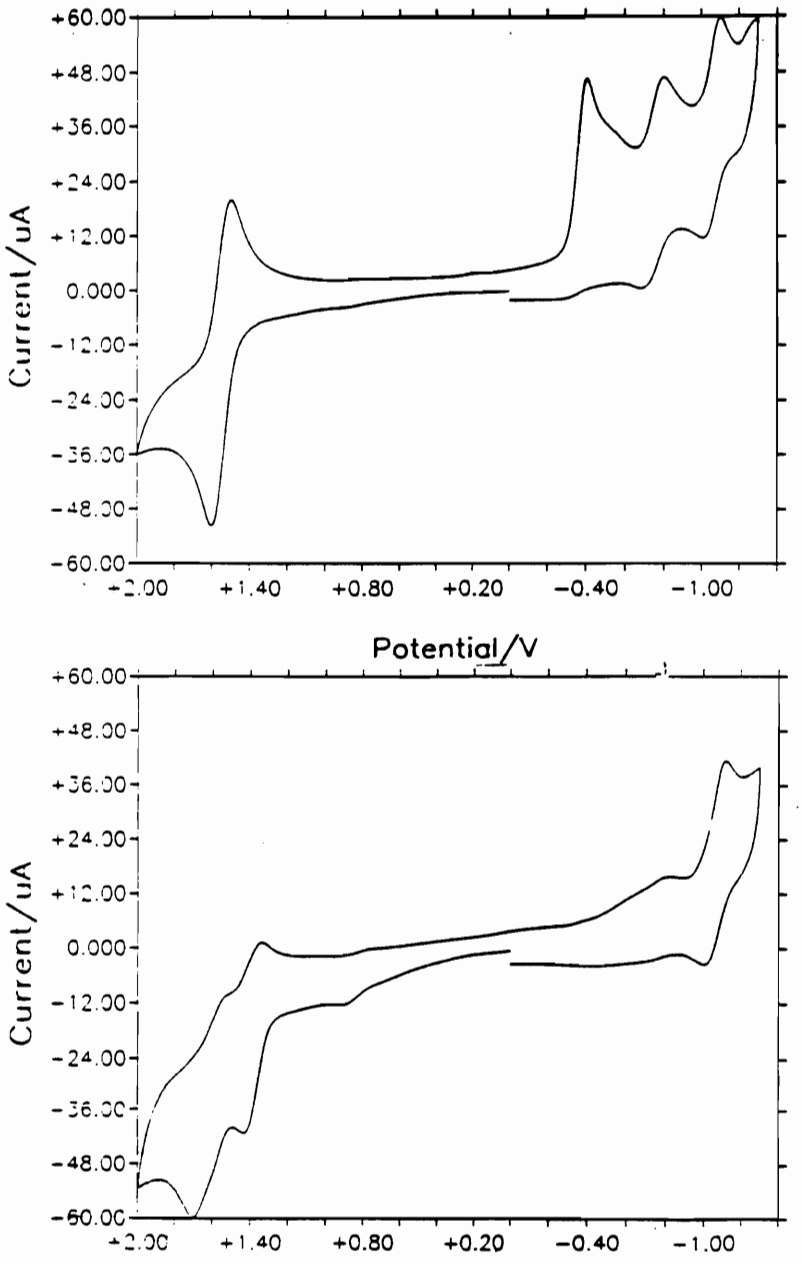

Figure 42. *Cyclic Voltammograms of the Original and Two Electron Reduced {[(bpy)$_2$ Ru(dpp)]$_2$RhCl$_2$}(PF$_6$)$_5$ (bpy = 2,2'-bipyridine and dpp = 2,3-bis(2-pyridyl)pyrazine).* [A] Original $\{[(bpy)_2Ru(dpp)]_2RhCl_2\}^{5+}$. [B] Two electron reduced species. These voltammograms were taken a scan rate of 200 mV/s, in spectral grade acetonitrile with 0.1 M Bu_4NPF_6 as the supporting electrolyte. The electrodes utilized were a platinum disk working electrode, a platinum wire auxiliary electrode, and a Ag/AgCl gel reference electrode (0.29 V vs. NHE).

was reacted with two equivalents of $TlPF_6$ in acetonitrile under inert atmosphere conditions which led to the formation of the solid TlCl . The ruthenium monometallic complex $[Ru(bpy)_2(dpp)](PF_6)_2$ was added to the solution. The stoichiometry of the monometallic to the Rh^I centers was 2 to 1. This solution was heated for 1 hour, the solvent was removed, and the solid stored in its reaction vessel. The cyclic voltammetry of this procedure's product was the same as the cyclic voltammogram produced upon bulk reduction by $2e^-$ of the $\{[(bpy)_2Ru\ (dpp)]_2RhCl_2\}(PF_6)_5$ complex. Figure 43 shows these two voltammograms. As one can see they are virtually indistinguishable. Therefore, the electrochemical product is the same as the chemical reaction product designed to produce a $\{[(bpy)_2Ru(dpp)]_2Rh^I\}(PF_6)_5$ trimetallic. More experiments are planned to establish the identity of these species.

Photolysis.

From the cyclic voltammetry and electronic absorption spectroscopy the orbital energy diagram of the trimetallic complex has been deduced. Figure 44 shows the molecular orbital diagram for the complex. As with the iridium trimetallic system, the rhodium trimetallic form the central LA-EC-LA core of the photoinitated electron collector, the light absorbing units being the $[Ru^{II}(bpy)_2(dpp)]$ moieties, and the Rh^{III} metal center the electron collector. Since this presents a promising picture of a photoinitated electron collection system, the photochemistry of the $\{[(bpy)_2Ru(dpp)]_2RhCl_2\}(PF_6)_5$ system was explored.

The trimetallic complex $\{[(bpy)_2Ru(dpp)]_2RhCl_2\}(PF_6)_5$ has been photolyzed, in the presence of a sacrificial electron donor, triphenylamine, in an attempt to

[A]

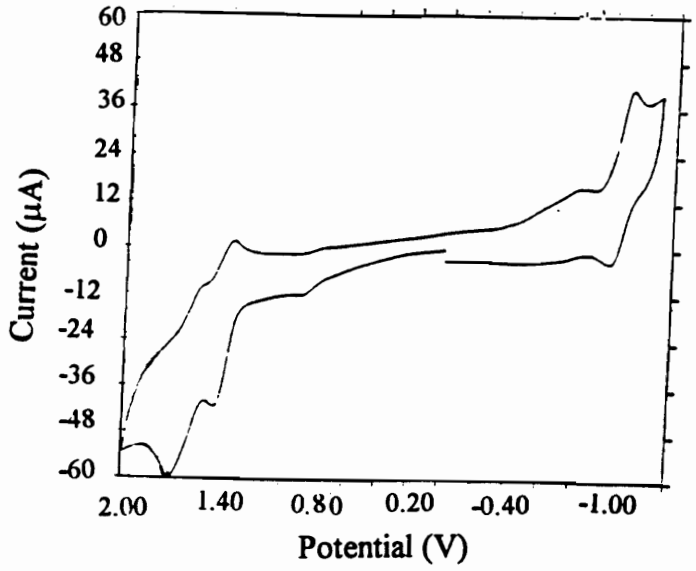

[B]

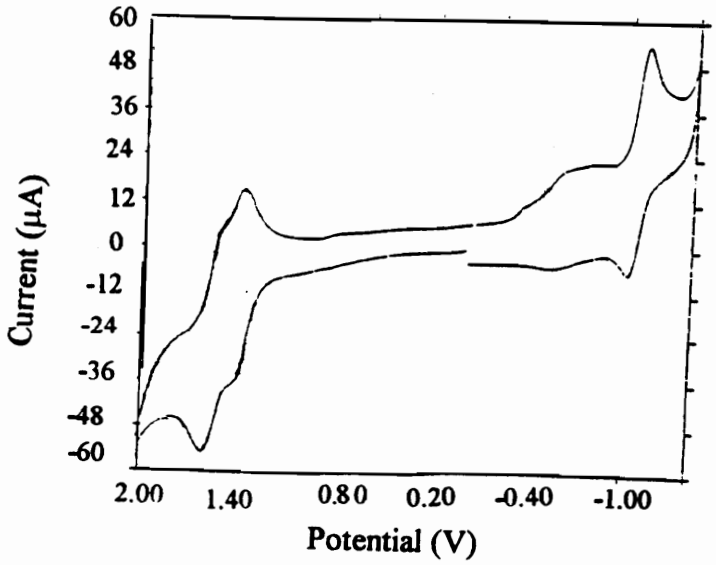

Figure 43. *Cyclic Voltammograms for the Electrochemical Product of the Two Electron Reduction of* $\{[(bpy)_2Ru(dpp)]_2RhCl_2\}(PF_6)_5$ *[A] and a Reaction Designed to Synthesize* $\{[(bpy)_2Ru(dpp)]_2Rh^{I}\}(PF_6)_5$ *[B].* These voltammograms were taken at a scan rate of 200 mV/s, in spectral grade acetonitrile with 0.1 M Bu_4NPF_6 as the supporting electrolyte. The electrodes utilized were a platinum disk working electrode, a platinum wire auxiliary electrode, and a Ag/AgCl gel reference electrode (0.29 V vs. NHE).

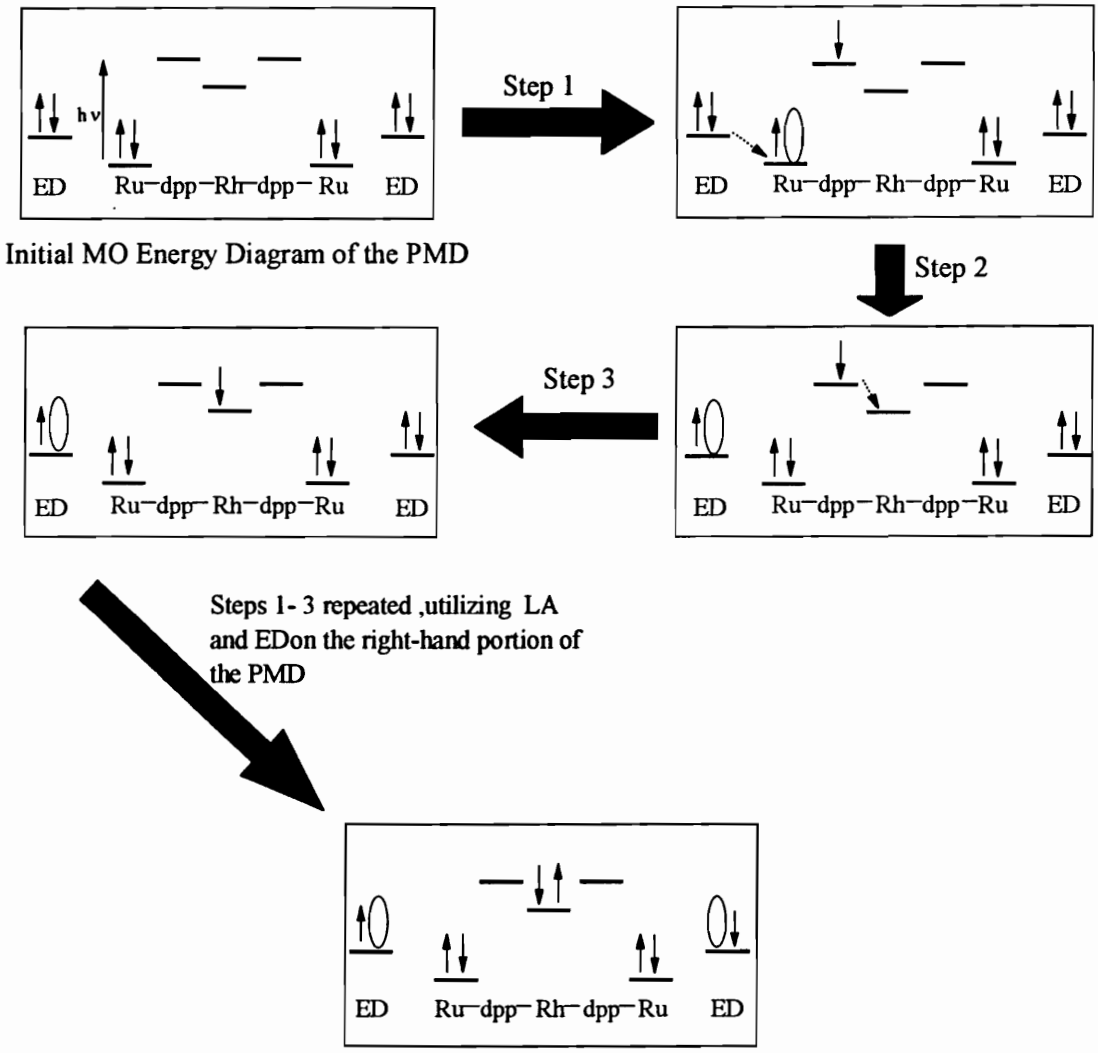

Figure 44. *Orbital Energy Diagram of the $\{[(bpy)_2Ru(dpp)]_2RhCl_2\}(PF_6)_5$ (bpy = 2,2'-bipyridine and dpp = 2,3-bis(2-pyridyl)pyrazine) Trimetallic Complex Before and After Light Absorption.*

photochemically produce the two electron reduced product of the system. The complex was dissolved in an acetonitrile solution of 0.1 M triphenylamine, and then placed in a sample cell with a 1 mm magnetic stirring bar. This system was deoxygenated and flame sealed. The trimetallic and electron donor solution was exposed to light using a 520 nm narrow bandpass filter. The $\{[(bpy)_2Ru(dpp)]_2RhCl_2\}(PF_6)_5$ complex was determined to be photostable in the absence of the electron donor. The solution of the $\{[(bpy)_2Ru(dpp)]_2RhCl_2\}(PF_6)_5$ complex and electron donor was also stable in the absence of light. Although the final product does not exactly overlap (see Figure 45) with the spectroelectrochemical counterpart, the two spectra do appear to have good agreement. It appears as though the photochemical product and electrochemical product are the same. Consequently, the use of this trimetallic complex as a PIEC device looks quite promising.

Conclusions.

The identity of the$\{[(bpy)_2Ru(dpp)]_2RhCl_2\}(PF_6)_5$ two electron reduced species, generated both electrochemically and photochemically is still not concrete. The loss of the chloride upon reduction and the appearance of the two oxidation waves in the combined experiment of bulk electrolysis and cyclic voltammetry would lead one to believe that the Rh^I square planar complex is being formed. Yet, the reductive potential of the dpp bridging ligand is the same as in the $[(bpy)_2Ru(dpp)]^{2+}$ monometallic complex. The reductive potential of the dpp should be shifted if the Rh^I complex is being formed. If the monometallic fragment is being produced, then only one oxidative wave, not two as is observed, should appear. Although many of the observations lead to the conclusion of a

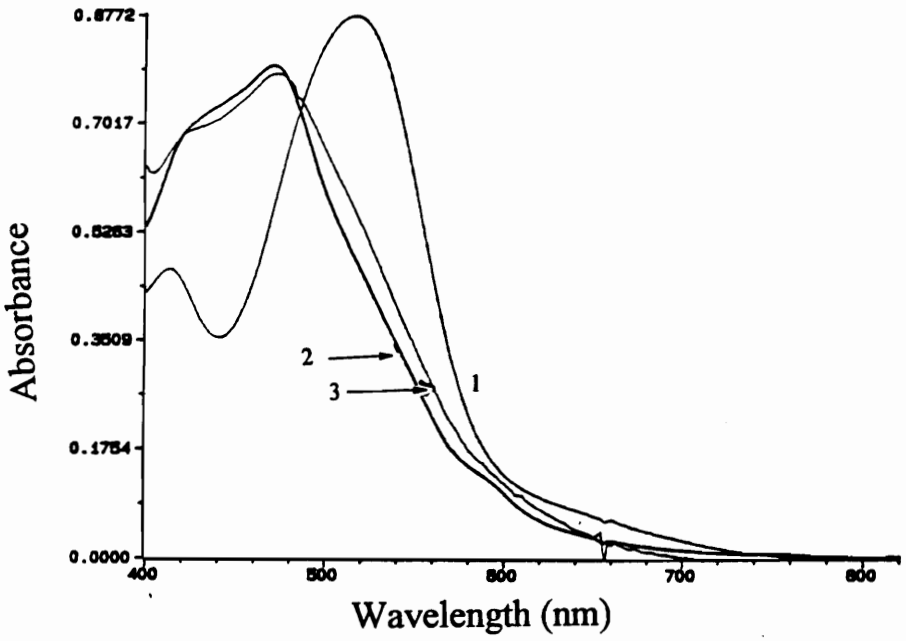

Figure 45. *Photolysis of {[(bpy)$_2$Ru(dpp)]$_2$RhCl$_2$}(PF$_6$)$_5$ (bpy = 2,2'-bipyridine and dpp = 2,3-bis(2-pyridyl)pyrazine) with an Electron Donor.* (1) $\{[(bpy)_2Ru(dpp)]_2RhCl_2\}^{5+}$ with 0.1 M triphenylamine in room temperature spectral grade acetonitrile; (2) after a 1.5 hour irradiation at 520 nm; (3) two electron reduced form of $\{[(bpy)_2Ru(dpp)]_2RhCl_2\}^{5+}$ generated electrochemically.

Rh^{I} product, others argue against that assumption. Therefore, the identity of the $\{[(bpy)_2Ru(dpp)]_2RhCl_2\}(PF_6)_5$ reductive product must be ruled still undetermined.

REFERENCES.

1. Balzani, V. *Supramolecular Photochemistry* NATO *Adv. Study Inst. Ser., Ser. D* **1987**, *214*, 135.

2. *Webster's Ninth New Collegiate Dictionary* Merriam-Webster Springfield, Massachusetts, **1988**.

3 Lever, A. B. P. *Inorganic Electronic Spectroscopy* Elsevier Publishing Company, New York, **1994**.

4. Balzani, V.; Bolletta, F.; Gandolfi, M.; Maestri, M. *Top. Curr. Chem* **1985,** *75*,1.

5. Gilbert, A.; Baggott, J. *Essentials of Molecular Photochemistry* CRC Press, London, **1992**.

6. Wayne, R. P. *Photochemistry* Butterworth & Co. London, **1970**.

7. Adamson, A. W.; Fleischauer, P. D. *Concepts of Inorganic Photochemistry* John Wiley & Sons, New York, **1975**.

8. Bard, A. J.; Faulkner, L. R. *Electrochemical Methods Fundamentals and Applications* John Wiley & Sons, New York, **1980**.

9. Kissinger, P. T.; Heineman, W. R. *Laboratory Techniques in Electroanalytical Chemistry* Marcel Dekker, Inc., New York, **1984**.

10. Gust, D.; Moore, T. A.; Moore, A. L.; Macpherson, A. N.; Lopez, A.; DeGraziano, J. M.; Gouni, I.; Bittersmann, E.; Seely, G. R.; Gao, F.; Nieman, R. A.; Ma, X. C.; Demanche, L. J.; Hung, S.-C.; Luttrull, D. K.; Lee, S.-J.; Kerrigan, K. *J. Am. Chem. Soc.* **1993**, *115*, 11141.

11. Gust, D.; Moore, T. A.; Moore, A. L.; Lee, S.-J.; Bittersmann, E.; Luttrull, D. K.; Rehms, A. A.; DeGraziano, J. M.; Ma, X. C.; Gao, F.; Belford, R. E.; Trier, T. T. *Science* **1990**, 190.

12. Lee, S.-J.; DeGraziano, J. M.; Macpherson, A. N.; Shin, E.-J.; Kerrigan, P. K.; Seely, G. R.; Moore, A. L.; Moore, T. A.; Gust, D. *Chem. Phys.* **1994**, *176*, 321

13. Osuka, A.; Yamada, H.; Maruyama, K.; Mataga, N.; Asahi, T.; Ohkouchi, M.; Okada, T.; Yamazaki, I.; Nishimura, Y. *J. Am. Chem. Soc.* **1993**, *115*, 9439.

14. Chambron, J.-C.; Harriman, A.; Heitz, V.; Sauvage, J.-P. *J. Am. Chem. Soc.* **1993**, *115*, 6109.

15. Chen, P.; Westmoreland, D.; Danielson, E.; Schanze, K. S.; Anthon, D.; Neveux, Jr. P. E.; Meyer, T. J. *Inorg. Chem.* **1987**, *26*, 1116.

16. Strouse, G. F.; Schoonover, J. R.; Duesing, R.; Meyer, T. J. *Inorg. Chem.* **1995**, *34*, 2725.

17. Schoonover, J. R.; Strouse, G. F.; Chen, P.; Bates, W. D.; Meyer, T. J. *Inorg. Chem.* **1993**, *32*, 2618.

18. Meyer, T. J.; Meyer, G. J.; Pfennig, B. W.; Schoonover, J. R.; Timpson, C. J.; Wall, J. F.; Kobusch, C.; Chen, X.; Peek, B. M.; Wall, C. G.; Ou, W.; Erickson, B. W.; Bignozzi, C. A. *Inorg. Chem.* **1994**, *33*, 3952.

19. Oppermann, K. A.; Mecklenburg, S. L.; Meyer, T. J. *Inorg. Chem.* **1994**, *33*, 5295.

20. Indelli, M. T.; Bignozzi, C. A.; Harriman, A.; Schoonover, J. R.; Scandola, F. *J.*

Am. Chem. Soc. **1994**, *116*, 3768.

21. Al-Obaidi, A. H. R.; Gordon, K. C.; McGarvey, J. J.; Bell, S. E. J.; Grimshaw, J. *J. Phys. Chem.* **1993**, *97*, 10942.

22. Wang, Y.; Schanze, K. S. *Chem. Phys.* **1993**, *176*, 305.

23. Ryu, C. K.; Wang, R.; Schmehl, R. H.; Ferrere, S.; Ludwikow, M.; Merkert, J. W.; Headford, C. E. L.; Elliott, C. M. *J. Am. Chem. Soc.* **1992**, *114*, 430.

24. Larson, S. L.; Cooley, L. F.; Elliott, C. M.; Kelley, D. F. *J. Am. Chem. Soc.* **1992**, *114*, 9504.

25. Wang, Y.; Hause, B. T.; Rooney, M. M.; Burton, R. D.; Schanze, K. S. *J. Am. Chem. Soc.* **1993**, *115*, 5675.

26. Mecklenburg, S. L.; McCafferty, D. G.; Schoonover, J. R.; Peek, B. M.; Erickson, W.; Meyer, T. J. *Inorg. Chem.* **1994**, *33*, 2974.

27. Burstall, F. H. J. *Chem . Soc.* **1936**, 173.

28. Roundhill, D. M. *Photochemistry and Photophysics of Metal Complexe,* Plenum Press, New York, **1994**.

29. Gafney, H. D.; Adamson, A. W. *J. Am. Chem. Soc.* **1972**, *94*, 8238.

30. Kavarnos, G. J. *Fundamentals of Photoinduced Electron Transfer* VCH Publishers, New York, **1993**.

31. Kalyanasundaram, K. *Photochemistry of Polypyridine and Phorphyrin Complexes* Academic Press, London, **1992**.

32. Kalyanasundaram, K.; *Coord. Chem. Rev.* **1982**, *46*, 159.

33. Krausz, E.; Ferguson, J.; *Prog. Inorg. Chem.* **1989**, *37*, 293.

34. Balzani, V.; Juris, A.; Barigelletti, F.; Campagna, s.; Belser, P.; Von Zelewsky, A. *Coord. Chem. Rev.* **1988**, *84*, 85.

35. Steel, P. J. *Coord. Chem. Rev.* **1990**, *106*, 227.

36. Braunstein, C. H.; Baker, A. D.; Strekas, T. C.; Gafney, H. D. *Inorg. Chem.* **1984**, *23*, 857.

37. Fuchs, Y.; Lofters, S.; Dieter, T.; Shi, W.; Morgan, R.; Strekas, T. C.; Gafney, H. D.; Baker, A. D. *J. Am. Chem. Soc.* **1987**, *109*, 2691.

38. Berger, R. M. *Inorg. Chem.* **1990**, *29*, 1920.

39. Rillema, D. P.; Mack, K. B. *Inorg. Chem.* **1982**, *21*, 3849.

40. Rillema, D. P.; Taghdiri, D. G.;Jones, D. S.; Keller, C. D.; Worl, L. A.; Meyer, T.J.; Levy, H. A. *Inorg. Chem.* **1987**, *26*, 578.

41. Rillema, D. P.; Callahan, R. W.; Mack, K. B. *Inorg. Chem.* **1982**, *21*, 2589.

42. Sahai, R.; Morgan, L.; Rillema, D. P. *Inorg. Chem.* **1988**, *27*,3495.

43. Cooper, J. B.; Macqueen, D. B.; Petersen, J. D.; Wertz, D. W. *Inorg. Chem.* **1990**, *29*, 3701.

44 . Rassmussen, S. C.; Richter, M. M.; Yi, E.; Place, H.; Brewer, K. J. *Inorg.Chem.* **1990**, *29*, 3926.

45. Kahl, J. L.; Hanck, W.; DeArmond, M. K. *J. Chem. Phys.* **1978**, *82*, 540.

46. Baiano, J. A.; Carlson, D. L.; Wolosh, G. M.; DeJesus, D. E.; Knowles, C. F.; Szabo, E. G.; Murphy, W. R. *Inorg. Chem.* **1990**, *29*, 2327.

47. DeArmond, M. K.; Hillis, J. K. *J. Chem. Phys.* **1971**, *54*, 2247.

48. Crosby, G. A. *Acc. Chem. Res.* **1975**, *8*, 231.

49. Kew, G.; DeArmond, K.; Hanck, K. *J. Phys. Chem.* **1974**, *78*, 727.

50. Nallas, G. N.; Brewer, K. J. *Inorg. Chim. Acta.* in press.

51. Skoog, D. A.; West, D. M.; Holler, J. F. *Fundamentals of Analytical Chemistry Fourth Edition* Saunders College Publishing, New York, **1988**.

52. Harris, D. C. *Quantitative Chemical Analysis Second Edition* W. H. Freeman and Company, New York, **1987**.

53. Braun, R. D. *Introduction to Instrumental Analysis* McGraw-Hill Book Company, New York, **1987**.

54. Gale, R. J. *Spectroelectrochemistry Theory and Practice* Plenum Press, NewYork, **1988**.

55. Brewer, K. J.; Lumpkin, R. S.; Otvos, J. W.; Spreer, L. O.; Calvin, M. *Inorg. Chem.* **1989**, *28*, 4446.

56. Adamson, A. W.; Wegner, E. E. *J. Am. Chem. Soc.* **1966**, *88*, 394.

57. Camus, A.; Coceuar, C.; Mestroni, G. *J. Organomet. Chem.* **1972**, *39*, 355.

58. Goodwin, H. A. ; Lions, F. *J. Am. Chem. Soc.* **1959**, *81*, 6415.

59. Buu-Hoi, N. P.; Saint-Ruf, G. *J. Chem. Soc.* **1961**, 2257.

60. Molnar, S. M.; Neville, K. R.; Jensen, G. E.; Brewer, K. J. *Inorg. Chim. Acta.* **1993**, *206*, 69.

61. Sullivan, B. P.; Salmon, D. J.; Meyer, T. J. *Inorg. Chem.* **1978**, *17*, 3334.

62. Bridgewater, J. S.; Vogler, L. M.; Molnar, S. M.; Brewer, K. J. *Inorg. Chim. Acta.* **1993**, *208*, 179.

63. Campagna, S.; Denti, G.; Serroni, S.; Ciano, M.; Balzani, V. *Inorg. Chem.* **1991**, *30*, 3728.

64. Molnar, S. M.; Jensen, G. E.; Vogler, L. M.; Jones, S. W.; Laverman, L.; Bridgewater, J. S.; Richter, M. M.; Brewer, K. J. *J. Photochem. Photobiol. A.: Chem.* **1994**, *80*, 315.

65. DeArmond, M. K.; Carlin, C. M. *Coord. Chem. Rev.* **1981**, *36*, 325.

66. Caspar, J. V.; Kober, E. M.; Sullivan, B. P.; Meyer, T. J. *Inorg. Chem.* **1978**, *29*, 3926.

67. Casper, J. V.; Meyer, T. J. *J. Am. Chem. Soc.* **1983**,*87*, 952.

68. Lever, A.B. P; Dodsworth, E. S. *Chem. Phys. Lett.* **1986**, *124(2)*, 152.

69. Lever, A. B. P. *Inorg. Chem.* **1990**, *29*, 1271.

70. Kaim, W.; Kasack, V. *Inorg. Chem.* **1990**, *29*, 4696.

71. Richardson, D. E.; Taube, H. *Inorg. Chem.* **1981**, *20*, 1278.

72. Cooper, J. B.; Vess, T. M.; Kalsbeck, W. A.; Wertz, D. W. *Inorg. Chem.* **1991**, *30*, 2286.

73. Murphy, W. R.; Brewer, K. J.; Gettliffe, G.; Petersen, J. D. *Inorg. Chem.* **1989**, *28*, 81.

74. Molnar, S. M.; Nallas, G.; Bridgewater, J. S.; Brewer, K. J. *J. Am. Chem. Soc.* **1994**, *116*, 5206.

75. Richter, M. R.; Brewer, K. *J. Inorg. Chem.*, **1993**, *32*, 5762.

76. Hand, R.; Nelson, R. F. *J. Electrochem. Soc.* **1970**, *11*, 1353.

77. Porter, G. B. In *Concepts of Inorganic Chemistry* Adamson, A. W.; Fleischauer, P. D., Eds. Wiley, New York, **1975**, p. 73.

APPENDIX I.

Infrared Spectra.

Figure A1. *Infrared Spectrum of 2,2'-Pyridyl.*

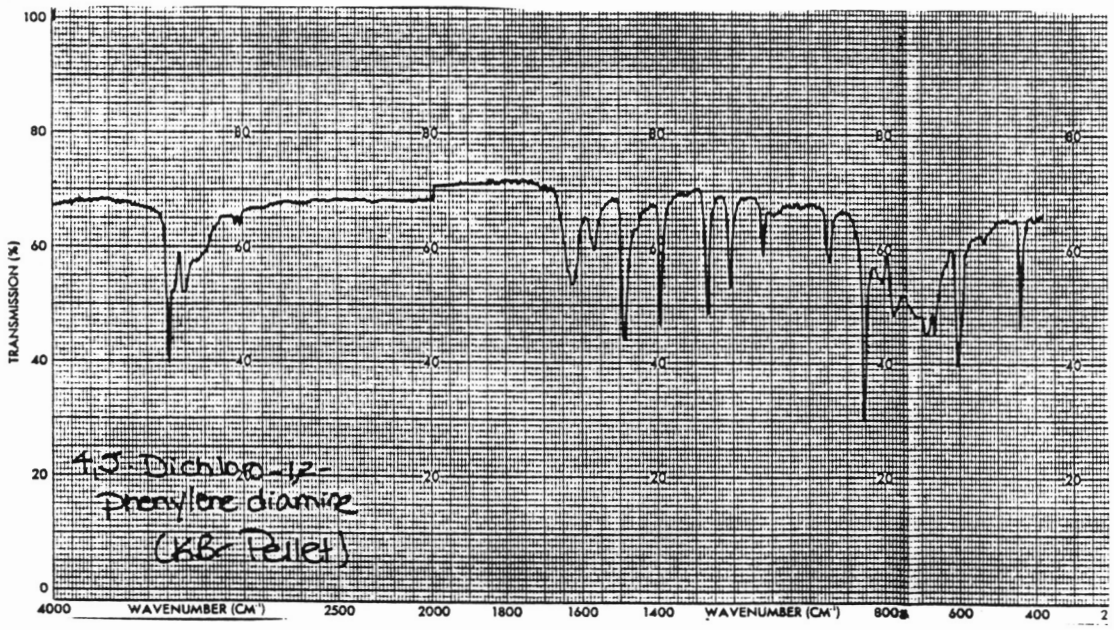

Figure A2. *Infrared Spectrum of 4,5-Dichloro-1,2-phenylenediamine.*

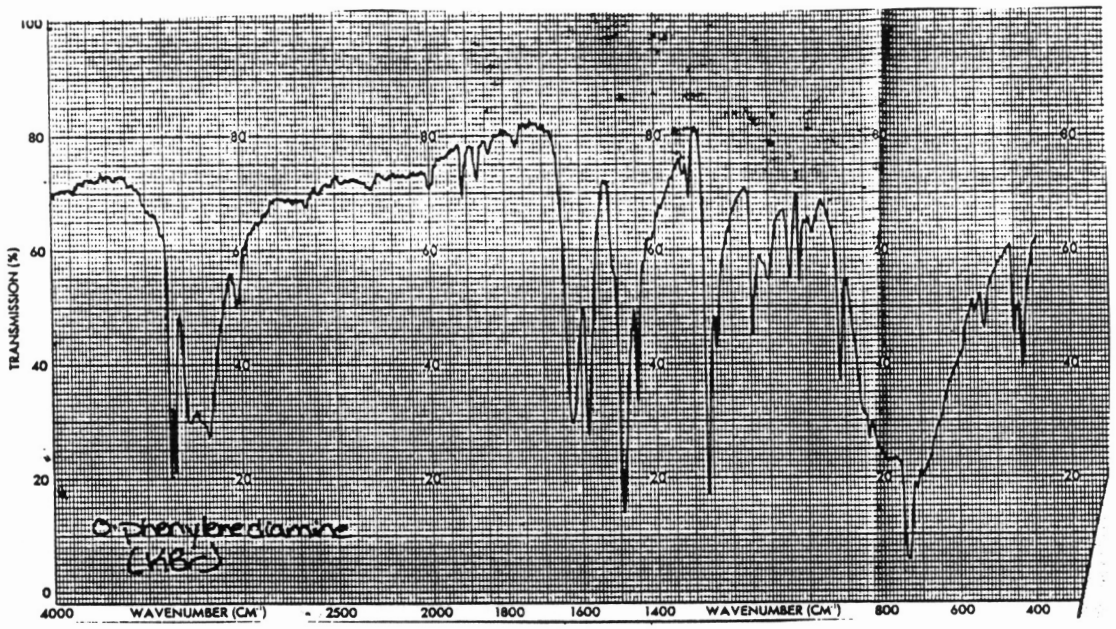

Figure A3. *Infrared Spectrum of o-phenylenedimine.*

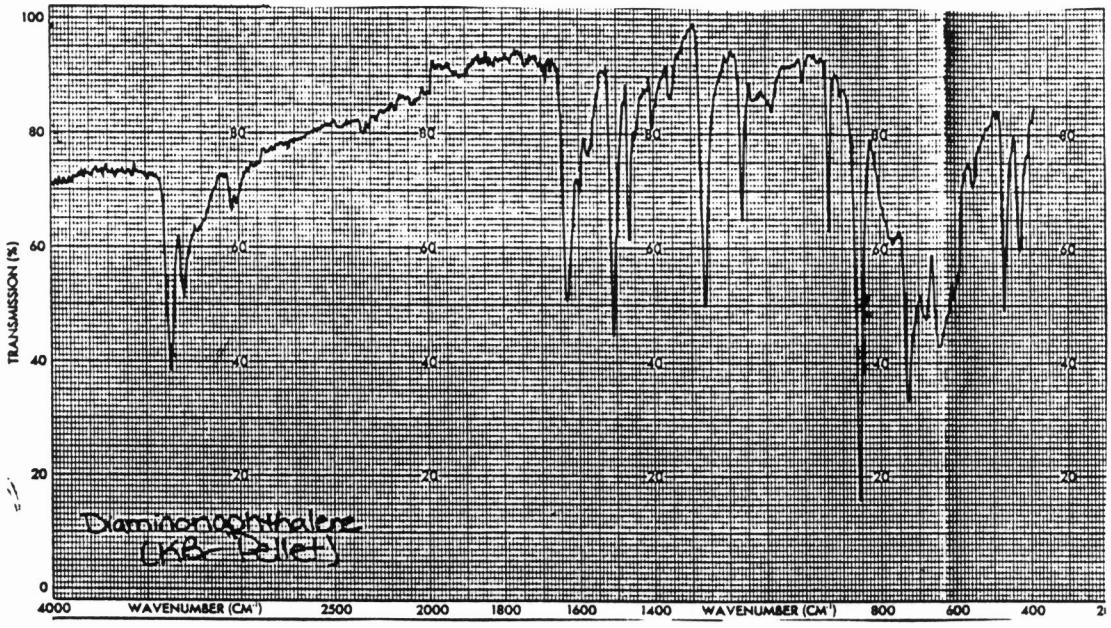

Figure A4. *Infrared Spectrum of Diaminonaphthalene.*

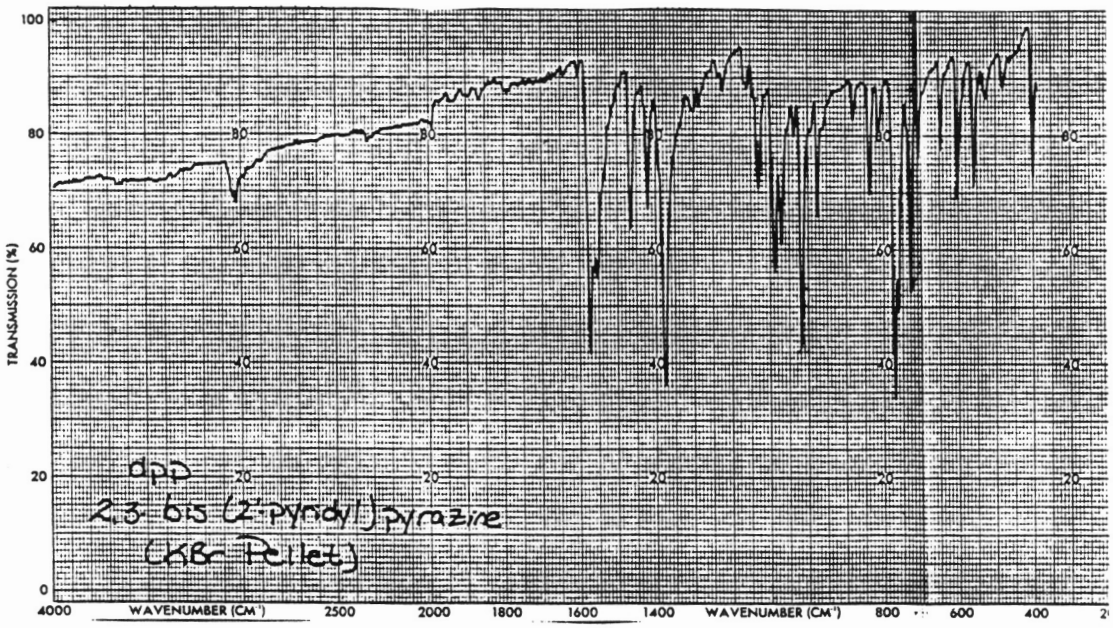

Figure A5. *Infrared Spectrum of 2,3-bis(2-pyridyl)pyrazine.*

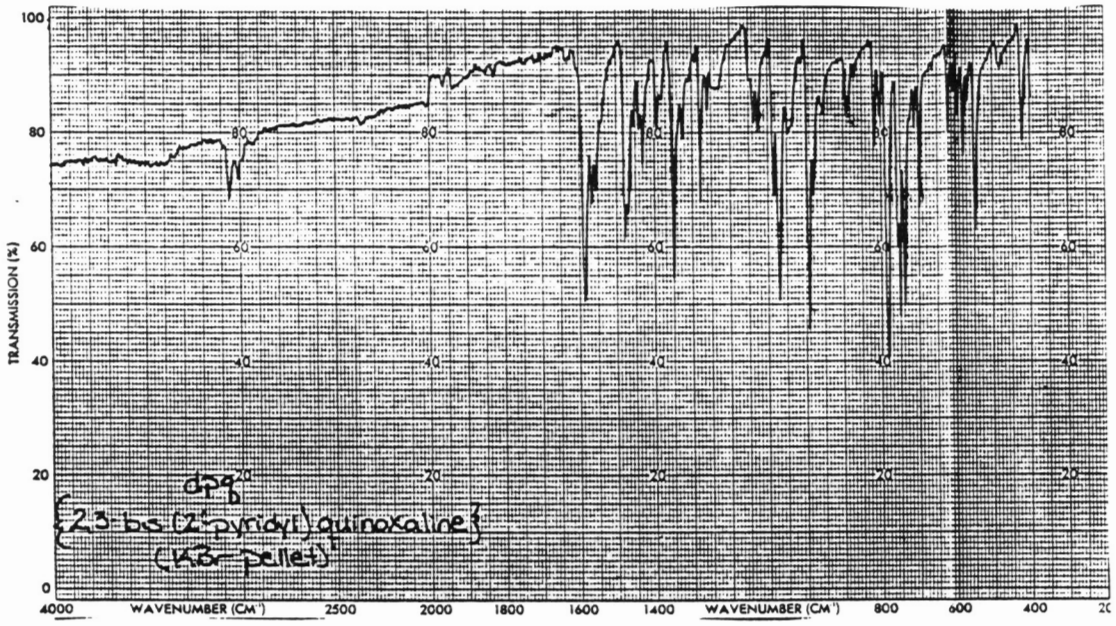

Figure A6. *Infrared Spectrum of 2,3-Bis(2-pyridyl)quinoxaline.*

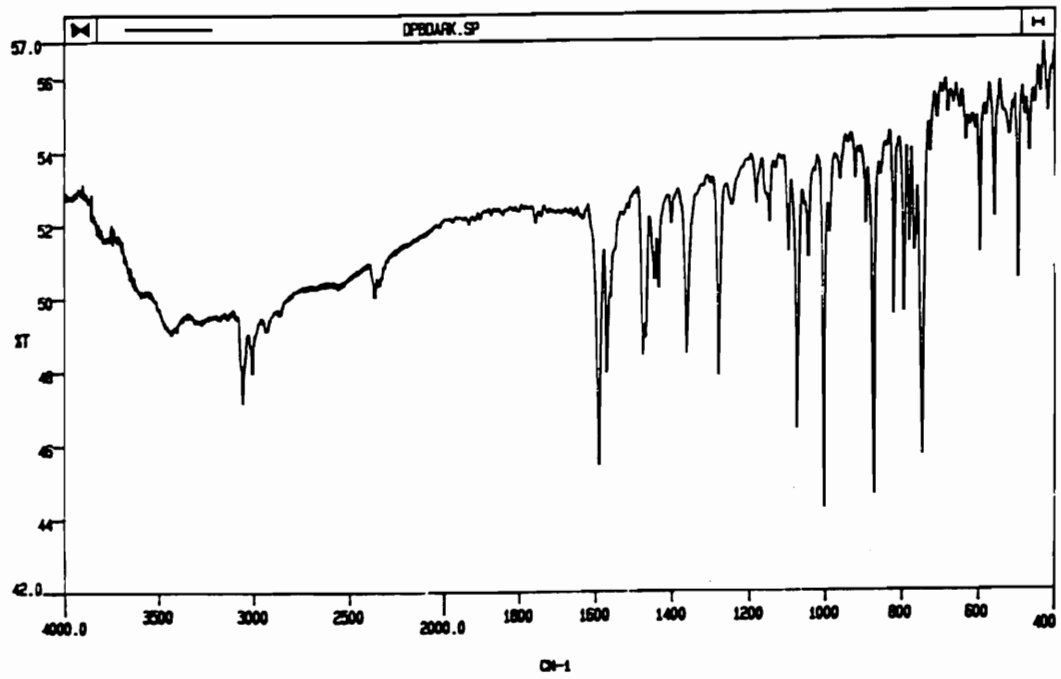

Figure A7. *Infrared Spectrum of 2,3-Bis(2-pyridyl)benzoquinoxaline.*

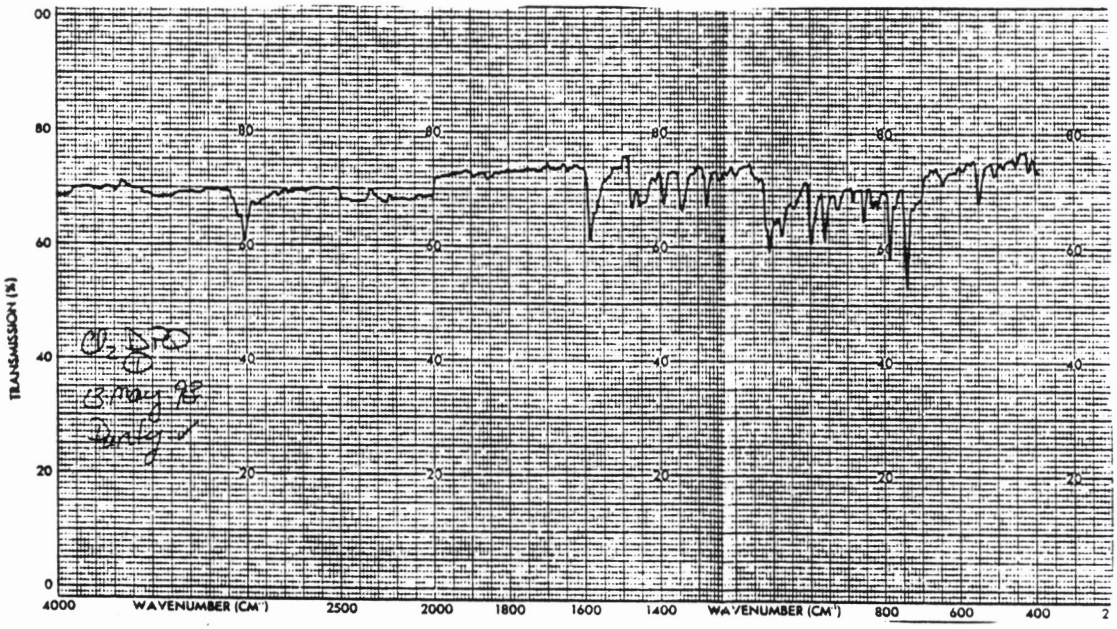

Figure A8. *Infrared Spectrum of 6,7-Dichloro-2,3-bis(2-pyridyl)quinoxaline.*

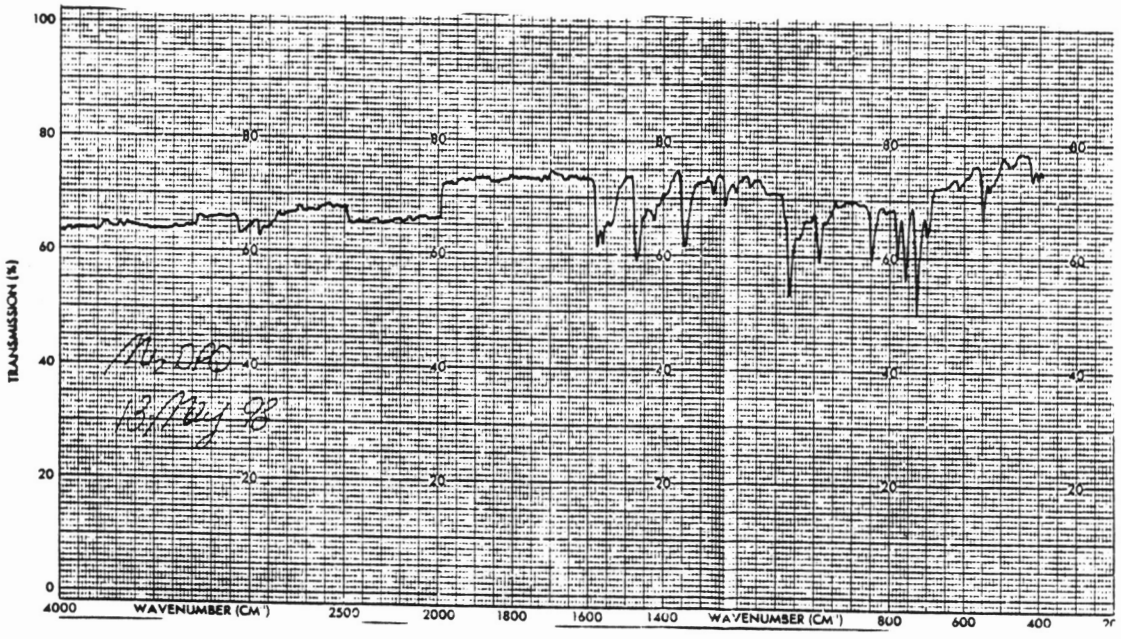

Figure A9. *Infrared Spectrum of 6,7-Dimethyl-2,3-bis(2-pyridyl)quinoxaline.*

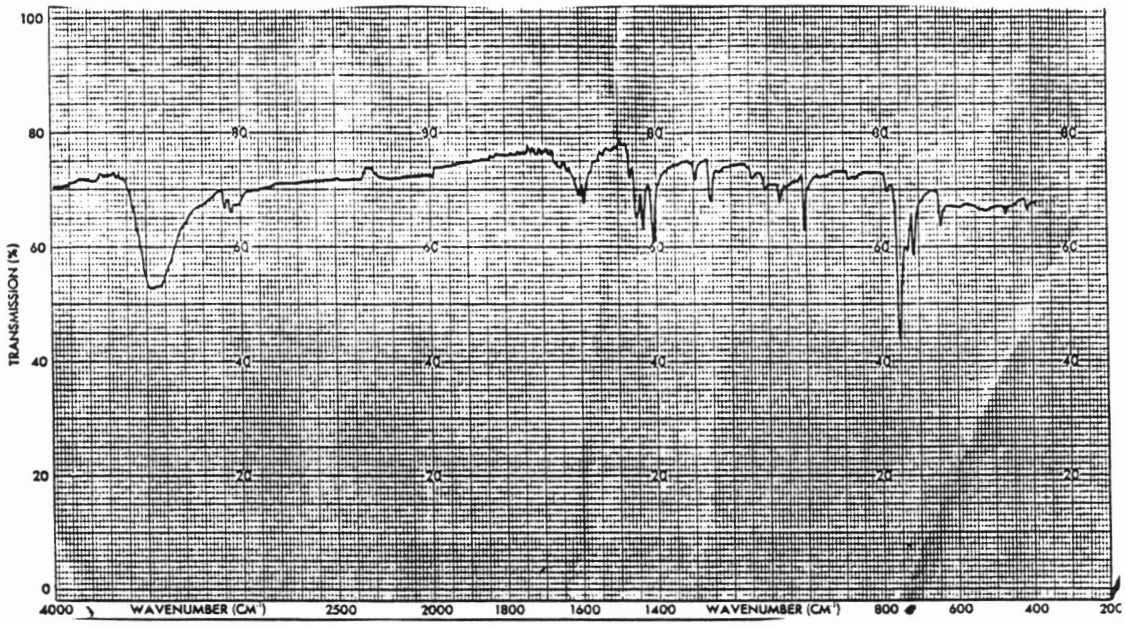

Figure A10. *Infrared Spectrum of $Ru(bpy)_2Cl_2$.*

APPENDIX II.

Photomultiplier Tube and Xenon Arc Lamp Supplementary Material.

[A]

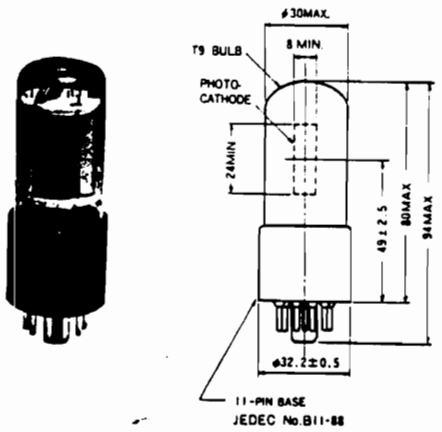

[B]

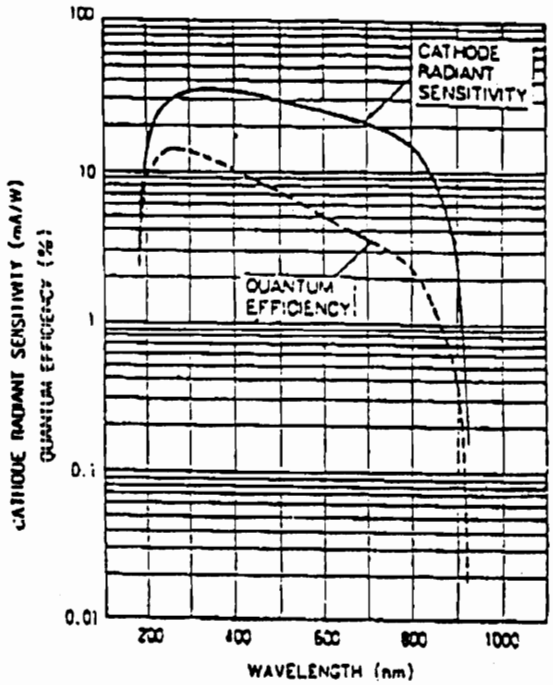

Figure A11. *Diagram and Wavelength vs. Signal Response of a Hammamatsu R666s Photomultiplier Tube.* [A] The diagram of the outer construction of the photomultiplier tube and the inner arrangement of the dynodes within a Hammamatsu R666s photomultiplier tube. [B] A plot of the wavelength dependence of the photomultiplier tubes signal response.

[A]

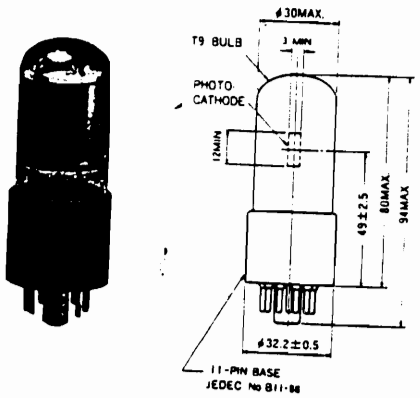

[B]

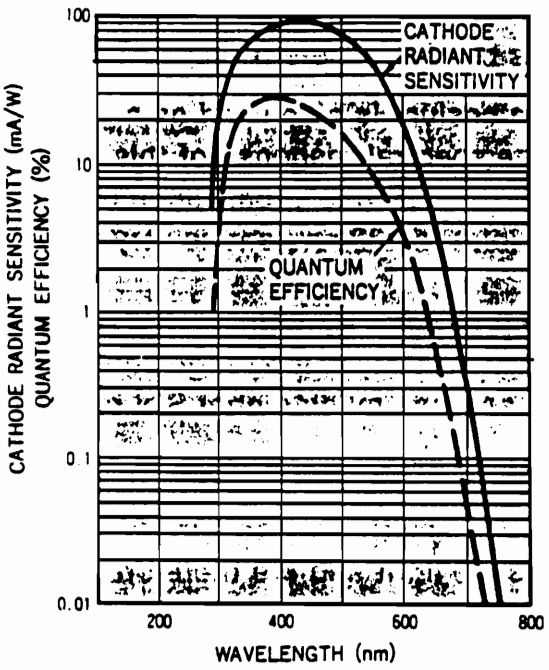

Figure A12. *Diagram and Wavelength vs. Signal Response of a Hammamatsu R928s Photomultiplier Tube.* [A] The diagram of the outer construction of the photomultiplier tube and the inner arrangement of the dynodes within a Hammamatsu R928s photomultiplier tube. [B] A plot of the wavelength dependence of the photomultiplier tubes signal response.

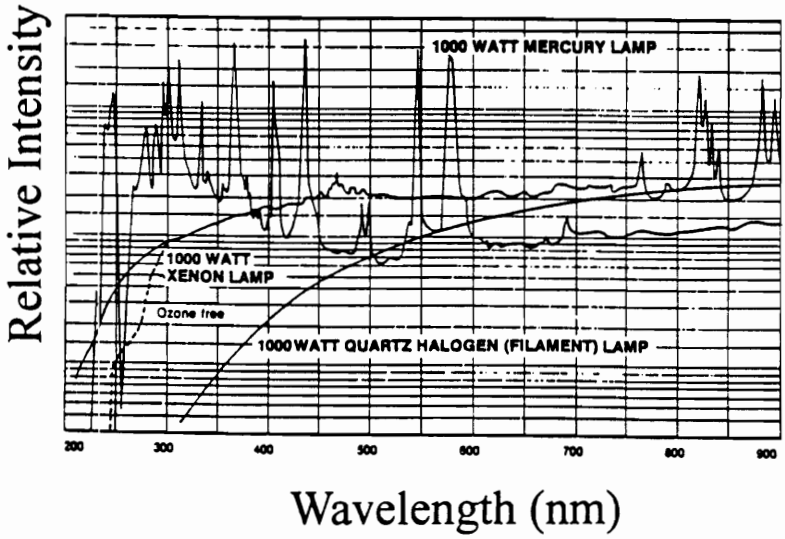

Figure A13. *Output of an Oriel 1000 W Xenon Arc Lamp.*

APPENDIX III.

Emission Lifetime Supplementary Material.

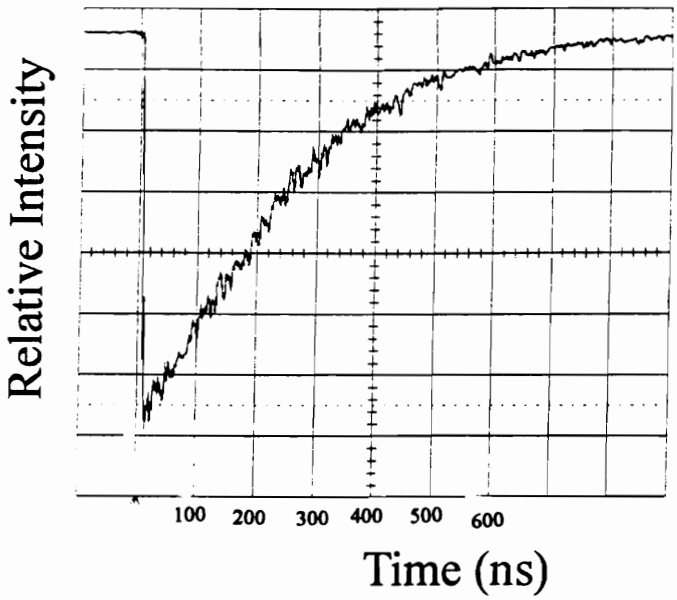

Figure A14. *An Example of an Emission Lifetime Signal versus Time Trace.* This time trace example is of $[(bpy)_2Ru(dpp)](PF_6)_2$ (bpy = 2,2'-bipyridine and dpp = 2,3-bis(2-pyridyl)pyrazine).

APPENDIX IV.

Photolysis Light Filtering Supplementary Material.

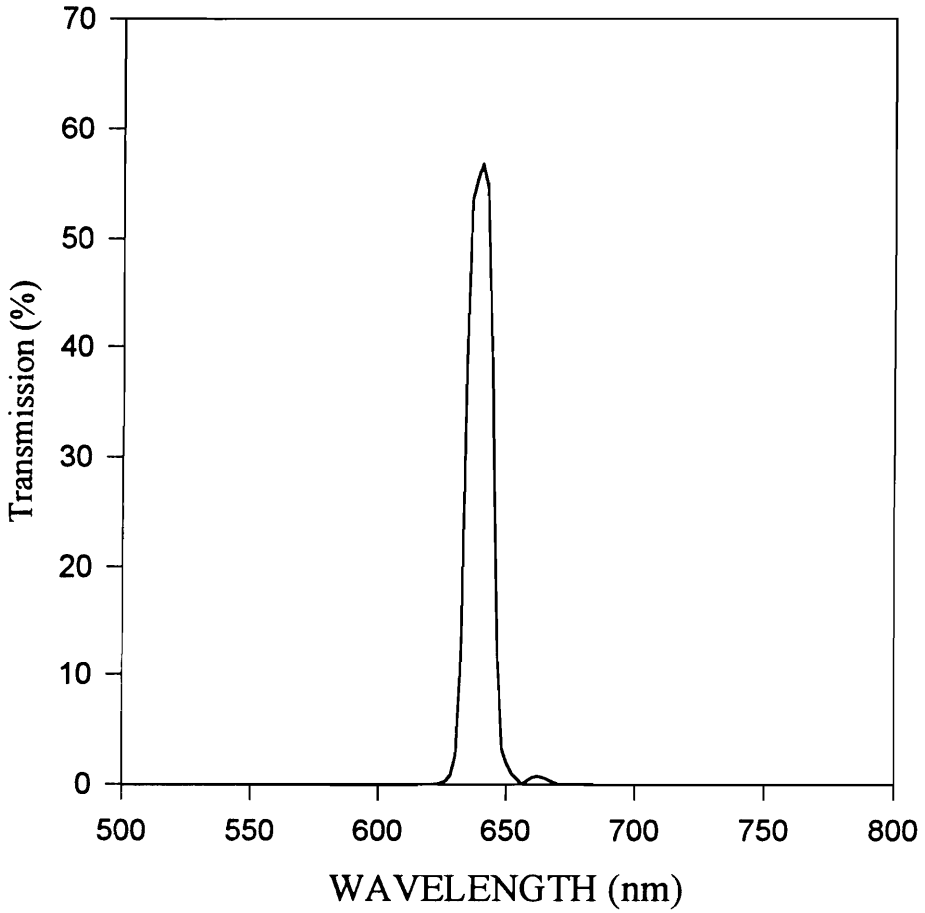

Figure A15. *The Transmittance Spectrum for the 640 nm Narrow Bandpass (10 nm) Filter.*

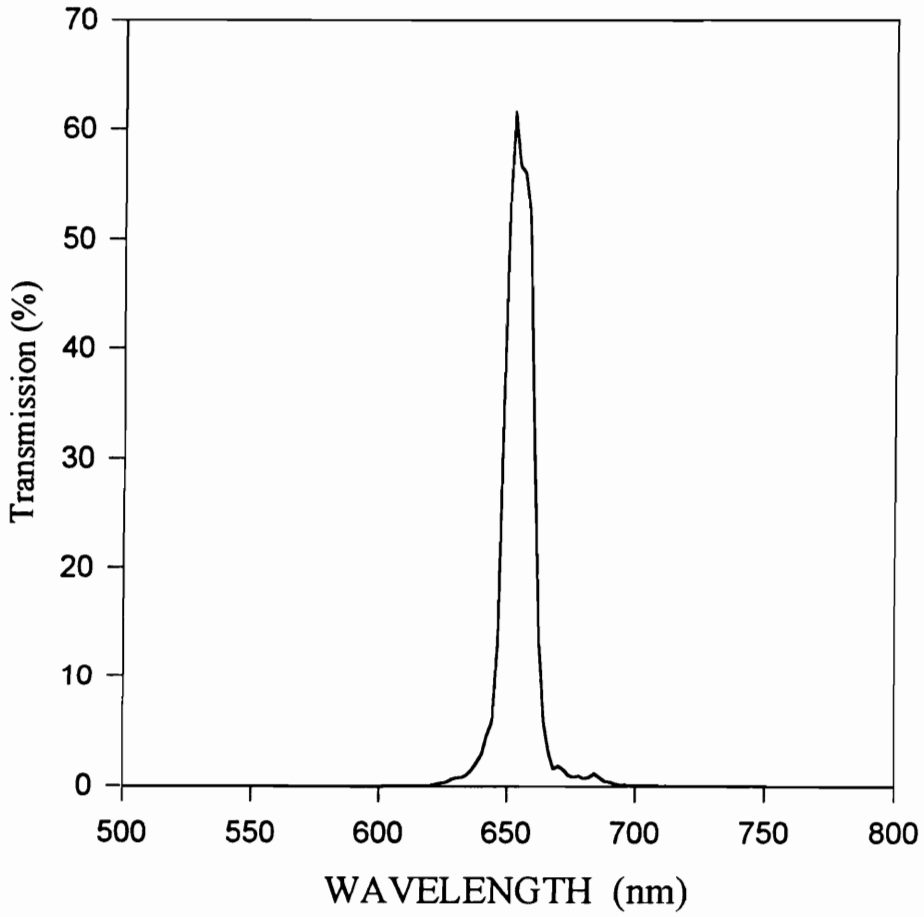

Figure A16. *The Transmittance Spectrum for the 660 nm Narrow Bandpass (10 nm) Filter.*

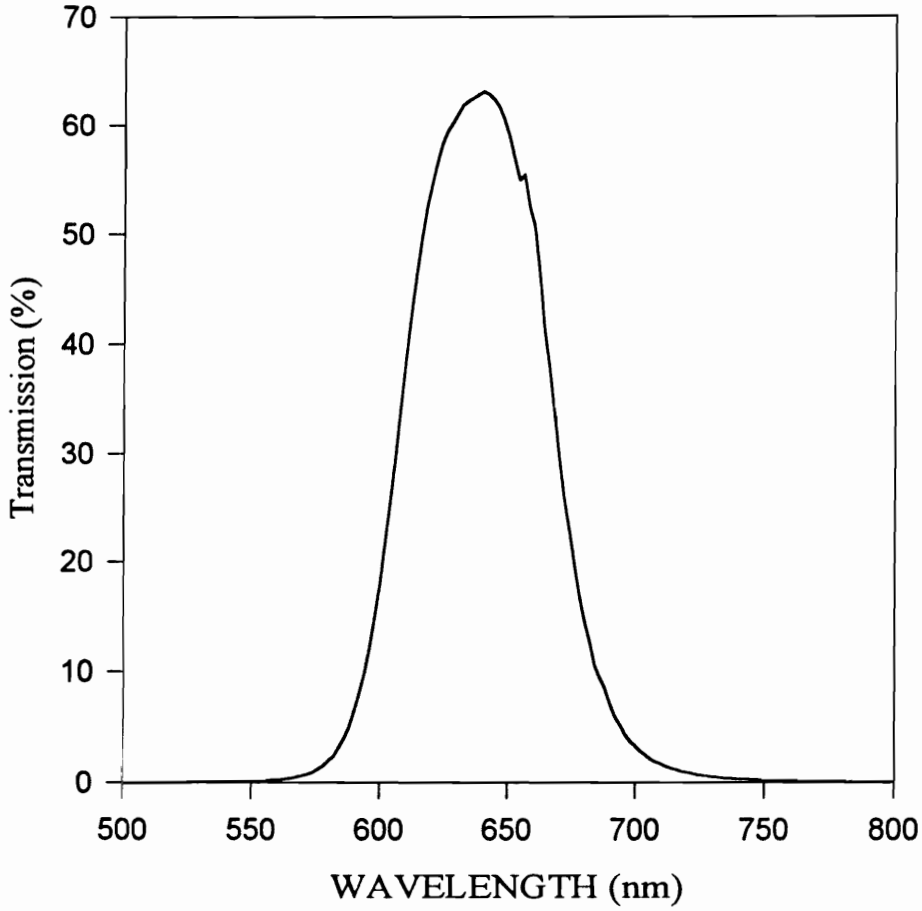

Figure A17. *The Transmittance Spectrum for the 660 nm Narrow Bandpass (50 nm) Filter.*

VITA

Sharon Marie Molnar was born in Detroit, Michigan in June of 1967. She has wanted to receive her Ph. D. in science ever since the tenth grade in high school. After graduating with a double major in chemistry and math at the College of St. Catherine (Spring, 1990), she attended graduate school at Washington State University in Pullman, Washington. Her research director was Karen J. Brewer, whom Sharon followed to Virginia Polytechnic Institute and State University to finish her doctoral degree.

PUBLICATIONS:

"PHOTOINITIATED ELECTRON COLLECTION IN A MIXED-METAL TRIMETALLIC COMPLEX OF THE FORM $\{[(bpy)_2Ru(dpb)]_2IrCl_2\}(PF_6)_5$ (bpy = 2,2' -bipyridine and dpb = 2,3-bis(2-pyridyl)benzoquinoxaline)." Sharon M. Molnar, Jon S. Bridgewater, Girlie Nallas, and Karen J. Brewer. *J. Am. Chem. Soc.* **1994**, *116*, 5206.

"PHOTOCHEMICAL PROPERTIES OF MIXED-METAL SUPRAMOLECULAR COMPLEXES." Sharon M. Molnar, Glen E. Jensen, Lisa M. Vogler, Leroy Laverman, Jon S. Bridgewater, and Karen J. Brewer. *J. Photochem. & Photobiol., Section A, Chem.* **1994**, *80*,315-322.

"TUNING THE SPECTROSCOPIC AND ELECTROCHEMICAL PROPERTIES OF POLYPYRIDYL BRIDGED MIXED METAL Ir(III)/ Ru (II) COMPLEXES: A SPECTROELECTROCHEMICAL STUDY." Jon S. Bridgewater, Lisa M. Vogler, Sharon M. Molnar, Karen J. Brewer. *Inorg. Chim. Acta* **1993**, *208*, 179.

"UTILIZATION OF SUBSTITUTED POLYAZINE BRIDGING LIGANDS TO TUNE THE SPECTROSCOPIC AND ELECTROCHEMICAL PROPERTIES OF BIMETALLIC RUTHENIUM COMPLEXES." Sharon M. Molnar, Kevin R. Neville, Glen E. Jensen, and Karen J. Brewer. *Inorg, Chem. Acta* **1993**, *206*, 69.

"SYNTHETIC DESIGN OF FERRIMAGNETIC MATERIALS: ONE DIMENSIONAL BIMETALLIC COORDINATION POLYMERS." Roger Willett, Zhenming Wang, Sharon Molnar, Karen Brewer, Christopher P. Landee, Mark M. Turnbull, and Wanru Zhang. *Mol. Cryst. Liq. Cryst.* **1993**, *233*, 277.

"THREE METAL (1,4,8,11-TETRAAZACYCLOTETRADECANE) HALIDE SALTS." Xin Chen, Gregory Long, Roger D. Willett, Tara Hawks, Sharon Molnar and Karen Brewer *Acta Cryst. C.* **1996**, *C52*, 1924.

"CRYSTAL STRUCTURE OF 1,4,8,12-TETRAZACYCLOTETRADECANE COPPER(II) TRIBROMOCUPRATE(I)." Xin Chen, Roger D. Willett, Tara Hawks, Sharon Molnar and Karen Brewer *J. Chem. Cryst.* **1996**, *26*, 261.

"MONOCLINIC FORM OF $Cu(C_{10}H_{28}N_4)CuCl_4$." Zhenming Wang, Roger D. Willett, Sharon M. Molnar, and Karen J. Brewer *Acta Cryst. C.* **1996**, *C52*, 581.